INFORMATION PROCESSING IN THE MAMMALIAN OLFACTORY BULB

Thesis by

Upinder Singh Bhalla

In Partial Fulfillment of the Requirements

for the Degree of

Doctor of Philosophy

California Institute of Technology

Pasadena, California

1993

(Submitted April 22, 1993)

To my family.

ACKNOWLEDGMENTS

This project owes much to the ideas and efforts of my friends and colleagues, to whom I am deeply indebted.

Jim Bower, who gave me the freedom to work in my own way and the opportunity to undertake projects that few biologists ever have a chance to try.

The Genesis developers - Matt Wilson, Mark Nelson, Erik De Schutter, Dave Bilitch, John Uhley, Dave Beeman, Michael Speight, and many others.

My fellow students and post-docs, who were a continual source of help, ideas, and perspective.

My teachers, who challenged me to accomplish things I had never imagined being able to do.

Henry Lester and the students I nominally taught, who made teaching a learning experience.

My well-intentioned friends in the GSC, and the equally well intentioned souls in the Administration, who showed me that that two good intentions an impasse make.

My family, for everything.

ABSTRACT

A combination of computer modeling and experimental approaches were taken to studying the mammalian olfactory bulb. First, detailed single cell models were developed for the main cell classes in the olfactory bulb. This involved development of simulation techniques and a parameter search method for assigning unknown parameters for neuronal models. This study demonstrated the feasibility of using indirect information, such as spike waveforms, to determine the detailed electrical properties of neurons. The models demonstrated that spikes propagate into the secondary dendrites, which may play a role in long-range spatial interactions in the bulb. Blockage of this spike propagation might be involved in bulbar information processing. Second, a series of recordings were made from neurons in the olfactory bulb of awake unrestrained rats exposed to a cyclical sequence of odorants. These recordings demonstrated a significant amount of variability in the response of individual neurons over time. The neuronal responses were well described as a combination of a consistent component with a component that varied over time. Comparisons made between response properties of the same neuron at different times, between adjacent neurons, between distant neurons and between unrelated neurons showed a clear sequence of increasing difference in the order: same < adjacent < unrelated < distant. However, during sniff periods, the sequence was: adjacent < same < unrelated < distant. This suggests the bulb normally responds evenly to a wide range of odorants, but during sniffing responses to familiar odorants are suppressed so as to preferentially detect novel odorants. The final stage of the study involved the development of detailed models of the bulb as a whole using both the single cell models, and the experimental results previously obtained. It was found that topographical organization of receptor input according to receptor type was not required to produce the range of responses seen in the experiments. The response variability of neurons in the model was much smaller than in experiment. We propose that the bulb can operate in multiple processing modes so as to optimize its responses for different situations and that this leads to variability in single neuron responses.

TABLE OF CONTENTS

LIST OF ILLUSTRATIONS

INTRODUCTION

The olfactory system is rich in paradoxes. It is regarded as one of the minor senses in humans, yet it elicits some of the strongest behavioral effects and memory associations of any modality (Slotnick et al. 1991). Olfaction combines the exquisite selectivity of the pheromone system, with a general sensitivity so broad as to recognize almost any chemical stimulus whatsoever (Lancet 1986). Olfactory receptor cells turn over as often as once a month (Graziadei and Monti Graziadei 1979), yet odor sensations are stable over a lifetime. These observations appear paradoxical, perhaps, because of a deeper paradox in our understanding of the system: olfaction is one of the best described, yet least understood of the sensory modalities. The objective of this project is to broaden this understanding, particularly as it applies to the information processing in the olfactory bulb.

The key to understanding how the system processes information is to learn how it represents information. This approach has proven very successful in other modalities such as vision, where the experiments of Hubel and Wiesel (Hubel and Wiesel 1962, 1968) laid the foundation for the field by providing deep insights into the representation of visual information in the cortex. There are clear indications in the olfactory literature, as discussed below, that both the temporal patterns of neural spike trains, and the spatial patterns of activity over the surface of the bulb, are important in this representation. A major goal of the experimental project was therefore to develop techniques for acquiring data on spike activity over long periods of time, and at different spatial separations on the bulb, under well defined behavioral and stimulus conditions. Briefly, we found not one but two distinct modes in which the bulb might spatially represent olfactory information. We also found that individual neurons represented information as a combination of a consistent response component, and a variable component. Based on this information about representation, we hypothesized that the processing in the bulb involves several different modes of representation, and that the variable component of single neuron response arises from switching between these modes.

In parallel with this experimental study, we developed computer simulation methods for modeling individual cells and networks at a high level of biological realism. We constructed a model of the bulb based on the structural data from the literature, and related this to the experimental observations. We found a functional correlate of the spatial organization of bulbar activity, in the form of active spike propagation along the secondary dendrites of bulbar mitral cells. These dendrites extend for distances comparable to the experimentally observed range of organization of bulbar activity. We further found that the receptor input itself is unlikely to generate the variability observed in the experiments, which strengthens the argument that this variability results from switching between processing modes under central control.

In summary, this project combines simulations with experiments in order to broaden understanding of bulbar information processing. In the context of some of the issues in olfactory research that we discuss below, we have contributed towards defining some of the aspects of olfactory processing in the bulb.

Background information.

Relation to other areas of the brain.

There are only two centers in the mammalian brain which are exclusively devoted to olfactory processing, in contrast to tens of visual areas. These are the olfactory bulb, and the piriform cortex (Figure 1). All the projections from the olfactory epithelium terminate in the ipsilateral olfactory bulb. The bulb in turn projects to, and receives feedback from, the ipsilateral piriform cortex. There are numerous feedback connections from higher and multimodal systems such as the amygdala, hippocampus and hypothalamus, mainly via the septum and diagonal band. Projections from the contralateral olfactory bulb arrive via the anterior commissure and anterior olfactory nucleus. Clearly, the olfactory system functions in the context of a great deal of information about the behavioral state of the animal and of the other senses.

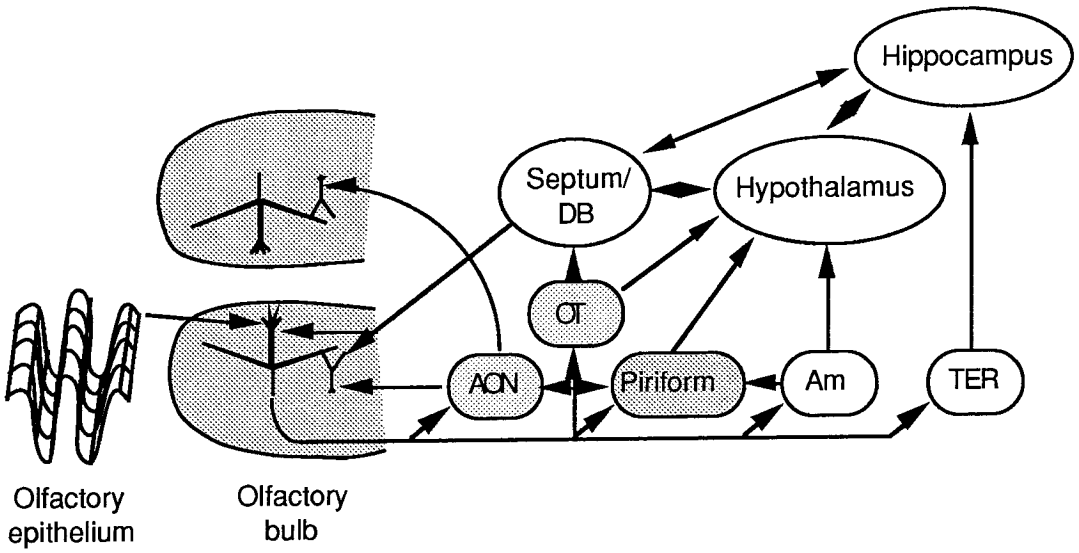

Figure 1. Olfactory processing centers in relation to other areas of the brain. (Adapted from Shepherd 1979). The olfactory areas are shaded. Abbreviations: AON: Anterior Olfactory Nucleus. OT: Olfactory tubercule. Am: Amygdala. TER: Transitional Entorhinal cortex. DB: Diagonal Band. The olfactory epithelium projects solely to the olfactory bulb. Mitral cells (represented by the large cell in the bulb) are the only output neurons. Granule cells receive most of the feedback projections. The AON and OT are small nuclei which appear to act mainly to relay olfactory information. The projection from the AON to the contralateral olfactory bulb occurs via the anterior commisure. There are extensive feedback projections throughout the system, except to the olfactory epithelium.

The subject of our investigations is the olfactory bulb. It is a highly organized structure, consisting of four layers: the glomerular layer, the external plexiform layer, the mitral cell layer, and the granule cell layer (Figure 2). In mammals the olfactory bulb is subdivided into the main olfactory bulb (MOB) and the accessory olfactory bulb (AOB). These are similar in layering and in the morphology of their cells. The AOB is concerned with pheromonal and species-specific olfactory processing, and receives specialized input from the vomeronasal organ as well as the olfactory epithelium (Meredith 1991). The MOB is involved in general olfactory processing, and receives input from the olfactory epithelium (Meredith 1991). This investigation focuses on information processing in the MOB.

Olfactory bulbs in other species.

Although the term olfactory bulb can only be applied to vertebrates, where this structure has a distinct identity, there are analogous structures in the corresponding position of the olfactory pathways of many animals. Glomerulus-like structures are apparent in the mushroom bodies of insects (Hansson et al. 1992). Furthermore, cell types with clear similarities to mitral cells are also visible. It seems likely that there are some aspects of the first stage of olfactory processing that glomerular-like structures are uniquely well adapted to serving.

Among vertebrates, there is a substantial amount of similarity in olfactory bulb structure. In many vertebrates the mitral cells bodies are not as cleanly organized into the mitral cell layer, which is especially prominent in the rat and rabbit olfactory bulb (Mori 1987). However, their morphology and projections remain essentially the same. Mitral cells in mammals tend to have a single apical dendrite, projecting to a single glomerulus. Mitral cells in other vertebrates frequently have two or more apical dendrites. The presence of additional apical dendrites does not seem to cause large differences in electrical properties of these cells (see Chapter 3).

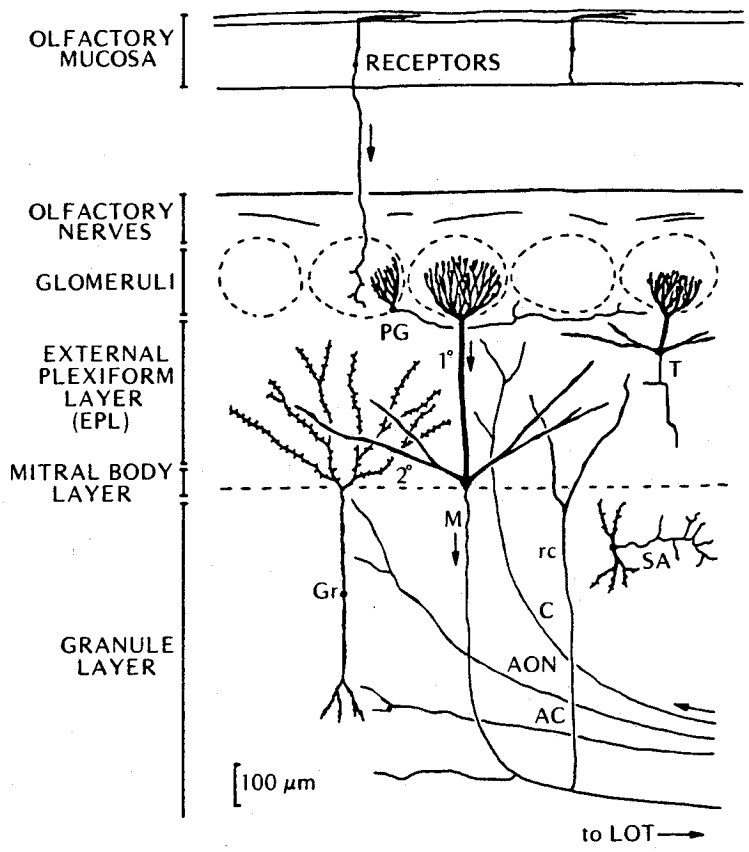

Neuronal elements of the mammalian olfactory bulb.

Inputs: afferent fibers (above) from olfactory receptors; central fibers (below) from three sources; centrifugal fibers (C) from the nucleus of the horizontal limb of the diagonal band; ipsilateral fibers from the anterior olfactory nucleus (AON); contralateral fibers from the anterior commissure (AC).

Principal neurons: mitral cell (M), with primary (1°) and secondary dendrites (2°) and recurrent axon collaterals (rc); tufted cell (T).

Intrinsic neurons: periglomerular short-axon cell (PG); deep short-axon cell (SA); granule cell (Gr). LOT, lateral olfactory tract.

(Based on Cajal, 1911; Price and Powell, 1971; Pinching and Powell, 1972; Shepherd, 1972.

Figure 2. Structure of the olfactory bulb. (From Shepherd 1979)

Cell types.

The major cell types in the bulb are the mitral cells and subtypes, the granule cell classes, and the periglomerular cells (Mori 1987). A number of smaller populations of short-axon cells have been described histologically but not as well characterized electrophysiologically.

The principal neurons of the bulb are the mitral cell and its subclasses. These cells receive direct synaptic input in the glomerular layer from the olfactory nerve and provide the only output to piriform cortex and other brain regions. They are a relatively small cell population numerically -- around 50,000 cells in each olfactory bulb of the rabbit (Shepherd 1993). Mitral cells possess two distinct dendritic areas: the glomerular tuft at the top of the primary dendrite(s), and the secondary dendrites which extend enormous distances laterally in the olfactory bulb (a 1-mm radius around the cell body in rabbits: Mori et al. 1983). Mitral cells are believed to be the only excitatory cells in the bulb (Wellis and Scott 1990; but see Martinez and Freeman 1984). Three main subclasses of mitral cells have been described: mitral, displaced mitral, and tufted. Displaced mitral cells are very similar in morphology and properties. As their name implies their cell bodies are slightly displaced from the mitral cell layer and lie in the lower part of the external plexiform layer. They also tend to be slightly smaller than mitral cells. The tufted cells are sometimes classed differently because their projection patterns are believed to be more restricted to within the bulb (Mori 1987). These are somewhat smaller than mitral cells and have fewer secondary dendrites (two or three in the rat). Their cell bodies lie scattered in the middle and upper portions of the external plexiform layer.

The electrical properties of all three mammalian mitral cell classes appear quite similar, except for the input resistance characteristics associated with the differences in size. This similarity extends to mitral cells derived from other vertebrate species, including turtles and salamanders (Mori 1987). The electrotonic size of the cells is large, over one lambda from measurements of charging time-courses (Mori et al. 1981). Mitral cells clearly have dendritic spiking activity in the glomerular region, as seen from fast

pre-potentials recorded at the soma (Mori et al. 1981). There is also evidence for spikes in the secondary dendrites from voltage-sensitive dye recordings (Cinelli and Salzberg 1992). Simulation studies (Chapter 3) also support the idea of a wide distribution of voltage-dependent channels throughout the mitral cell dendritic tree. Experiments with blockers have confirmed that the spikes have both a sodium as well as a calcium component, since it requires both TTX and cobalt to block spiking activity (Mori et al. 1981). Mitral cells have receptors both for excitatory input from the olfactory nerve (presumed to be glutamate) and also for GABA, which appear to be located at dendro-dendritic synapses from periglomerular and granule cells (Mori 1987).

Periglomerular cells are, as their name implies, clustered closely around the glomeruli. Their dendrites enter the glomerulus and make extensive dendro-dendritic contacts with mitral cells and also receive direct synaptic input from the olfactory nerve axons. Their cell bodies are small (5 um). These cells are quite numerous, there being about 20 for every mitral cell.

Periglomerular cells are difficult to identify and record from in vivo, but recent whole-cell and culture methods have provided improved electrical characterization (Bufler et al. 1992 a,b). There appear to be a number of subclasses, some of which do not spike. Receptors for both glutamate and GABA have been reported on these cells (Bufler et al. 1992 a). There is some disagreement about the role of these cells in the bulbar circuitry. The general consensus is that they are likely to have an inhibitory effect on mitral cells (Mori 1987) and more recent evidence suggests that they might inhibit each other as well (Bufler et al. 1992 b). Freeman and co-workers, however, have inferred from a number of studies that periglomerular cells play an excitatory role and that this effect is mediated by the transmitter GABA (Martinez and Freeman 1984).

Granule cells are by far the most numerous cell type in the olfactory bulb, being present in about a 200:1 ratio to mitral cells, making a total population of 10 million (Mori 1987). They are somewhat unusual for cells in the central nervous system, being axonless. Granule cells have small cell

bodies with small descending dendrites, and a larger ascending trunk which branches a few times. The granule cell dendrites have large numbers (200 - 1000s) of dendritic spines or gemmules, which are both the main input and output terminals for these cells (Mori et al. 1983). These cells are rather small electrically (Mori 1987) (< 0.5 lambda). The difficulty of obtaining stable intracellular recordings from granule cells has limited the available data, but at least a sub population of them are clearly capable of spiking. Granule cells utilize GABA as their transmitter at the dendro-dendritic synapses with mitral cells and possess receptors for glutamate (Trombley and Shepherd 1992). NMDA receptors in the olfactory bulb have been localized to granule cells (Trombley and Shepherd 1992), which raises the possibility of ongoing synaptic modification. LTP has not yet been fully demonstrated at mitral-granule synapses, though infusion of NMDA blockers in the bulb has been shown to impair olfactory learning (Staubli et al. 1987) and other experiments (Patneau and Stripling 1992) strongly support the notion of LTP at these synapses.

There have been reports of other cell classes in the olfactory bulb, mainly short-axon cells. These occur both in the EPL and in the granule cell layer. They form a relatively small population, and their role and properties are unclear.

Synaptic pathways in the olfactory bulb.

There are at least two distinct levels of organization of the bulbar circuitry. The first is at the glomerular level, where mitral cell dendritic tufts, periglomerular cell dendrites, and olfactory nerve terminations interact (Pinching and Powell 1971 a,b). The second is at the external plexiform layer, where mitral and granule cells form extensive reciprocal dendro-dendritic contacts (Price and Powell 1970; Rall and Shepherd 1968). At both levels, dendrodendritic interactions are believed to play a major role.

Glomeruli are remarkable synaptic structures, with dense dendritic terminations from both mitral and periglomerular cells. Glomeruli are widely believed to be functional units of organization in the olfactory bulb (Lancet et al. 1982). It has been pointed out that their numbers (approx. 2000 in

mammals) is similar to the number of distinguishable odorants (Lancet et al 1982). Furthermore, tests of activity such as 2-deoxyglucose studies invariably stain individual glomeruli uniformly, though neighboring glomeruli may have quite different levels of staining (Lancet et al. 1982).

Several configurations of synapses have been observed in the glomerulus, including reciprocal dendrodendritic contacts between mitral and periglomerular cells, synaptic triads including the olfactory nerve terminations, and axo-dendritic terminations from the olfactory nerve to one of the dendritic types (Pinching and Powell 1971a). The tight glial sheath around the glomeruli has been proposed as a mechanism for localizing diffusible substances. Evidence for his sort of local confinement of potassium ions has in fact been demonstrated (Khayari 1988) using ion-selective electrodes. It has recently been suggested that nitric oxide, NO, may also play a role as a transmitter confined within a glomerulus, since there is dense diaphorase staining in the glomeruli (Breer and Shepherd 1993, Vincent and Kimura 1992). Additional interactions in the glomerular layer occur through the periglomerular cell axons, which typically terminate within a few (2-3) glomerular radii, but not in the originating glomerulus (Pinching and Powell 1971b).

The second major level of bulbar synaptic organization is at the external plexiform layer (EPL). The reciprocal dendro-dendritic contacts at this level were suggested on the basis of electrophysiological evidence (Philips et al. 1963), simulations (Rall and Shepherd 1968) and finally confirmed by electron-microscopic studies (Price and Powell 1970). The large extent of mitral cell secondary dendrites (Mori et al. 1983) means that interactions at this level can take place across most of the extent of the bulb. It has been shown (Mori et al. 1983) that the density of synapses is greatest approximately halfway down the secondary dendrites. This would imply a radius of influence of 0.5 to nearly 2 mm from mitral to mitral cell, via intermediary granule cells. Since the extent of the rabbit olfactory bulb is only 4 mm, this represents a very substantial portion of the bulb.

Another important synaptic pathway is from the mitral/tufted cell axons, which send out collaterals into the external plexiform layer en route to the LOT. These synapse onto the granule cells in

the EPL and potentially provide an even wider range of influence than the dendro-dendritic synapses on mitral cell secondary dendrites. It is not clear what the relative importance of the two pathways is.

Principal issues in olfaction.

Olfactory stimuli.

In order to understand how the olfactory system encodes information, it is necessary to describe the stimuli it represents. The stimulus space for olfaction is in sharp contrast to that for most other modalities. In vision, for example, there is a two-dimensional mapping of stimulus space onto the retina. Each point in this space has two further attributes: intensity and color. Furthermore, each of these features is continuous, monotonic, and single-valued.

In olfaction, the stimulus space is multidimensional. This has been shown both by electrophysiological studies (recordings from receptor neurons, Sicard and Holley 1984) and from the large family of presumed olfactory receptor proteins (Buck and Axel 1991). Such a multidimensional stimulus space seems inevitable, given the variety of chemical stimuli and identifying molecular features that the system must resolve.

If one regards a particular chemical compound as a point in olfactory stimulus space, further differences between olfaction and other sensory modalities emerge. There is no continuity to chemical compounds, for example, no halfway point between H_2O and H_2S. Olfactory sensations are not monotonic, either at the perceptual or receptor level. Perceptually, an increasing concentration of a particular compound does not necessarily increase the perceived intensity of odorant. Instead, the perceived quality of the odor may change. For example, isoamyl acetate smells like bananas or pears depending on the concentration. At the electrophysiological level, the firing rate of receptor neurons (Sicard and Holley 1984) and mitral cells (Duchamp-Viret et al. 1990) does not always vary monotonically with odorant concentration. Finally, olfactory stimuli are not single-valued. At the perceptual level, the same pure compound may smell differently depending on context or concentration (e.g., isoamyl acetate). At the receptor level, a single odorant typically elicits responses from a large number of receptor neurons, each with a different profile of odorant selectivity (Sicard and Holley 1984). This has been explained by the

observation that a molecule is likely to have a number of functional groups which would be expected to bind to a number of completely different receptor proteins.

A fundamental question regarding olfactory reception has been the nature of the individual receptor molecules. The discovery of a large (N > 500) family of putative olfactory receptor proteins by Buck and Axel (1991) has opened the field to study using a wide array of molecular biological techniques. Some issues that may soon be resolved include the specificity and sensitivity of individual receptor molecules, the distribution of receptor molecules on receptor neurons and over the surface of the olfactory epithelium, and the projection from the epithelium to the bulb. At this stage, one can certainly infer that the dimensionality of olfactory space is at least of the same order as the number of receptor molecules.

Many of these issues are relevant to this thesis. In the experimental study we have taken care to keep odorant concentrations at a low, constant level, so as to avoid some of the complications mentioned above. The broad tuning of individual receptor neurons was an integral part of our model of the olfactory epithelium, in the bulb simulation study.

Issues in olfactory receptor turnover.

Olfactory receptor neurons are unique among neurons of the mammalian nervous system in that they continually undergo turnover. This is probably related to the harsh chemical environment which they are exposed to. The average lifetime of a receptor neuron has been estimated to be approximately 30 days (Graziadei and Monti Graziadei 1979; but see Mackay-Sim and Kittel 1991); clearly this depends on environmental factors. There are also studies which indicate that the population of granule cells may also undergo renewal, but at a much slower rate (Altman 1972; Bayer 1983). The regrowth of olfactory neurons leads to many interesting regulatory and developmental questions. The most salient of these, with respect to the information processing in the olfactory bulb is: how is the representation of odorants preserved?

A conceptually simple mechanism by which this may be accomplished requires preservation of the status quo at two stages of the regeneration process. First, the parent stem cells must give rise to a

receptor neuron with the same odorant selectivity as its predecessor. Second, the axon of this new neuron must find its way to the same or to a functionally identical set of synapses in the olfactory bulb. The first condition may be met by a number of clonal mechanisms which may occur in the stem cell. The second condition poses some interesting problems in axonal guidance and specificity. Regrowth along pre-existing axons of the olfactory nerve is not likely to be a complete answer, since complete recovery of olfactory recognition can occur after chemical (Alberts and Galef 1971) and surgical (Alberts 1974) ablation of the entire receptor (and axon) population. For the same reason, selective termination based on activity patterns in the olfactory bulb cannot fully explain the regeneration of appropriate synapses, since complete ablation would eliminate the requisite ordered activity patterns.

Some aspects of regrowth guidance may be explained by the presence of a number of molecular markers for various subpopulations of olfactory nerve axons, with correspondingly delimited target regions in the olfactory bulb. Markers identified so far include carbohydrate epitopes, lectins, and membrane proteins (reviewed in Mori 1993). Although increasing numbers of such localized markers are being identified, they are not likely to be a complete explanation for regrowth specificity. One difficulty is the sheer number of olfactory receptor types. Experiments involving ablation of part of the bulb, mentioned previously, also pose problems for any mechanism relying solely on pre-existing chemical markers.

Variations on the above general idea of receptor guidance have been proposed. In particular, a slightly more sophisticated axonal guidance mechanism would eliminate the need for clonally identical replacement neurons during turnover. The selectivity of the receptors themselves could be sufficient to determine their final target glomeruli.

A completely different mechanism for maintaining response specificity may be proposed, which assumes a distributed representation of olfactory information in the bulb and piriform. This mechanism relies on relationships within the olfactory stimuli themselves to uniquely identify them, and therefore could tolerate a large amount of variability in the spatial patterns of regrowth. The role of the bulb and piriform cortex in such a context would be to identify such relationships. This sort of processing has been

studied in artificial neural networks of various kinds, notably back-propagation and auto-associative memories (Rumelhart and McClelland 1988). These networks display a considerable amount of robustness both in categorizing novel stimuli, and when damaged. It is not clear if real olfactory stimuli could be categorized in such a manner. Furthermore, this mechanism fails to account for the observed topographical features of the olfactory representation.

A striking observation, whose significance in this context is unclear, is that regenerating olfactory axons are capable of inducing ectopic formation of glomeruli in other brain structures. When the entire olfactory bulb is ablated, and the olfactory nerve is forced to regrow into the piriform and anterior cortex, glomeruli are formed at these inappropriate targets (Monti-Graziadei and Graziadei 1987). There are indications that these structures may even be functional. The converse side of this ability of olfactory axons to induce the formation of glomeruli is their dependence on them for survival (Alberts 1974). Clearly, the role of the incoming axons is more complex than to simply locate an appropriate termination site.

Many of these issues, particularly those dealing with targeting and molecular markers, are being addressed though the use of molecular biological techniques (Mori 1993). The familiar question of distributed vs. topographic representation also bears on the mechanisms involved in olfactory axonal regrowth.

In the behavioral experiments that supplement the recording study, we directly induce a mass olfactory turnover in the form of chemical ablation of the bulb. The time for recovery is consistent with the turnover periods previously reported. Our longest recordings were not quite long enough to be able to directly address issues of mitral cell tuning on the time scale of receptor turnover, and this would be an interesting issue for further study.

Issues in topography - projections.

A topic closely related to the issues of turnover above concerns the actual patterns of interconnectivity being maintained. Both the epithelial - bulbar projection (via the olfactory nerve) and the

bulbar - piriform projection (via the lateral olfactory tract) are non-topographic in the strict one-to-one, spatially organized sense (Mori 1993; Haberly and Price 1977). A range of specificity is seen in the projection from the olfactory epithelium to the bulb (Mori 1993, Shepherd 1993). This range of specificities has led to conflicting interpretations regarding the existence or lack of spatial organization. For example, the dorsal regions of the bulb tend to receive more organized projections than the ventral (Shepherd 1993). The accessory olfactory bulb, which is related to the pheromonic system, receives a number of specific projections (Mori 1993). Additional confusion arises from the difference between microsmatic (salamander, turtle, etc.) and macrosmatic (mammals) olfactory bulbs. In microsmatic animals, the number of glomeruli is much smaller (~ 50) and the projections much more diffuse than in the macrosmatic animals (~2000 glomeruli).

Similar disagreements in interpretation enliven accounts of the projection from bulb to piriform cortex. This has been reported to be almost completely diffuse (Haberly and Price 1977). More recent studies (Buonviso et al. 1991) indicate, however, that some of the fine details of the projection, such as the projections of neighboring mitral cells, may be more organized.

Our modeling study addresses some aspects of the epithelial-bulbar projection. We find that within the scale of the model, even a completely random projection is capable of producing results close to those from our recording experiments. This greatly relaxes requirements for specificity of projection in the real system. On a small scale, therefore, the projections may indeed be quite random, but over the bulb as a whole there may be some general constraints on the organization of this projection.

Issues in topography - mapping stimulus space.

Given the multidimensional nature of the olfactory stimulus, and the essentially two-dimensional layout of neural circuitry, it is not surprising that olfactory stimuli are not represented by the straightforward topographic mappings familiar in the visual, auditory and somatosensory systems. Any representation of a multidimensional space onto a biologically constrained two-dimensional surface must at best be patchy. This does not preclude some degree of organization to these mappings, and this issue is

under active investigation. As we have already seen, a recurring theme in olfactory research is the difference in interpretation of results relating to spatial organization. Some authors emphasize topographic representations of odorants on the bulb (Lancet et al. 1982), while others favor a distributed representation (Slotnick et al. 1987; Monti Graziadei, A. G., and Graziadei 1987). There is evidence for both viewpoints.

Some of the strongest evidence for a spatial map of odor space onto the bulb comes from 2-deoxyglucose studies, which reveal preferential activity in small clusters of glomeruli upon stimulation with specific odorants (Lancet et al. 1982). These patterns are fairly consistent between animals. These results are confounded, however, by experiments where large fractions of the bulb are ablated, including the putative glomeruli responding to a specific odorant, without loss of the ability to recognize the odorant (Slotnick et al. 1987).

Electrophysiological evidence can be cited both for spatially organized and for distributed encoding of olfactory information. Experiments since the 1950s (Adrian 1950) have indicated that there clearly is some spatial organization to the responses of olfactory bulb neurons. This result has been well established using a wide array of techniques, including multi-unit recordings (Adrian 1950), EEG studies (Freeman and Grajski 1987), single-unit recordings (Meredith 1986, Mori et al. 1992), multielectrode recordings (Buonviso et al. 1992, Chapter 4), and optical recordings (Kauer 1988; Cinelli and Salzberg 1992). The consensus from these experiments favors a fairly stable mapping, consistent between animals within a species, of responses in the bulb to odorant stimuli. On the other hand, there is ample evidence for individual mitral cells in the bulb responding to many odorants, typically 1/3 to 1/4 of all the odorants presented out of a large sample (Duchamp-Viret 1990). Conversely, about 1/3 to 1/4 of the mitral cells tend to respond to any particular odorant. This clearly points to an overlapping, distributed representation, where information pertaining to a particular odorant is carried over a substantial proportion of the neurons in the bulb. A further complicating factor is the observation over short time scales (under 10 min) that individual mitral cells display some variability in their responses to odorants (Chaput and

Holley 1985, Macrides and Chorover 1972). The key to combining all these observations into a unified picture is to quantify the degree of spatial organization, of response specificity, and of variability.

In our experimental study we have taken pains to quantify the temporal and spatial aspects of bulbar response. We find that instead of extremes of specific or distributed representations, the responses appear to lie along a smooth continuum, with examples for both extremes. For example, some neurons will respond very consistently over time, and others vary considerably. Similarly, we also observe a strong spatial organization of responses, but this can be maintained even when individual neurons are responding differently. The bulb modeling study takes this result a step further and suggests that the spatial organization may in part emerge from activity-based interactions between neurons, and in part be 'hard wired' in the form of specific connectivity.

Issues related to behavioral context of responses.

The dependence of olfactory perception on behavioral context has been noted above. This is an issue that has largely been avoided in the literature, simply because most studies have been performed in anesthetized preparations. In studies which have been carried out in awake animals, there have been a few suggestive results indicating state-dependent responses in the bulb. In general, this is an issue that complicates responses and has therefore received less attention.

EEG responses in the bulb have previously been shown to depend on behavioral state of the animal. For example, differences in EEG spatial patterns have been seen depending on odorant and also on behavioral outcome of trials in classical conditioning (Freeman and Grajski 1987). While the main effort in these studies has been to find odor-specific spatial patterns, it has been shown that such patterns fail to arise in the absence of reinforcement. Temporal differences in field potentials have also been reported depending on the degree of familiarity with the set of odorants (Gray and Skinner 1988a). A particularly elegant demonstration of centrifugal modulation of EEG and single unit activity in the bulb was carried out by Gray and Skinner (Gray and Skinner 1988b). They used cooling probes to reversibly block

transmission through the olfactory peduncle in awake rabbits. The effect of blockage was to increase regularity of firing and decrease variability in the EEG patterns.

Multiunit recordings on rats have revealed differences in response to food odors depending on whether the animals were satiated or hungry (Pager 1978). Furthermore, these changes were shown to be dependent on centrifugal feedback by comparing responses with animals whose LOT had been lesioned. Single unit comparisons made between the same neuron recorded during conscious and anesthetized states (Chaput and Holley 1979) have demonstrated changes in temporal firing patterns.

There is an intriguing correspondence between these results and our hypothesis of multiple modes of bulbar processing. Our results relate to features that characterize a mode of processing, rather than to individual odors. Taken in conjunction with our results on variability of individual neurons, we propose that there may be several such processing modes in the bulb. It seems likely that the above cases are specific examples of different modes of processing, for example, selectivity for odorants in relation to conditioning and nutritional state. The bulb may therefore be reorganizing its processing attributes to optimize for different tasks depending on context.

Simulation context of this study.

This introduction has outlined a large body of knowledge and many lines of experimental investigation relating to olfaction and the olfactory bulb. Computer simulations provide a complementary approach, which combines the investigative aspects of these studies with the integrative methods of theoretical study. The investigative angle comes from the ability of simulations to raise questions and suggest avenues for further study. The integrative angle is inherent to simulations with any significant amount of realism, since a great deal of experimental information must be incorporated into an accurate model. The tightening of the interaction between experiment and theory, embodied in simulations, is likely to be a major driving force in neurobiological studies in the coming years.

Neural computer simulations have been carried out at many levels of detail, from single molecules to abstract models of entire sensory modalities. While it is likely that processes occurring at all

these levels are relevant for understanding the behavior of neural systems (Churchland and Sejnowski 1988), the level of detail ranging from single-cells to small networks is most suited to addressing biological questions at the present time. This is because of the many constraints on constructing a useful model: what is known about the system; what one wishes to learn; what one needs to know in order to set up a good model; the availability of simulation techniques; the computer requirements; and so on. At this time these constraints are best met at the single-cell modeling level.

The physical underpinnings of neural activity are relatively well understood at the level of detail pertaining to single neurons. Almost all neuronal simulations at the present time utilize a few basic physical descriptions: the cable equations (devised by Lord Kelvin) for describing the passive electrical properties, the ionic equilibrium descriptions (Goldman-Hodgkin-Katz, Nernst); the Hodgkin-Huxley or similar equations for describing voltage-dependent channels; and sometimes simple physical models of diffusion. With the addition of models for the synapse (a simple alpha-function is adequate for most non-modifiable synapses), one can in principle begin to model networks as well.

It has been known for nearly four decades that these simple physical models can model real single neuron behavior to a high degree of accuracy (Rall 1964; Cooley and Dodge 1966). In recent years developments in numerical techniques (Hines 1984; Mascagni 1989) and in computing hardware have made the basic calculations relatively easy to carry out. This has brought more attention to the experimental information required to make valid models, and this is the major bottleneck in devising single cell simulations at the present time. As we discuss in Chapter 3, parameter search techniques offer means for simplifying this aspect of the simulation process as well.

The detailed simulation of larger systems of neurons has proven more difficult both from the parameter specification and from the methods and resources points of view. For this reason, network models have tended to be more abstract and to gloss over biological details. There are a few notable exceptions to this. A growing number of pattern generating networks have benefited both from extensive study and the relatively small size of the networks. This has resulted in the development of a number of detailed models of such pattern generators (reviewed in Harriswarrick and Marder 1991). Among

mammalian central nervous system structures, a few systems have the requisite combination of relative simplicity and extensive physiological characterization. Perhaps the first such system to be modeled with a substantial amount of biological detail was the olfactory bulb (Rall and Shepherd 1968). Since then the bulb has been the subject of a large number of modeling studies at various levels of detail, which will be discussed later. More recently, the hippocampus has been modeled in careful detail by Traub and co-workers (e.g., Traub, Miles, and Wong 1989). The piriform cortex is another structure where detailed models have been constructed (Wilson and Bower 1992). Many other parts of the mammalian nervous system such as the cerebellum, visual system, and auditory system are now becoming amenable to the modeling approach, as experimental information and simulation techniques reach the point where realistic models can be constructed.

In the course of this project, we have developed Genesis as our simulation tool (Wilson et al. 1989; Chapter 1). It has become widely used by other researchers as well. Our simulation efforts have introduced new techniques to the field, such as the parameter search methods discussed in Chapter 3. As a technical achievement, the bulb model is the first detailed network simulation to have been implemented on a parallel machine. At a more fundamental level, our study establishes an especially close link between simulation and experiment. We are able to relate high-level issues, such as spatial encoding, to the details of single-cell properties, for example the propagation of spikes into mitral cell secondary dendrites. Our approach to the study of the brain is to try to close the loop between model and experiment, so that each contributes to the development of the other.

REFERENCES

ADRIAN, E.D. Sensory discrimination with some recent evidence from the olfactory organ. *Br. Med. Bull.* 6:330-331, 1950.

ALBERTS, J.R., AND GALEF, B. G., JR. Acute anosmia in the rat: a behavioral test of a peripherally induced olfactory deficit. *Physiol. Behav.* 6:619-621, 1971.

ALBERTS, J.R. Producing and interpreting experimental olfactory deficits. *Physiol. Behav.* 12:657-670, 1974.

ALTMAN, J. Autoradiographic and histological studies of postnatal neurogenesis IV. Cell proliferation and migration in the anterior forebrain, with special reference to persisting neurogenesis in the olfactory bulb. *J. Comp. Neurol.* 137: 433-458, 1972

BAYER, S. A. 3H-thymidine-radiographic studies of neurogenesis in the rat olfactory bulb *Exp. Brain Res.* 50: 329-340, 1983.

BREER, H., AND SHEPHERD, G.M. Implications of the NO/cGMP system for olfaction. *TINS* 16:5-9, 1993.

BUCK, L., AND AXEL, R. A novel multigene family may encode odorant receptors: a molecular basis for odor recognition. *Cell* 65: 175-187, 1991.

BUFLER, J., ZUFALL, F., FRANKE, C., AND HATT, H. Patch clamp recordings of spiking and nonspiking interneurons from rabbit olfactory bulb slices: Membrane properties and ionic currents. *J. Comp. Physiol.* 170: 145-152, 1992 a.

BUFLER, J., ZUFALL, F., FRANKE, C., AND HATT, H. Patch clamp recordings of spiking and nonspiking interneurons from rabbit olfactory bulb slices: GABA and other transmitter receptors. *J. Comp. Physiol.* 170: 153-159, 1992 b.

BUONVISO, N., CHAPUT, M. A., AND BERTHOMMIER, F. Temporal pattern analyses in pairs of neighboring mitral cells. *J. Neurophysiol.* 68: 417-424, 1992.

BUONVISO, N., REVIAL, M.F., AND JOURDAN, F. The projections of mitral cells from small local regions of the olfactory bulb: an anterograde tracing study using PHA-(Phaseolus vulgaris Leucoagglutinin). *Eur. J. Neurosci.* 3: 493-500, 1991.

CHAPUT, M. A., AND HOLLEY, A. Spontaneous activity of olfactory bulb neurons in awake rabbits with some observations on the effects of pentobarbitol anaesthesia. *J. Physiol. Paris* 75: 939-948, 1979.

CHAPUT, M. A., AND HOLLEY, A. Responses of olfactory bulb neurons to repeated odor stimulations in awake freely-breathing rabbits. *Physiol. and Behav.* 34: 249-258, 1985.

CHURCHLAND, P.S., AND SEJNOWSKI, T.J. Perspectives on cognitive neuroscience. *Science* 242:741-745, 1988.

CINELLI, A. R., AND SALZBERG, B. M. Dendritic origin of late events in optical recordings from salamander olfactory bulb evoked field potentials from salamander olfactory bulb. *J. Neurophysiol.* 68: 786-806, 1992.

COOLEY, J. W., AND DODGE, F. A. Digital computer solutions for excitation and propagation of the nerve impulse. *Biophys J.* 6: 583-599, 1966.

DUCHAMP-VIRET, P., DUCHAMP, A., AND SICARD, G. Olfactory discrimination over a wide concentration range. Comparison of receptor cell and bulb neuron properties. *Brain Res.* 517: 256-262, 1990.

FREEMAN, W.J., AND GRAJSKI, K.A. Relation of olfactory EEG to behavior: Factor Analysis *Behav. Neurosci.* 101: 766-777, 1987.

GRAY, C.M., AND SKINNER, J.E. Field potential response changes in the rabbit olfactory bulb accompany behavioral habituation during the repeated presentation of unreinforced odors. *Exp. Brain Res.* 73: 189-197, 1988a.

GRAY, C.M., AND SKINNER, J.E. Centrifugal regulation of neuronal activity in the

olfactory bulb of the waking rabbit as revealed by cryogenic blockade. *Exp. Brain Res.* 69: 378-386, 1988b.

GRAZIADEI, P.P.C., AND MONTI GRAZIADEI, A.G. Neurogenesis and neuron regeneration in the olfactory system of mammals. I. Morphological aspects of differentiation and structural organization of the olfactory sensory neurons. *J. Neurocytol.*, 8:1-18, 1979.

HABERLY, L. B., AND PRICE, J. L. The axonal projection patterns of the mitral and tufted cells of the olfactory bulb in the rat. *Brain Res.* 129: 152-157, 1977.

HANSSON, B. S., LJUNGBERG, H., HALLBERG, E., AND LOFSTEDT, C. Functional specialization of olfactory glomeruli in a moth. *Science* 256: 1313-1315, 1992.

HARRISWARRICK, R.M., AND MARDER, E. Modulation of neural networks for behavior. *Ann. Rev. Neur.* 14:39-57, 1991.

HINES, M. Efficient computation of branched nerve equations. *Int. J. Bio-Medical Computing.* 15: 69-76, 1984.

HUBEL, D.H., AND WIESEL, T.N. Receptive fields, binocular interaction and functional architecture in the cat's visual cortex. *J. Physiol.* 160:106-154, 1962.

HUBEL, D.H., AND WIESEL, T.N. Receptive fields and functional architecture of monkey striate cortex. *J. Physiol.* 195: 215-243, 1968.

KAUER, J. S. Real-time imaging of evoked activity in local circuits of salamander olfactory bulb. *Nature* 331: 166, 1988.

KHAYARI, A., MATH, F., AND DAVRAINVILLE J.L. Electrical stimulation of primary olfactory nerve induces two types of variation in the extracellular potassium activity within the glomerulus of the rat olfactory bulb. *Brain Res.* 457: 188-191, 1988.

LANCET, D., GREER, C.A., KAUER, J. S., AND SHEPHERD, G. M. Mapping of odor-related neuronal activity in the olfactory bulb by high-resolution 2-deoxyglucose autoradiography. *Proc. Natl. Acad. Sci.* 79: 670-674, 1982.

MACKAY-SIM, A., AND KITTEL, P.W. On the life span of olfactory receptor neurons. *Eur J Neurosci.* 3: 209-215, 1991.

MACRIDES, F., AND CHOROVER, S.L. Olfactory bulb units: activity correlated with inhalation cycles and odor quality. *Science* 175: 84-87, 1972.

MARTINEZ, D.P., AND FREEMAN, W.J. Periglomerular cell action on mitral cells in olfactory bulb shown by current source density analysis. *Brain Res.* 308:223-233, 1984.

MASCAGNI, M. Numerical methods for neuronal modeling. In: *Methods in Neuronal Modeling: from Synapses to Networks.* Edited by C. Koch and I. Segev, Cambridge. MIT Press, 1989, p. 439-484.

MEREDITH, M. Patterned response to odor in mammalian olfactory bulb: the influence of intensity. *J. Neurophysiol.* 56: 572-597, 1986.

MEREDITH, M. Sensory processing in the main and olfactory systems: comparisons and contrasts. *J. Steroid Biochem. Molec. Biol.* 39: 601-614, 1991.

MONTI GRAZIADEI, A. G., AND GRAZIADEI, P.P.C. Sensory reinnervation after partial removal of the olfactory bulb. *J. Comp. Neurol.* 257: 442-452, 1987.

MORI, K. Membrane and synaptic properties of identified neurons in the olfactory bulb. *Progress in Neurobio.* 29: 275-320, 1987.

MORI, K., KISHI, K., AND OJIMA, H. Distribution of dendrites of mitral, displaced mitral, tufted, and granule cells in the rabbit olfactory bulb. *J. Comp. Neurol.* 219: 339-355, 1983.

MORI, K., MATAGA, N., AND IMAMURA, K. Differential specificities of single mitral cells in rabbit olfactory bulb from a homologous series of fatty acid odor molecules. *J. Neurophysiol.* 67: 786-789,1992.

MORI, K., NOWYCKY, M. C., AND SHEPHERD, G. M. Electrophysiological analysis of mitral cells in the isolated turtle olfactory bulb. *J. Physiol. Lond.* 314: 281-294, 1981.

MORI, K. Molecular and cellular properties of mammalian primary olfactory axons. *Micr. Res. and Tech.* 24: 131-141, 1993.

PAGER, J. Ascending olfactory information and centrifugal influxes contributing to a nutritional modulation of the rat mitral cell responses. *Brain Res.* 140: 251-269, 1978.

PATNEAU, D. K., AND STRIPLING, J. S. *Brain Res.* Functional correlates of selective long-term potentiation in the olfactory cortex and olfactory bulb. 585: 219-228, 1992.

PHILIPS, C.G., POWELL, T.P.S., AND SHEPHERD, G.M. Responses of mitral cells to stimulation of the lateral olfactory tract of the rabbit. *J. Physiol. Lond.* 168:65-88, 1963.

PINCHING, A.J., AND POWELL, T.P.S. The neuropil of the glomeruli of the olfactory bulb. *J. Cell Sci.* 9: 347-377, 1971a.

PINCHING, A.J., AND POWELL, T.P.S. The neuropil of the periglomerular region of the olfactory bulb. *J. Cell Sci.* 9: 379-409, 1971b.

PRICE, J.L., AND POWELL, T.P.S. The synaptology of the granule cells of the olfactory bulb. *J. Cell Sci.* 7: 125-155 , 1970.

RALL, W. Theoretical significance of dendritic trees for neuronal input-output relations. In: *Neural theory and modeling.* Edited by R. Reiss Stanford. Stanford University Press, 1964, p. 73-97.

RALL, W., AND SHEPHERD, G.M. Theoretical reconstruction of field potentials and dendrodendritic synaptic interactions in olfactory bulb. *J. Neurophysiol.* 31:884-915, 1968.

RUMELHART, D.E., AND MCCLELLAND, J.L. *Parallel distributed processing. Explorations in the microstructure of cognition.* MIT Press, Cambridge, MA. 1988.

SHEPHERD, G.M. *The synaptic organization of the brain. 2nd edn.* OUP, Oxford. 1979.

SHEPHERD, G. M. Principles of specificity and redundancy underlying the organization of the olfactory system. *Micr. Res. and Tech.* 24:106-112, 1993.

SICARD, G., AND HOLLEY, A. Receptor cell responses to odorants: similarities and differences among odorants. *Brain Res.* 292: 283-296, 1984.

SLOTNICK, B.M., GRAHAM, S., LAING, D.G. AND BELL, G.A. Detection of propionic acid vapor by rats with lesions of olfactory bulb areas associated with high 2-DG uptake. *Brain Res.* 417: 343-346, 1987.

SLOTNICK, B.M., KUFERA, A., AND SILBERBERG, A.M. Olfactory learning and odor memory in the rat. *Physiol. and Behav.* 50: 555-561, 1991.

STAUBLI, U., FRASER, D., FARADAY, R., AND LYNCH, G. Olfaction and the 'data' memory system in rats. *Behav. Neurosci.* 101:757-765, 1987.

TRAUB, R.D., MILES, R., AND WONG, R.K.S. Model of the origin of rhythmic population oscillations in the hippocampal slice. *Science* 243:1319-1325, 1989.

TROMBLEY, P.Q., AND SHEPHERD, G.M. Noradrenergic inhibition of synaptic transmission between mitral and granule cells in mammalian olfactory bulb cultures. *J. Neurosci.* 12(10): 3985-3991, 1992.

VINCENT, S.R., AND KIMURA, H. Histochemical mapping of Nitric Oxide synthase in the rat brain. *Neuroscience* 46: 755-784, 1992.

WELLIS, D. P., AND SCOTT, J. W. Intracellular Responses of Identified Rat Olfactory Bulb Interneurons to Electrical and Odor Stimulation. *J. Neurophysiol.* 64: 932-947, 1990.

WILSON, M. A., BHALLA, U. S., UHLEY, J. D., AND BOWER, J. M. Genesis: A system for simulating neural networks. In: *Advances in Neural information processing systems, Vol 1*. Edited by D. Touretzky. San Mateo, Morgan Kaufman Publishers, 1989, p. 485-492.

WILSON, M., AND BOWER, J. M. Cortical oscillations and temporal interactions in a computer simulation of piriform cortex. *J. Neurophysiol.* 67(4): 981-995, 1992.

SECTION 1. MODELING.

This section describes the development of the basic simulation techniques used in this project and their application to an effort to model single neurons in the olfactory bulb. Chapter 1 (published in Neural systems: Analysis and modeling, ed. Eeckman, F.H. Kluwer, Norwell 1993) is an overview of the simulator developed in our lab. The development of Genesis is a large and ongoing project to which many individuals have contributed, notably Dr. Matthew Wilson (Wilson et al. 1989). The main contributions of the author include writing the graphical user interface (Xodus), the development of single cell modeling techniques in Genesis, parallelizing Genesis, and developing parameter search techniques as described in Chapter 3.

An important component of the development effort in Genesis was the validation of the numerical techniques used. Chapter 2 (published in Trends in Neurosciences, 15:453-458 1992) resulted partly from our efforts to confirm the numerical accuracy and reliability of Genesis. The development of a suite of benchmarks has implications beyond our own work, since a common standard for simulators is valuable for the community of simulator developers and users as a whole. This set of benchmarks has the additional benefit of allowing one to predict the computational resources required to obtain a desired accuracy in a particular simulation.

Chapter 3, accepted for publication in the Journal of Neurophysiology, describes the development of a set of models of cell types in the olfactory bulb. This part of the thesis work involved the development of techniques for systematically searching parameter space to obtain the best match of model to experiment. Beyond the intrinsic interest of the cell models on their own, these were essential components of the detailed model of the olfactory bulb (Chapter 5).

Genesis : a neuronal simulation system.

Upinder S. Bhalla and James M. Bower

Division of Biology

California Institute of Technology

Pasadena, CA 91125

Introduction

The use of numerical simulation techniques to study neurobiology has grown over the past few years to encompass systems ranging from molecular level processes occurring in real neurons to systems of many thousands of highly abstract neuron-like elements (Touretzky, 1990, Koch and Segev, 1989; Zornetzer et al 1990). It is increasingly apparent that all these levels of analysis are interrelated and may be essential to the understanding of the functioning of the nervous system (Bower, 1991)

In principle, numerical simulation techniques can provide a means of performing an analysis of neurobiological structure / function relationships over many levels of biological investigation. Such an effort is likely to benefit from the availability of a simulation environment capable of representing neurobiological assemblies at levels of detail ranging from molecules to complete systems. This is one of the principal design objectives of the GENESIS system.

Design Philosophy.

We have developed Genesis (GEneral NEuronal SImulation System) and its graphical interface Xodus (X-based Output and Display Utility for Simulators) primarily as a means of constructing biologically realistic neuronal simulations. There are three basic elements of our design philosophy. One, the simulator must be capable of addressing problems at many levels of detail. Two, the system should facilitate communication between groups working on many kinds of modeling problems. Three, the system should be open-ended : it should not place limits on the kinds of problems that can be addressed

and should allow the incorporation of user extensions. The following specific features of the system have evolved based on these criteria.

Modular Design.

As a key principle conferring both flexibility and organization on Genesis, a highly object-oriented programming approach has been adopted. Simulations are constructed of 'building blocks' or modules, each of which perform well-defined functions and have standardized means for communicating with each other. The level of detail of a simulation is then determined by the nature of the building blocks one chooses. For example, one could use more realistic (and computationally expensive) Hodgkin-Huxley type conductances to describe the spiking properties of a neuron, or just simple threshold elements. The user has complete freedom to assemble a model with any set of modules, so the system does not constrain the kind of simulation developed. Object-oriented design also enables the user to easily add new modules to extend Genesis for a particular application.

Flexible interface.

The Genesis user interface consists of two parts. The underlying level is the Script Language Interface, or SLI. This is an interpretive programming language similar to the UNIX shell, with an extensive set of commands related to building simulations. The interpreter can read SLI programs (scripts) either interactively from the keyboard, or from files.

The graphical interface, Xodus, provides a higher level and user-friendly means for developing simulations and monitoring their execution. Xodus consists of a set of graphical modules which are exactly the same as the computational modules from the user's point of view, except that they perform graphical functions. Like the computational modules, Xodus modules can be set up in any manner that the user chooses to display or enter data. Furthermore, the graphical modules can call functions from the script language, so the full power of the SLI is available through the graphical interface.

These two aspects of the Genesis user interface give the user complete freedom to specify the structure of a simulation, including graphical input and output.

Device independence.

In order to make the simulator portable and available to the maximum number of users, the system has been designed to run under UNIX and X-windows. The code has been tested on a number of machine architectures. This facilitates communication by enabling groups utilizing different machines to run each other's simulations. A parallellized implementation is also being developed with the objective of extending the range of problems which Genesis can address.

Using Genesis.

The user interacts with Genesis at a number of levels.

Simulation Library.

Each registered GENESIS user has access to a library containing demonstration simulations, tutorials, and high level simulation tools. These completed simulations are manipulable through a user-friendly graphical interface without any need for interaction with the GENESIS scripting language. The demonstration simulations are intended to illustrate the range diversity of simulations that can be carried out in Genesis. They also provide starting points for the design of new simulations. Tutorials are simulations specifically designed to introduce students to fundamental concepts, and classical models, in computational neurobiology. These tutorials are currently being used in a number of graduate and undergraduate training programs in computational neurobiology (Beeman and Bower, 1991). Some tutorials also serve to introduce new GENESIS users to the structure of the scripting language. Finally, the simulation tools are complete interfaces for developing new research simulations. One of the most useful tools is "neurokit", which provides an environment for developing, editing, and testing multicompartment models of single neurons.

Prototype library.

At a slightly greater stage of sophistication, one can develop simulations using the script language directly. Such new simulation development takes advantage of the simulation component prototypes in the extensive and growing library of ion channels, cellular compartments, whole neurons,

and even networks. These prototypes are genesis modules, or assemblies thereof, which have already through use in other simulations, been assigned appropriate parameters.

Implementing new prototypes.

At the next level of interaction with GENESIS, users can implement new prototypes by collecting data from the literature or their own experiments and assigning these parameters to the appropriate pre-existing computational elements.

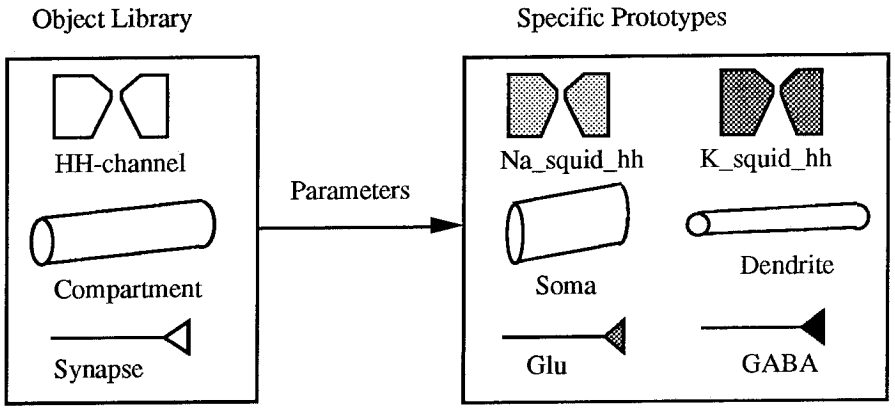

Figure 1. Implementing new prototypes.

Implementing new modules.

Finally, the most advanced level of interaction with GENESIS involves the construction of new modules to perform new computational tasks. This interaction with the simulator is the only level that requires advanced programming skills. However, the object-oriented nature of Genesis means that only a few basic rules must be observed in writing new modules, to ensure that they mesh smoothly with existing GENESIS structure.

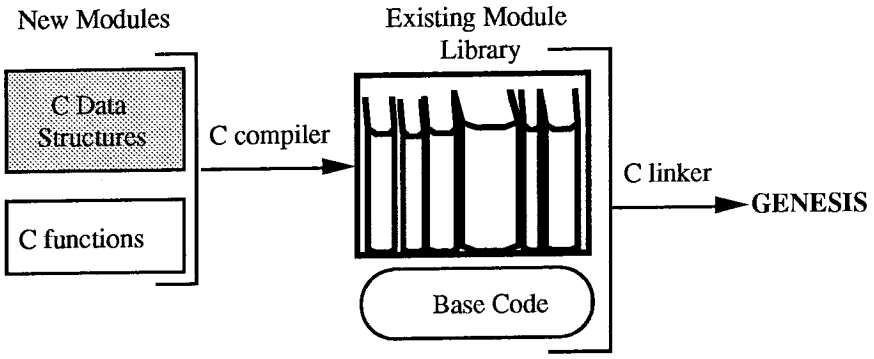

Figure 2. Implementing New Modules.

Users Group.

In order to support the continued development and use of GENESIS, we have established a active users group called Babel. The objective of the users group is to act as a simulation clearing house and to facilitate communications between groups doing neuronal modeling, using GENESIS. Accordingly, all serious users of GENESIS are encouraged to interact with the users group, to send their innovations and keep up with developments from other users. Babel makes extensive use of the internet for correspondence, support, and the distribution of new GENESIS related materials.

The structure of Genesis.

In the follow sections, we will briefly describe the overall structure of GENESIS. Readers who would like more information should address correspondence to the email address listed at the end of this article.

Base code.

All the housekeeping activities, allocation of memory and CPU resources, and maintenance of simulation state is handled by the base code. It also provides the most basic functions available in the Script Language.

Objects.

As we have stressed earlier, GENESIS is written in an object-oriented manner. The building blocks of all simulations within Genesis are objects, which we have loosely referred to as modules. In programming terms, an object is both the data structure associated with a module, and the numerical operations which that module carries out. An element is an actual instance of a Genesis object. Each element has its own memory area for storing state variables and parameters associated with it, and performs the numerical operations defined for the object.

Hierarchy.

The elements in Genesis are arranged in a UNIX directory-like hierarchy. This makes it very natural to group related elements together and provides a straightforward means for identifying each individual element.

Messages and connections.

Inter-element communications are performed in two ways. For instantaneous information transfer between elements, such as is needed for evaluating electrical properties for the integration routines, messages are used. For delayed transfer of information, as in spike propagation down an axon to a synapse, connections are used.

Simulation setup

As already alluded to, the Script Language Interface contains all the commands for setting up a simulation in genesis. A typical simulation might be set up in the following stages :

1 **Creating elements**

create compartment /soma

create hh_channel /soma/Na

create hh_channel /soma/K

2 **Assigning parameters**

set /soma Rm 1e7 *// Ohms*

set /soma Cm 0.01 *// Farads/m^2*

3 **Establishing inter-element communications**

sendmsg from /soma to /soma/Na VOLTAGE Vm

sendmsg from /soma/Na to /soma CHANNEL Ek Gk

4 **Setting up input/output**

create xform /form

create xgraph /form/graph

sendmsg from /soma to /form/graph PLOT Vm

5 **Running the simulation**

step 100

Single Neuron specification

One of the central functions of any neuronal simulator is the specification of multicompartmental models of single neurons. This process is greatly simplified in Genesis by the use of a special set of functions and tools. The most important of these is the cell-reader function. This Genesis utility reads a neuronal specification file which contains the geometry, branching structure, and channel distribution of a particular neuron. In association with "neurokit" (see above), this provides a

straightforward way for single neuron models to be made and tested with minimal knowledge of the details of GENESIS and the script language.

Numerical aspects.

The main numerical operation carried out by most objects in Genesis is numerical integration of time-varying state variables. In keeping with the object-oriented methodology, each element is responsible for updating its own variables. At the present time there are eleven integration methods available in Genesis, including Euler, Gear, Adams-Bashforth, Runge-Kutta, Backward Euler and Crank-Nicolson. All of these are intercompatible, so one can evaluate different methods using different integration schemes. The two implicit methods are based on the Hines algorithm (Hines, 1984), and are intrinsically non-object oriented and are available only to compartment and channel objects.

Input/Output.

Three interconvertible forms of IO are available in Genesis. The first is simply the script language, which can be used to explicitly set variables and have them printed out on the screen. The second in Xodus, the graphical interface. This is usually the main method for controlling and monitoring a simulation. It can also read output stored into files. The third option is file I/O. Typical file inputs are for stimulus patterns, cell parameters, and so on. File output can be used, for example to save the entire time history of a simulation. An additional I/O feature is the SAVE/RESTORE option, which can save the current state of a simulation to a file, for resumption later.

Libraries.

The development of Genesis as a multipurpose simulation tool has led to the establishment of libraries of components of the system, at different levels.

1 Code/object libraries. These are functions and objects developed for different simulations and projects. There are currently over 200 commands and over 50 different Genesis objects in the various code libraries.

2 Prototype libraries. These are simulation components such as voltage dependent channels, synapses, compartments and even complete neurons whose parameters have been worked out from experiments and the literature. They greatly simplify the task of developing new simulations.

3 Simulation libraries. These are complies simulations at a wide range of detail and complexity, providing a resource of examples and demonstrations of the use of Genesis.

Simulator Specifications.

Memory requirements

Genesis currently consists of about 45000 lines of simulator code and about 25000 lines of graphics code in Xodus. The size of the binaries are strongly machine dependent, varying from 1 to 2 Meg. The amount of additional memory needed for a particular simulation can be estimated from the size and number of modules in the simulation. Typically, elements use about 100 bytes, connections 16 and messages 20. Graphical elements use from 5 to 20 K each. In a typical simulation, messages and connections account for the bulk of the memory use.

Performance.

This varies roughly linearly with the number and type of elements in the simulation. As an example, a simulation of the olfactory bulb with 7 kinds of neuron having from 9 to 52 compartments and roughly 2 channels per compartment occupies 10 meg for a 400 cell model. On a Sun Sparc2 this simulation runs at about 1 second per time step.

Access/use of Genesis

A demonstration version of Genesis is freely available over the network by anonymous ftp from genesis.cns.caltech.edu. This includes a number of example simulations and full source for GENESIS.

Babel newsgroup.

Serious users of Genesis are encouraged to join the Babel newsgroup which provides access to the latest versions of Genesis, bugfixes, new simulations and libraries, and a forum for

interacting and exchanging simulations. Interested persons should contact Chris Ploegaert (cp@smaug.cns.caltech.edu).

Acknowledgements

Genesis was devised and brought into being principally by Matt Wilson. Many people have contributed to its development, and continue to do so. To acknowledge the contributions of a few of them: Dave Bilitch and Matt Wilson : the Script Language Interface; John Uhley : Xodus; Matt Wilson, Mark Nelson, Erik de Schutter and many others : the function and module libraries; Dave Beeman, Matt Wilson, Mark Nelson, Erik De Schutter, and several generations of students at the "Methods in Computational Neuroscience" course at the Marine Biological Laboratory, Woods Hole : the library of simulations, demos and tutorials; The National Science Foundation (DIR-9017153), Sun Microsystems Inc., Digital Equipment Corporation, Intel Corporation, and the Lockheed Corporation : financial support.

References

TOURETZKY, D. S. 1990 *Advances in neural information processing systems.* Morgan Kaufman.

KOCH, C. AND SEGEV, I. 1989 *Methods in Neuronal Modeling.* MIT Press.

ZORNETZER, S. F., DAVIS, J. L., AND LAU, C. 1990 *An Introduction to Neural and Electronic Networks.* Academic Press.

BOWER, J. M. 1991 *Piriform cortex and olfactory object recognition.* In: Olfaction as a Model System for Computational Neuroscience. Edited by J. Davis and H. Eichenbaum. MIT Press, Cambridge, MA. (in press).

BEEMAN, D. AND BOWER, J. M. *Soc Neurosci Abstr.* 1991.

HINES, M. Efficient computation of branched nerve equations. *Int J. Bio-Med. Comp.* 15:69-76, 1984.

Rallpacks : A set of benchmarks for neuronal simulators.

Upinder S. Bhalla, David H. Bilitch, James M. Bower.

Division of Biology, California Institute of Technology.

The field of computational neurobiology has advanced to the point where there are several general purpose simulators to choose from. These cater to various niches of the world of realistic neuronal models, ranging from the molecular level to descriptions of entire sensory modalities. In addition, there are numerous custom designed simulations, adaptations of electrical circuit simulators, and other specific implementations of neurobiological models. As a first step towards evaluating this disparate set of simulators and simulations, and towards establishing standards for comparisons of speed and accuracy, we describe a set of benchmarks. These have been given the name 'Rallpacks', in honor of Wilfrid Rall who pioneered the study of neuronal systems through analytical and numerical techniques.

History

Numerical methods for computing the properties of neuronal models have existed at least since the 19th century, when Lord Kelvin first studied the equations describing signal propagation for the first undersea cables. This problem is mathematically identical to the description of the passive properties of cellular membranes, and the *cable equations* underlie all realistic neuronal models. The description of active properties of membranes by Hodkin and Huxley[1] in the 1950s was the second major conceptual advance in the field. Even the most sophisticated simulations carried out today are essentially implementations, in greater and greater detail, of the formulation of neurons in terms of these passive and active properties. The application of these equations to neuronal systems was undertaken from the 50's onward, notably by Wilfrid Rall[2].

Levels of description.

Neuronal systems have features of interest and functional significance at all the levels of detail that have been studied[3], from the molecular to the systems level. An especially keenly studied section of this field has been the single neuron level, which has consequently seen a proliferation of simulations and simulators[4,5] The present set of Rallpacks are intended to provide a standard for evaluation of the basic numerical capabilities of this disparate variety of simulators at the single neuron level, and to provide a degree of confidence in the reproducibility of simulations carried out on them.

What simulators do.

As alluded to above, realistic single neuron simulators must at least solve the equations describing the passive and active properties of neurons. A brief overview of this process follows.

Passive Properties

The passive cable equations are partial differential equations, and may be expressed as

$$\lambda^2(\partial^2 V/\partial x^2) - V - \tau(\partial V/\partial t)=0$$

where λ is the cable length constant and τ is the time constant.

Several methods may be employed in solving these[6], including Laplace transforms and discretization in space and time. The latter is the method of choice for almost all neuronal simulators. Briefly, it may be thought of as a process of subdividing the description of the model in space and in time, so that values calculated for discrete positions and times may be used to approximate the real, smoothly varying system. The process of spatial discretization is accomplished by dividing the neuronal model in to *compartments* , which are simply short cylindrical lengths of cell membrane of uniform diameter and electrical properties. The problem is then reduced to a system of coupled ordinary differential equations which may be solved by any of a large number of numerical integration techniques, which carry out the discretization in time. There are two main classes of numerical integration methods applicable to compartmental models: *explicit* and *implicit* integration schemes. These bear strongly on the numerical stability of the model. Explicit methods are conceptually simpler, but suffer from the drawback that as one improves the spatial discretization (i.e., makes the compartments smaller) one has to use much smaller time steps to

retain numerical stability. Implicit methods are more complex, but are always stable. This permits the use of longer and fewer timesteps in the solution. A scheme developed by Hines[7] for evaluating the implicit solutions in a time linearly proportional to the number of compartments makes this highly preferable for neuronal simulators, many of which now incorporate Hines' method.

Active Properties

A number of alternative schemes have been employed for describing active behaviour of neuronal models. Among these are the FitzHugh-Nagumo[8,9] systems of reduced equations which embody the behaviour of all the channels in a single set of equations; and simple integrate-and-fire models, where a depolarization above a threshold causes firing and resetting of the neuronal potential. The most common description of active properties is the Hodgkin-Huxley[1] formalsm (Box 1). It has been pointed out[10] that this formalism is inadequate in describing the detailed behaviour of many kinds of channels as they are now understood. Despite these considerations, the capability to model active Hodgkin-Huxley type channels is *de rigeur* for realistic single neuron simulators.

The Hodgkin-Huxley description naturally lends itself to spatial discretization in small equipotential compartments, as pioneered by Cooley and Dodge[11]. The highly nonlinear Hodgkin-Huxley equations contribute to the linear cable equations only in the conductance terms, leading to a system of conditionally linear equations which are amenable to the same numerical methods described above.

Other capabilities.

Most simulators provide the capability to do far more than the minimal set described above. Typical numerical capabilities include calcium dynamics, Calcium-dependent ion channels, Nernst potentials, synaptic input using alpha functions, and synaptic learning. From the user's perspective, the non-numerical capabilities such as interfaces and flexibility are often an even more important component of a simulator. These features are discussed elsewhere in this issue[5]. Our evaluation of the basic numerical capabilities of simulators will be confined to passive properties and the computation of the Hodgkin-Huxley equations.

The Rallpack suite.

The Rallpacks are primarily intended to objectively evaluate simulator performance on measures such as speed and accuracy. The performance information generated in this way also provides a means for making informed decisions on model parameters such as size and timestep which are constrained by accuracy requirements and computer time and memory limitations.

The components of these benchmarks include :

The establishment of standard computational tasks

The provision of utilities and references for the model output.

The definition of performance measures and a set of conditions for

which measurements are to be taken.

Specification of the format of the report on the simulator.

Computational tasks.

The computational tasks set by the Rallpacks are simulations which address different aspects of modeling calculations. The three models currently comprising the Rallpacks are :

Rallpack 1 : Linear cable model

Rallpack 2 : Branched cable model

Rallpack 3 : Linear axon model.

These are specified in detail in Box 1.

The choice of this set of basic simulations for the benchmarks is determined by their relevance to the classes of model most commonly studied at the present time and by the availability of analytical and/or thoroughly investigated solutions. This set will be extended in the future as simulator capabilities broaden.

The linear cable model in Rallpack 1 tests the most basic ability of a simulator to model a uniform unbranched cable. Current is injected at one end, and the transmembrane voltage measured at each end of the modeled cable. If the simulator generates the correct curves for each end of the model, the entire

solution must be correct, since the cable equations are linear and therefore all intermediate solutions must be linear superpositions of the solutions at the ends.

The branched cable model in Rallpack 2 tests simulator performance on a highly branched model with non-uniform branch sizes. Since the model obeys Rall's 3/2 power law[12], it is electrically equivalent to a single cable, and the stimulus and recording arrangements are therefore equivalent to those for Rallpack 1.

Rallpack 3 introduces Na and K channels into the uniform cable model of Rallpack 1. This tests simulator capabilities in solving the Hodgkin Huxley equations.

Taken together, these three models exercise all the capabilities of a simulator that are needed to deal with any combination of Hodgkin-Huxley channels and branching (non-looping) structure.

Reference curves and utilities.

The Rallpack suite provides the reference output data for each model, programs for generating this output, and programs for doing the comparison between the correct output and the output from the simulator being tested.

1 Reference output. Each Rallpack set includes two data files containing time and voltage data points sampled at 50 μsec, to serve as a reference for the output from each end of the model. For Rallpack 3 two such reference pairs are provided, from the reference simulations performed on the simulation packages NEURON[13] and GENESIS[14], respectively.

2 Reference programs. The output for the two passive models can be analytically determined. These curves are calculated based on a Laplace transform solution for the time-varying behaviour of the cable[6], numerically calculated as the sum of a convergent series. The C program for performing this calculation is included in the Rallpack suite.

The correct solution for the axon model in Rallpack 3 cannot be obtained analytically. We therefore provide the simulator setup code used to generate the results in NEURON and in GENESIS. These models were run at a timestep of 1 μsec using full calculation of all exponential terms. The correspondence between the two, as calculated by the comparison programs (below) is better than 1%

3 Comparison programs. These are provided to compare simulator output to the reference curves. A simple root mean squared difference in voltage is used for the exponential charging curves for the models in Rallpacks 1 and 2. A slightly more sophisticated measure is used for spike output waveforms of the axon model. In this case spike peaks are aligned for the voltage calculations, and interspike interval differences are separately added to the root mean squared total.

Performance measures.

Two main performance measures are defined for the benchmarks: *raw speed* and *accuracy*

Raw speed is the number of compartmental calculations per second:

Raw speed = compartments * steps/simulation run time.

Accuracy. This is defined as the average normalized root mean squared difference between the simulator output and the reference curve, for each of the two output points on the model. These calculations are performed by the utility routines provided with the benchmark suite to ensure compatibility. Values are reported as percentage errors.

Each of these measures is dependent on specific model parameters such as model size and timestep. The following tables and/or curves in the detailed report for each model illustrate different aspects of simulator performance.

1. Accuracy vs. Timestep. This is a measure of the intrinsic numerical accuracy of the simulator algorithms. It provides one with information on the best expected accuracy, and the appropriate simulation timestep needed to obtain results with a desired accuracy.

2 Accuracy vs. Simulation Speed. The simulation speed is the product of timestep and raw speed. In most cases the raw speed does not depend on timestep, so the simulation speed is directly proportional to timestep for the purposes of this plot. This measure is most relevant to choosing between simulators. It directly displays which simulator will be fastest in a desired accuracy range, and assists in making the tradeoff between desired accuracy and speed.

3. Raw Speed vs. Model size. This curve shows how the speed performance of the simulator scales with increasing model size and gives an estimate of the computational overhead associated with the simulator.

4 Memory use per compartment vs. Model size. This auxiliary measure indicates the memory overhead associated with different kinds of model. It is valuable for estimating the memory that will be required to run a particular model.

Format of the Rallpack Report.

The Rallpack report consists of a general section, followed by a detailed report for each of the three Rallpack models. The complete benchmark report is of the form displayed in Box 2, which contains the reports for NEURON and GENESIS.

The general section concisely (and sometimes misleadingly) summarizes the performance figures for the simulator. The Peak speed and compartment equivalent values are the basis for evaluating the sheer number crunching capabilities of a simulator. The peak speed corresponds to the best raw speed obtained for Rallpack 1, the linear cable. The compartment equivalents are the ratios of CPU time required for compartments, branched compartments, and Hodgkin-Huxley-channels. Together these enable one to estimate the total time it would take to run a model involving any combination of these components.

A partial measure of the simulator accuracy is provided by the asymptotic accuracy (The best accuracy obtained with Rallpack 3) and semi-accurate timestep (The longest timestep which will give an error less than twice the asymptotic error). Rallpack 3 is the most demanding model of the three from the accuracy viewpoint, and is therefore used as the criterion. In most cases the semi-accurate timestep will be an adequate compromise between run time and accuracy.

The detailed report for each model includes data for speed, accuracy and memory use over a range of model sizes and timesteps. These curves are described above and illustrated in Box 2. The detailed reports are the basis for any but the most cursory evaluation of a simulator. They also provide a tool for making informed trade-offs between speed and accuracy for a particular simulation.

Concluding remarks

The three models presented here as Rallpacks test only the very basic, universally accepted features of neuronal simulators. Existing simulators already support a much wider range of numerical

capabilities[4,5,13,14]. It is to be hoped that it will take less time than the decades since the introduction of the model of the squid axon, before some of these capabilities become universally accepted and embodied as benchmarks. Two classes of models already deserve consideration for future Rallpack tests : a complex single cell model with calcium dynamics, to test simulator capabilities on realistic neuronal models; and a model of a network with extensive synaptic interactions to evaluate performance of synapses. A performance related aspect of simulators that may be worth quantifying in future benchmarks is scaling of simulator speed with increasing numbers of nodes on parallel computer architectures.

Benchmarks as a whole offer a very narrow view of the real usability of simulators. Speed and accuracy are important, but less quantifiable features such as interfaces and documentation may have a much greater impact on the time taken to generate a simulation, and the validity of the results can never be any better than the model parameters. What these benchmarks do seek to offer are standards. It is a sign of the growing importance of neuronal simulations to neurobiology that there are so many disparate simulators available to the community. This is a valuable resource, in that each has its own strengths and is developing in different directions. However, it would be unfortunate if this profusion led to doubts about the generality of the results, since each simulator is far too complex for users to analyze in great detail. The Rallpacks are intended to be a common reference for the community, to lend a measure of confidence that all these sophisticated packages produce the same answers, and the *right* answers.

Acknowledgments.

The development of the Rallpacks could not have occurred without the insights and suggestions of many people. The original idea was discussed at the symposium on Analysis and Modeling of Neural Systems in 1991 in San Francisco. Among those involved were Frank Eeckman, Michael Hines and John Miller. Feedback and assistance during the development of the Rallpacks was provided among others by Erik De Schutter, Michael Hines, Mark Nelson and Tony Zador.

Obtaining the Rallpacks.

The Rallpack suite may be obtained by anonymous ftp from mordor.cns.caltech.edu. We would appreciate feedback on the suite and the results for simulators tested with it.

Selected References.

1 Hodgkin, A.L. and Huxley, A.F. (1952) *J. Physiol. Lond.* 117, 500-544

2 Rall, W., (1989), in *Methods in Neuronal Modeling,* Ch 2. ed Koch and Segev., MIT Press..

3 Churchland and Sejnowski (1988) *Science* 242, 741-745

4 Miller, J., (1990), *Nature,* 347, 783-784.

5 De Schutter, E., and Bower, J.M. (1992) *TINS* this issue

6 Jack J.J.B., Noble, D., Tsien R.W. (1983) in *Electrical current flow in excitable cells* , OUP.

7 Hines, M. (1984) *Int. J. Bio-Medical computing* 15, 69-76

8 FitzHugh, R. (1961) *Biophys. J.* 1, 445-466

9 Nagumo, J.S., Arimoto, S., Yoshizawa, S. (1962) *Proc. IRE.* 50, 2061- 2070

10 Hille, B. in *Ionic channels of Excitable Membranes, 2nd ed.* , ch 14, Sinauer.

11 Cooley and Dodge (1966) *Biophys. J.* 6, 583-599

12 Rall, W. (1959). *Exp Neurol* 1, 491-527

13 Hines, M. (1989) *Int. J. Bio-Medical computing* 24, 55-68

14 Wilson, M.A., Bhalla, U.S., Uhley, J.D., and Bower, J.M. (1989). *Advances in Neural Information Processing Systems* 1, 485-492.

Box 1. Model specifications.

Rallpack 1 : Uniform unbranched cable with a length constant of 1, a diameter of 1 micron, and a total length of 1 mm, and sealed ends. The cable is divided into 1000 compartments. The membrane properties are :

RA = 1.0 Ωm = 100 Ω cm
RM = 4.0 Ωm^2 = 40000 Ωcm^2
CM = 0.01 F/m^2 = 1.0 $\mu F/cm^2$
EM = -0.065 V = -65 mV.
$E_{Initial}$=EM

A current of 0.1 nA is injected in the first compartment. Membrane voltages are recorded for the first and last compartments.

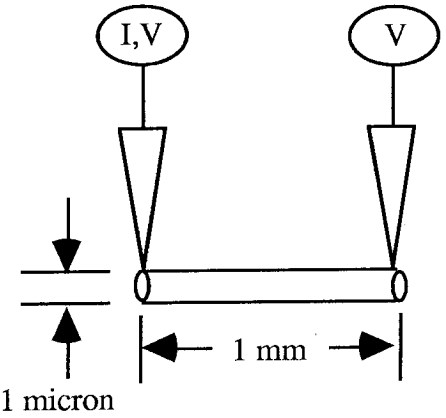

Rallpack 2 :

Binary branched structure obeying Rall's 3/2 power law. It consists of 1023 compartments corresponding to 9 levels of branching. Each branch has an electrotonic length of 0.008 . At each branch away from the root the diameter decreases by a factor of $2^{2/3}$, in accordance with the power law, and the length by a factor of $2^{1/3}$. The detailed geometry of the compartments is

Depth	N	L	Dia
0	1	32.0	16.0
1	2	25.4	10.08
2	4	20.16	6.35
3	8	16.0	4.0
4	16	12.7	2.52
5	32	10.08	1.587
6	64	8.0	1.0
7	128	6.35	0.63
8	256	5.04	0.397
9	512	4.0	0.25

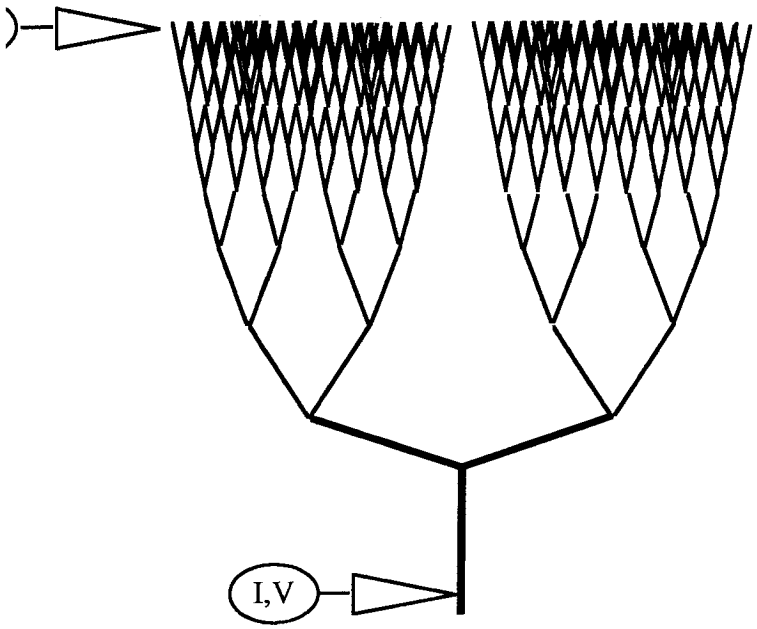

The membrane properties are as for Rallpack 1.

A current of 0.1 nA is injected into the root compartment. Membrane voltages are recorded for the root and a terminal branch compartment.

Rallpack 3

This model consists of the cable from Rallpack 1 with the addition of squid Na^+ and K^+ channels from Hodgkin and

Huxley. The channel properties are as described by Hodgkin and Huxley, as follows (We have reversed their sign convention, and take the resting potential to be -65 mV) :

E_{Na} = 0.050 V = 50 mV; E_K = -0.077 V = -77 mV

G_{Na} = 1200 S/m^2 = 120 m.mho/cm^2 ; G_K = 360 S/m^2 = 36 m.mho/cm^2

For each compartment :

$\overline{G}_{Na} = 3.77\times10^{-9}\text{S} = 3.77\times10^{-6}\text{m.mho}$; $\overline{G}_K = 1.131\times10^{-9}\text{S} = 1.131\times10^{-6}\text{m.mho}$

The conductance of each channel is given by :

$g_{Na} = \overline{G}_{Na} m^3 h$; $g_K = \overline{G}_K n^4$

where m, h, and n satisfy equations of the type

$dm/dt = \alpha_m - (\alpha_m+\beta_m)m$

α and β are given by (units are msec and mV) :

$\alpha_m = 0.1(-V+25)/(e^{(-V+25)/10}-1)$ $\beta_m = 4e^{-V/18}$

$\alpha_h = 0.07e^{-V/20}$ $\beta_h = 1/(e^{(V+30)/10}+1)$

$\alpha_n = 0.01(-V+10)/(e^{(-V+10)/10}-1)$ $\beta_n = 0.125e^{-V/80}$

A current of 0.1 nA is injected in the first compartment. Membrane voltages (V) are recorded for the first and last compartments.

Box 2. Rallpack reports for GENESIS and NEURON

General report.	**GENESIS version 1.4**	**NEURON version 2.43**
Peak speed	44,000	43,000
Compartment equivalents	1 : 1 : 0.5	1 : 1.8 : 0.75
Asymptotic accuracy	0.9%	1.1%
Semi-accurate timestep	50 µsec	50 µsec
Hardware information	Sun sparc 2; Sun OS 4.1; 26 MIPS	Sun sparc 2; Sun OS 4.1; 26 MIPS
Simulation setup time	13 Sec	1 Sec
Base memory	3.42 Megabytes	1.6 Megabytes
Integration method	Hines/Crank-Nicolson	Hines/Crank-Nicolson
Specific report for Rallpack 1		
Peak speed/model size compartments	44,000 for >= 1000 compartments	43,000 for >= 1000
Asymptotic accuracy	0.02%	0.02%
Semi-accurate timestep	100 usec	100 usec
Setup time	9 sec	< 1 sec
Specific report for Rallpack 2		
Peak speed/model size	44,000 for >= 511 compartments	23,962 for >= 127 compartments
Asymptotic accuracy	0.016%	0.017%
Semi-accurate timestep	1000 usec	100 usec
Setup time	8 sec	< 1 sec
Specific report for Rallpack 3		
Peak speed/model size	22,000 for >= 1000 compartments	17,400 for >= 100 compartments
Asymptotic accuracy	0.9%	1.1%
Semi-accurate timestep	50 usec	50 usec
Setup time	13 sec	1 sec

Rallpack 1

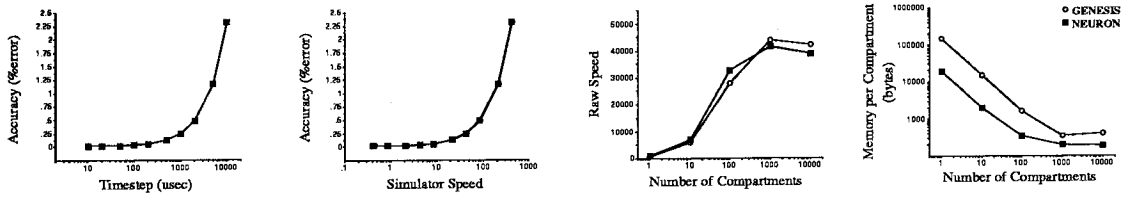

Rallpack 2

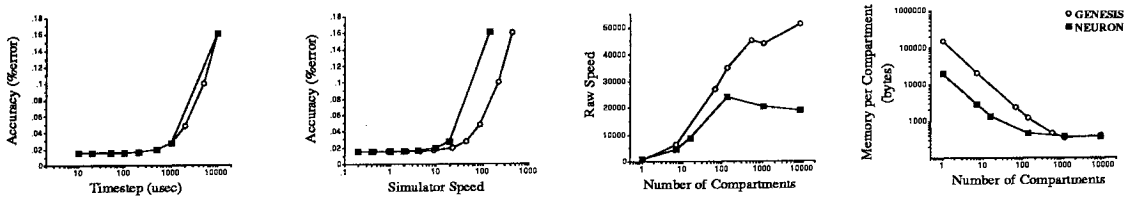

Rallpack 3

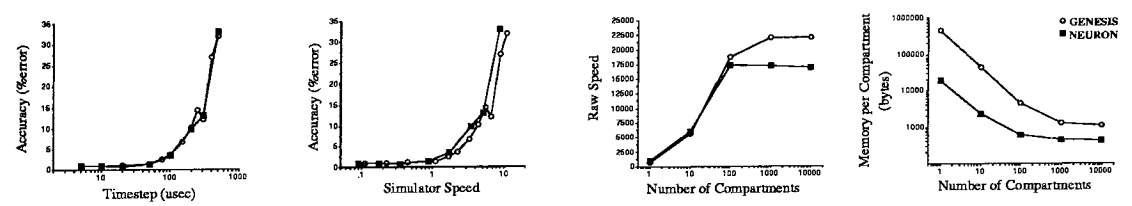

Exploring parameter space in detailed single neuron models: Simulations of the mitral and granule cells of the olfactory bulb.

Upinder S. Bhalla and James M. Bower.

Division of Biology,

California Institute of Technology, Pasadena, CA 91125

SUMMARY AND CONCLUSIONS

1. Detailed compartmental computer simulations of single mitral and granule cells of the vertebrate olfactory bulb were constructed using previously published geometrical data. Electrophysiological properties were determined by comparing model output to previously published experimental data, mainly current clamp recordings.

2. The passive electrical properties of each model were explored by comparing model output with intracellular potential data from hyperpolarizing current injection experiments. The results suggest that membrane resistivity in both cells is non-uniform with somas having a substantially lower resistivity than the dendrites.

3. The active properties of these cells were explored by incorporating active ion channels into modeled compartments. Based on evidence from the literature, the mitral cell model included 6 channel types: Fast Na, fast delayed rectifier (Kfast), slow delayed rectifier (K), Transient outward K current (KA), voltage and Ca dependent K current (KCa), and L-type Ca current (LCa). The granule cell model included four channel types: rat brain sodium (Na_{gran}), K, KA and the non-inactivating muscarinic potassium current KM. Modeled channels were based on the Hodgkin-Huxley formalism.

4. Representative kinetics for each of the channel classes above were obtained from the literature. The experimentally unknown spatial distributions of each included channel were obtained by systematic parameter searches. These were conducted in two ways: large-scale simulation series in which each parameter was varied in turn, and by an adaptation of a multidimensional conjugate gradient method. In each case the simulated results were compared to experimental data using a curve-matching function evaluating mean squared differences of several aspects of the simulated and experimental voltage waveforms.

5. Systematic parameter variations revealed a single distinct region of parameter space in which the mitral cell model best fit the data. This region of parameter space was also very robust to parameter variations. Specifically, optimum performance was obtained when Ca and slow K channels were

concentrated in the glomeruli, with a lower density in the soma and proximal secondary dendrites. The distribution of sodium and fast potassium channels, on the other hand, was highest at the soma and axon with a much lighter distribution throughout the secondary dendrites. The KA and KCa channels were also concentrated near the soma.

6. The parameter search of the granule cell model was much less restrained by experimental data. Several parameter regimes were found which gave a good match to the data. In the simplest of these, Na and K channels were present at high density both at the soma and in the peripheral dendrites, while the KA and KM channels were present only in the soma.

7. Further manipulation of the mitral cell model suggests that the predicted channel distributions can be verified physiologically. If the channel distributions suggested by the model are correct, voltage clamping the soma to potentials near the spiking threshold should result in the generation of independent local dendritic action potentials reflecting the effective decoupling of the active membranes of the different dendrites. The model predicts that the glomerular tuft, the soma, and the secondary dendrites of each mitral cell have distinct local electrical properties resulting largely from the localized distribution of ion channels. They may also be functionally distinct.

8. Our extensive search of model parameters suggests that neurons operate in regions of parameter space that are most robust to changes in parameter values. In particular, changes in channel densities by as much as an order of magnitude may have relatively little effect on the behavior of the neuronal model.

INTRODUCTION

This paper describes an effort to model each of the two major neuronal cell classes found in the vertebrate olfactory bulb (Mori 1987). We first describe models of the mitral cell and the related tufted and displaced mitral cells. These cells provide the only bulbar output to higher centers including piriform cortex (Haberly and Price 1977). We then present models of three classes of granule cells which are the largest population of cells in the bulb and are involved in the centrifugal feedback from piriform cortex

and other higher areas to the bulb (Mori 1987). This work extends our network modeling efforts in the olfactory cortex (Wilson and Bower 1992) to the neurons composing the brain structure that provides the primary afferent input to piriform cortex.

The pioneering modeling studies on the olfactory bulb (Rall et al. 1966; Rall and Shepherd 1968; Rall 1970) introduced multicompartmental models of the mitral and granule cells. These consisted of 5 to 10 compartments and involved reduced (FitzHugh 1961) active properties. These single-cell and network models were consistent with many of the experimental details available at the time and demonstrated the power of simulation techniques as a means for understanding physiological observations. The accumulation of much more detailed experimental data on these cell types, and the availability of vastly greater computational resources, makes it possible to now model the cells in considerably more detail. As with the original modeling studies, the development of single cell models is a necessary prelude to a detailed model of the bulb as a whole.

As is the case with most modern efforts to model single neurons (Segev et al. 1990; Woolf et al. 1991a; De Schutter and Bower 1991), the approach taken here involved first constructing an anatomically correct compartmental representation of each neuron of interest and then studying the passive properties of the model. Active channels were subsequently incorporated into the passive model based on evidence from the literature for the presence of particular channel types. Parameters such as channel densities and kinetics were then varied in order to replicate previously published physiological response properties.

As is also the case for most detailed single cell models, values for many of the parameters of interest, especially ion channel densities and channel kinetics, are not available directly from conventional experimental data such as intracellular somatic recordings (Koch and Bower 1992). Traditionally, models have either relied on additional data (Calcium imaging, dendritic recordings) or have involved estimates of channel properties that lack quantitative precision. It has usually been an open question whether the particular parameter values selected are the only viable parameters, or just one of several possible solutions. This issue becomes more serious as models become more realistically detailed and the number of parameters increases.

In this paper we have employed a systematic and semi-automated method to explore possible parameters for models of the two major types of olfactory bulb neurons, and their subclasses. These extensive searches of parameter space were performed on a parallel supercomputer, the Touchstone Delta at Caltech. In the case of the experimentally well studied mitral cell, we have discovered a single region of parameter space in which the similarity of model output and experimental data is preserved for a fairly large range of most parameter values. In fact, some parameters allow up to an order of magnitude leeway around the optimal value. The robust behavior of this cell model suggests that real neurons may seek to operate in regions of parameter space that are tolerant of small or even sizable changes in their physical characteristics (e.g., channel densities). This may have important implications for the robustness of the nervous system to small differences during development, to damage, and to the many environmental changes that are known to affect the detailed properties of ion channels.

In the case of the less well studied granule cell, several equivalent regions of parameter space have been found. These results demonstrate the importance of experimental data as constraints on model parameters, as well as the utility of careful studies of parameter space as a guide to future experimental work.

METHODS

General Simulation procedures.

The models described here are all in the class of single neuron models in which neuronal structure is represented as a series of electrically linked compartments (Figure 1; Rall 1964; Cooley and Dodge 1966).

In general, the same modeling approach was taken to construct and parameterize each of the models discussed in this paper. In each case, the first step was to establish the overall compartmental structure of the model based on previously published quantitative descriptions of cellular anatomy. Once an anatomically accurate model was constructed, the passive electrical properties of the cells were

established. Finally, active properties were explored by adding ionic conductances to the different compartments.

As described in the introduction, the principal effort in modeling these cells involved finding parameter values that produce model behavior consistent with experimental results. In some cases good estimates of parameters can be obtained from the literature, e.g., cellular anatomy or the presence of certain channel types. In other cases (channel distributions or kinetics), information is either difficult to obtain or not available. For channel kinetics we used parameters determined for other neuronal types as described below. Values for channel densities were estimated based on parameter searches which compared model output to physiological records which are relatively easy to obtain experimentally.

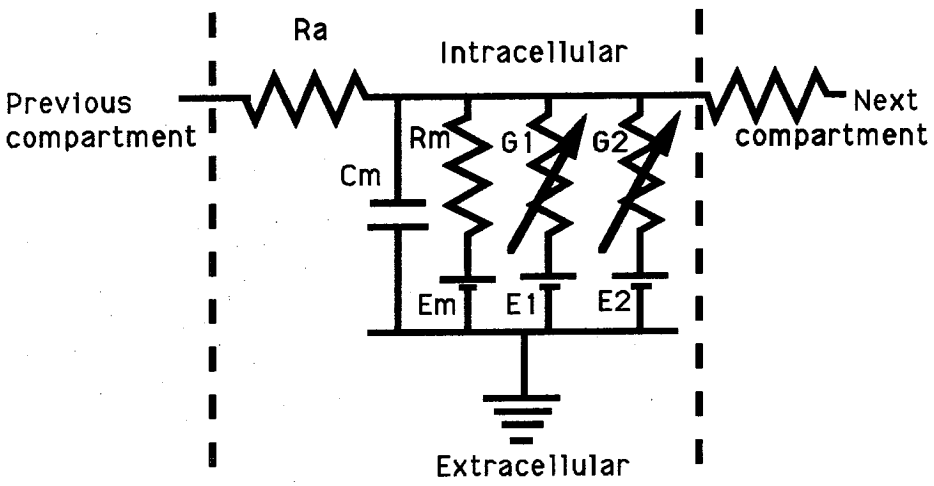

Figure 1: Circuit diagram for compartmental model. Following the classical description of an active compartment (Rall 1959), it is represented as a membrane resistance (Rm) in parallel with a membrane capacitance (Cm); and an axial resistance (Ra) which combines the cytoplasmic and extracellular axial resistance. The channel conductances are represented as variable conductances (G1, G2 and so on) in parallel with the membrane resistance. Each of the transmembrane conductances (Rm, G1, G2, etc.) is in series with the appropriate potential. These potentials are derived from the reversal potentials for the ions passing through the conductance and are kept fixed in these models.

Our models utilize parameters from many different sources and species. This is necessitated by the lack of complete data from any one species. In particular, the cell geometry is based largely on mammalian data and is scaled to correspond to the size of nominal rabbit neurons. The electrophysiogical data is largely (but not exculsively) from turtle, since that preparation has proven most amenable to detailed single-cell analysis of the sort required. As we shall discuss for specific instances, in most cases we do have comparable data from turtle, rabbit, and other species. This provides bounds on the expected variability in properties, and in most cases demonstrates a high level of consistency between species. The judicious use of data from several sources is common in modeling studies where experimental data on the system under study is inadequate (e.g., combining channel density information: Belluzi and Sacchi 1991; channel kinetics: Yamada et al. 1989). For many well-defined neuronal classes, a single canonical model is expected to provide a good representation for a particular neuron type over a fairly wide range of species and brain regions (Shepherd 1992).

Source of Known parameters

ANATOMICAL ORGANIZATION. The morphological data used to obtain the basic structure of each cell type was taken primarily from rabbit (Mori et al. 1983) but also from mouse (Greer 1987) and rat (Price and Powell 1970a,b). These studies reveal that the morphology of the cells in the olfactory bulb is remarkably consistent among vertebrates (Mori 1987), the main difference being one of scale. The specific model for each cell type was constructed by averaging published values for soma size, length of inter-branch segments, diameter of branches, branching probabilities and density and size of any spines.

PASSIVE PROPERTIES. Once the anatomical organization of a particular model was established, basic parameters governing the passive electrical properties of each cell type were added to the model. Values of membrane capacitance (C_m) and axoplasmic resistivity (R_a) have fairly consistent

values in the literature (Jack et al. 1983). For the models described here, the R_a was set at 50 Ω.cm (granule cell) and 200 Ω.cm (mitral cell). C_m was taken to be 1.0 μF/cm^2. Membrane resistivity (R_m) is more difficult to measure experimentally (Rall 1959; Jack et al. 1983), and therefore was determined in the current models by matching intracellular current clamp data using hyperpolarizing pulses (Mori et al. 1981a; Jahr and Nicoll 1982). Values used for R_m were made uniform throughout the dendritic structure but lower at the soma. This modification was intended to take into account the leak due to damage caused by the somatic recording electrode (Segev et al. 1990; Pongracz et al. 1991). When comparing published time courses and input resistances to simulated data, charging curves were fitted with a two-exponential curve using the Levenberg-Marquardt (nonlinear least squares) method (Press et al. 1988).

ACTIVE CHANNEL PROPERTIES. The identity of the channels included in each model were inferred from the published effects of specific channel blockers on the electrical properties of each cell. Good data on this subject exists for the mitral cell but less data is available for the granule cell. Accordingly, fewer channel types were assumed to exist for the latter case (see below).

Determining appropriate channel kinetics is a somewhat more complex process in that detailed descriptions of channel kinetics are not available for these specific cell types. The starting points for channel kinetic parameters were therefore derived from the values for similar channels in other cell types. In this study, initial channel kinetics were obtained from a wide variety of sources and then implemented in Hodgkin-Huxley (Hodgkin and Huxley 1952) form as discussed below in detail for each cell type. In principle, the parameter search approach could also be applied to the channel kinetics. This was not done in this study for the following reasons. First, each channel requires the specification of as many as 18 kinetic parameters: 4 for each of the forward and backward rate functions, in each of the two gates, plus a power term for each gate. (see Appendix C: channel parameters). This would be difficult to handle with the present parameter search methods (Appendix B). Second, neuronal properties tend to be very sensitive to variations in channel kinetics, unlike their more robust behavior with channel densities. Finally, an unconstrained automatic search could potentially distort channel

properties beyond the range normally expected for their channel class. Given the availability of well described channels of the desired classes from other systems, we chose to base our channel kinetics more directly on data from the literature.

Unknown parameter estimation

In general, the properties of each cell depend, in varying degrees, on a vast number of parameters, many of which are not known in detail or at all for the cells modeled here. In active cell models the number of such free parameters is enormous. For example, information on channel distributions and densities is not yet readily available for each channel type but is critical to model behavior. Accordingly, possible values for the spatial distribution of channels must be explored by matching model output to existing physiological data. Simplifying assumptions must be made to reduce the number of degrees of freedom in a complex neuronal model (Rall 1990) to a tractable range, in a systematic manner.

We have adopted the following basic approach to defining the parameter space of our models: First, we establish as many model parameters as we can in an unambiguous manner. This includes the morphology, passive properties, and a minimal set of X channel types that would be consistent with the data. These parameters are then held fixed. Second, we subdivide the model into Y distinct regions within which the channel distributions are assumed to be uniform. For each of these regions we assign the entire set of channel types. This establishes our basic parameter space of X.Y dimensions. Finally, as the parameter search indicates that certain channel classes may not play a significant role in a given region, those channels are eliminated from that region of the model.

We have found that the process just described can readily be automated if two conditions can be met. First, there must be a means of evaluating the 'goodness' of a particular set of parameters. Second, there must be a mechanism for systematically sampling parameter space. The approach used here to accomplish these two objectives is described in more detail in appendices A and B.

Mitral cell parameters and variations.

ANATOMICAL ORGANIZATION. Three classes of mitral cell models were constructed: mitral, displaced mitral and tufted cells . Very good statistical information is available on the morphology of these cells (Mori et al. 1983; Price and Powell 1970 a,b).

MATCHED PHYSIOLOGICAL DATA. Electrophysiological data from current clamp experiments in the turtle mitral cell (Mori et al. 1981a; Mori et al. 1982) was the main source of physiological data used in this study. Turtle mitral cells frequently have more than one primary dendrite (Mori 1987), but are otherwise similar in geometry to their mammalian counterparts. Whole cell current-clamp recordings from mammalian mitral cells have been made (Bufler et al. 1992; Nickell et al. 1992) in the slice, and have qualitatively similar appearance to the turtle recordings. However, the very large mitral cell dendritic arborization is invariably damaged in slice prepartions, which makes the data hard to interpret. Spike thresholds appear to be in the same range as for the turtle data, but the resting potential for the whole cell recordings is approx -80 mV (Bufler et al. 1992), which is 15 mV lower. Whole-cell current clamp recordings from mitral cells in primary cultures of mammalian olfactory bulb (Trombley and Shepherd 1992) also show very similar voltage waveforms to the turtle recordings.

Further evidence for the similarity in electrophysiological properties of mitral cells in turtle and mammals is available from intracellular recordings under a variety of stimulus conditions. Fast pre-potentials which can be isolated by hyperpolaraization are evident in responses to olfactory nerve stimulation in rabbit (Mori and Takagi 1975) and turtle (Mori et al 1982; Jahr and Nicoll 1982). Similar fast pre-potentials have been reported in rats (Wellis et al. 1989) in the absence of hyperpolarization. In all cases these pre-potentials are interpreted as originating from apical dendritic spikes. Close correspondence between turtle (Mori et al. 1981a; Jahr and Nicoll 1982) and rabbit (Mori and Takagi 1975; Mori and Takagi 1978) is also seen in experiments where the LOT is stimulated and intracellular recordings made from the mitral cell soma. In each case, a distinctive sequence of M, A, and B spikes is observed, which is interpreted as the successive activation of the myelinated axon (M), the axon hillock

(A), and the soma-dendritic membrane (B). Based on these observations a strong case can be made for similarity in mitral cell active properties across vertebrates, and specifically between rabbits and turtles, which provide much of our morphological and electrophysiological data respectively.

CHANNEL TYPES. A large amount of data is available on the types of channels found in mitral cells. Blockage of fast spikes by TTX (Mori et al. 1981a, reproduced in Figure 4 A below; Jahr and Nicoll 1982) shows the presence of sodium channels (Na). Blockage of the remaining spikes using cobalt ions (Mori et al. 1981a, Jahr and Nicoll 1982) reveals a calcium current (modeled as an L-type calcium current, LCa). The situation with potassium currents is, as is frequently the case, less distinct. The rapid repolarization following the action potential (Figure 4 A) makes it clear that a fast delayed rectifier (Kfast) is present. In addition, the somewhat less rapid hyperpolarization (Figure 4 A) following the Ca spike in the presence of TTX and TEA suggests a remaining, slower, delayed rectifier current (K). The slow rate of charging of the membrane (Figure 4 A) when current is being injected suggests that an anomalous rectifier current (KA) is active. Both Ca- and Na- dependent K channels have been shown to exist in the mitral cell (Jahr and Nicoll 1982; Egan et al. 1992). The presence of cation-dependent K currents can also be deduced from the increase in inter-spike interval following the first spike induced with current injection (Mori et al. 1981a; Figure 4 A,D). We have chosen to model the Ca-dependent K channel (KCa) because the whole cell experiments do not reveal Na-dependent currents except at very high concentrations of Na (Egan et al. 1992). Accordingly, four classes of K channels were modeled: fast K, slow K, KA and KCa. Under the experimental conditions of channel block (10 mM TTX, 5 mM TEA, see Mori et al. 1981a), fast K channels are likely to be completely blocked, slow K channels partially blocked and the KA and KCa channels not much affected (Connor and Stevens 1971).

CHANNEL KINETICS. The following final set of channels were used in the mitral cell model: 1) Fast sodium (Na) channel (slightly modified from Traub 1982); 2) Fast delayed rectifier (Kfast) channel and 3) slow delayed rectifier (K) channel (both modified from Aldrich et al. 1979; and Adams et al. 1977); 4) Anomalous outward current (KA) channel (Yamada et al. 1989); 5) Calcium L-type current (LCa) (modified from De Schutter 1991; and Hirano and Hagiwara 1989); and 6) Calcium-

dependent K channel (KCa) (modified from Traub 1982). The calcium dependence of this last channel was modeled by establishing a single pool of intracellular calcium which decays after calcium channel activation to a baseline of 10 nanomolar with a single time constant of 10 msec. Accordingly, calcium influx is assumed to be due only to the action of the LCa current and lateral diffusion of Calcium is not modeled.

Most of the selection of appropriate channels and kinetics was done on a single compartment model by varying the channel parameters under conditions of current clamp using the `neurokit' tool in the GENESIS script libraries (Wilson et al. 1989). This more readily allowed the comparison of modeled voltage traces to experimental data. Channels tuned in this manner were then incorporated into the full mitral cell model for further evaluation.

SPATIAL DISTRIBUTION OF CHANNELS. Channel density distributions have not been directly measured in mitral cells, but numerous experiments (e.g., Mori and Takagi 1975; Mori et al. 1982; Jahr and Nicoll 1982) suggest the presence of active channels distributed over various parts of the mitral cell dendritic arbor. In the absence of direct data on channel densities, a very conservative approach was taken to estimating these parameters. Six regions of the cell were considered as having distinct channel densities: the soma, primary dendrite, glomerular tuft, proximal secondary dendrites, distal secondary dendrites and axon (See Figure 3 below). Within each region, a uniform distribution was assumed.

The availability of current clamp records in the presence of applied blockers (Mori et al. 1981a; Jahr and Nicoll 1982) is very valuable for constraining the parameter search process. Under blockage of Na channels by TTX, and Kfast by TEA, we can conduct a parameter search with these channels missing from each of the six regions of the mitral cell, resulting in a far more tractable 24 parameters. Having fixed more than half of the model parameters using this initial parameter search, finding channel densities for the unblocked model involved a much smaller parameter space. Further refinement was possible for special cases where additional information was available. For example, the experimentally

demonstrated propagation of antidromic spikes into the mitral cell soma (Mori et al. 1981a; Mori et al. 1982) requires a higher channel density in the axon initial segments than in the rest of the axon.

OTHER CLASSES OF MITRAL CELLS. In general, displaced mitral and tufted cells are believed to have similar properties and functions to the more extensively studied mitral cells (Mori 1987). It has therefore been assumed that the channel kinetics and density parameters obtained for the mitral cells apply directly to the different geometries (Mori et al. 1983) of these other cell types. It has also been reported that a small percentage of mitral cells in mammalian olfactory bulb have two primary dendrites (Mori et al. 1983). As mentioned previously, multiple primary dendrites are quite common in turtle and amphibian mitral cells (Mori et al. 1981a) which are the source of much of the physiological data used in these simulations. Accordingly, channel properties and distributions from the basic mitral cell model were also tested in additional models with the geometries appropriate to the tufted, displaced mitral, and turtle mitral cells.

Granule cell parameters and variations

ANATOMICAL STRUCTURE. Three types of previously described granule cells were also modeled: Type I, Type II, and Type III. Morphological data is available from several species: rabbit (Mori and Kishi 1982; Mori et al. 1983), rat (Price and Powell 1970b), and mouse (Greer 1987; Woolf et al. 1991a,b). The convoluted morphology that the above studies reveal in granule cell dendrites was taken into account by increasing the equivalent membrane area by a factor of 2.0. Granule cell spines were simulated by assigning each model the same number and spatial distribution of spines as reported in the literature (Mori et al.. 1983). All spines consisted of identical neck and head compartments (Shepherd and Brayton 1987) with no attempt being made to include the considerable anatomical variability in spine morphology that has previously been reported (Woolf et al. 1991a,b).

MATCHED PHYSIOLOGICAL DATA. The difficulty of obtaining stable intracellular recordings in the granule cell has limited the amount of data available for assessing the detailed electrical properties of the granule cell (Jahr and Nicoll 1982; Wellis and Scott 1990; Mori and Kishi 1982). For the same reason, there is also a lack of information on the effects of channel blockers during current injection. Accordingly, a limited set of channels was used for simulating granule cell spikes (see below). An additional complication in the data for hyperpolarizing current injections used in the 'passive' granule cell model was a large (two-fold) discrepancy in the time courses for charging and repolarization of the cell. This issue is dealt with in the discussion. Recordings from current injection experiments in rat (Wellis and Scott 1990) and turtle (Jahr and Nicoll 1982) show substantial similarity in spike waveforms, suggesting that it is reasonable to combine morphological and electrophysiological data from these different sources.

CHANNEL TYPES. Granule cell spikes were assumed to be due to sodium and potassium channels based on the Hodgkin-Huxley formalism. Based on the previously reported increasing interval between spikes during the depolarizing current pulse (Jahr and Nicoll 1982), an additional non-inactivating muscarinic K channel (KM) was incorporated into the model. The kinetics and spatial distributions of these channels were varied to obtain matches to the experimental data that does exist for depolarizing current clamp (Jahr and Nicoll 1982).

CHANNEL KINETICS. The library of channels assembled in GENESIS was used to select channels which satisfied the slower kinetics seen in the granule cell data. The following final set of channels was used in the granule cell models: Rat brain Na (Na_{gran}) channel (Stuhmer et al. 1987), Modified delayed rectifier (K) channel (Aldrich et al. 1979; Adams et al. 1980), and the bullfrog sympathetic ganglion neuron KM and KA channels (Yamada et al. 1989).

SPATIAL DISTRIBUTION OF CHANNELS. A similar analysis was applied to the granule cell channel distribution as with mitral cells. In this case only four channels were considered. The regions of

the granule cell considered as electrically distinct were: soma, trunk, peripheral processes, and the descending (deep) dendrites (See Figure 6 below). Additional simulations also considered the possibility of ion channels in the spines. Simulations were performed while varying channel densities over each of these regions. The parameter searches revealed several distinct channel distributions which adequately matched experimental data.

OTHER CLASSES OF GRANULE CELLS. Three types of previously described granule cells were modeled: Type I; Type II; and Type III (Greer 1987; Mori et al. 1983). As with the mitral cell types, it was assumed for simplicity that the basic channel properties and distributions in each granule cell type are the same and that the only variation in classes was morphological. The channel distribution from the simplest (least number of channels/compartment) Type I model was applied to the Type II and Type III cells.

Computational Issues

SIMULATION ENVIRONMENT. All simulations were performed on the GENESIS simulator developed at Caltech (Wilson et al. 1989). Interactive simulations and parameter variations were performed using a special single cell simulation tool within GENESIS called Neurokit. As described in appendix B, exhaustive parameter searches were performed in batch mode under the control of GENESIS script language programs. The library of ion channels that has been constructed within GENESIS based on data in the literature was used extensively during these simulations. Initial simulations were performed on a variety of UNIX workstations while extensive parameter variations have employed the Intel Touchstone Delta parallel supercomputer at Caltech.

NUMERICAL TECHNIQUES. Implicit (Backward Euler, Crank Nicolson) as well as explicit (forward exponential Euler) integration methods were used to evaluate the systems of coupled differential equations that arise from the compartmental modeling scheme. In both cases, the time step

was empirically chosen so that the change in ISI with a halved time step was less than 0.5 %. Typical time steps used were 50 μsec using the implicit method, and 5 μsec for the explicit method. In the case of granule cells, however, the presence of numerous spines renders the system of equations numerically very stiff, and time steps of 20 nanoseconds were required for accuracy when using the explicit method.

The Hines numbering scheme (Hines 1984) was used to reduce the number of operations for solution using the implicit method and Gaussian elimination, to the order of the number of compartments. Hodgkin-Huxley equations were evaluated in the implicit method on a staggered time grid (Hines 1984; Mascagni 1989) to obtain second-order accuracy, except for the Calcium-dependent Potassium channels. The more complex form of these channels (Traub 1982; see appendix C) necessitated the use of the explicit method in their evaluation. This combination of integration methods did not lead to serious difficulties, as the relevant time constants were an order of magnitude slower than the time step.

Simulations performed using the implicit and explicit methods were checked against each other to verify consistency. The accuracy of these solutions was further confirmed by simulation of a constant current injection to obtain the input resistance of the cell from the asymptotic potential. The input resistance was then directly calculated using Ohm's Law and the circuit equivalent of the cell, and found to be identical with the previous estimate. Additional comparisons were made with values for input resistance calculated using full cable theory (Rall 1959; Rall and Rinzel 1973; Jack et al. 1983). These differ slightly due to the compartmental approximations, with the difference depending on the size of the compartments. In a 286 compartmental model of the mitral cell, where all compartments are smaller than 0.02 length constants, the difference is less than 1% .

The Hodgkin-Huxley equations were implemented using a tabulated lookup scheme, with a large number of sample points (every 50 μVolt) to retain numerical accuracy (Hines 1984; Mascagni 1989). The use of tables permits one to directly utilize experimental curves for voltage dependencies, without resorting to curve-fitting. Additionally, it is computationally much more efficient than calculating exponentials. In cases where the curves were directly taken from published data, the limited number of

experimental data points were interpolated using Bezier splines (Enns 1986) to obtain sufficient sample points for the table.

The correctness and accuracy of the GENESIS simulator as a whole has been evaluated using the Rallpack set of benchmarks (Bhalla et al. 1992). Briefly, the accuracy benchmarks calculate the normalized root-mean-squared difference between the simulated and the correct voltage waveform for a particular model. The Rallpack axon model incorporates Hodgkin-Huxley type channels in a 1000 compartment cyclindrical membrane and is appropriate for testing simulator performance for active models of the kind discussed in this study. At the timesteps used in these simulations, the error for the axon model in the Rallpacks is 1.3%.

Parameter availability.

All model parameters are available from the authors or by ftp from Babel, the GENESIS users group. Scripts for running these simulations within the GENESIS environment are also available from the same source. Inquiries should be addressed to babel.cns.caltech.edu.

RESULTS

In the course of this study a great number of parameter variations were explored while comparing model output to physiological data. In the following sections, the resulting final state of each neuronal model will be presented. In each case the final parameters were determined on the basis of two criteria: First, the ability of the resulting model to replicate physiological data as evaluated by the curve-matching function. Second, the robustness of the model as determined by varying parameters in the vicinity of the final solution and observing how well the simulations continued to match experiment. In terms of the curve matching function, this translates to smoothness of the function in the region of the best match (Figure 2).

While it is very likely the case that some other more complicated combination of channels, channel kinetics and/or channel distributions could meet the same criteria, we will describe the simplest combination of parameters that our models suggest satisfy the data. Following the description of the final models, we then describe a number of manipulations performed on them to explore their behavior in various physiological and experimental contexts.

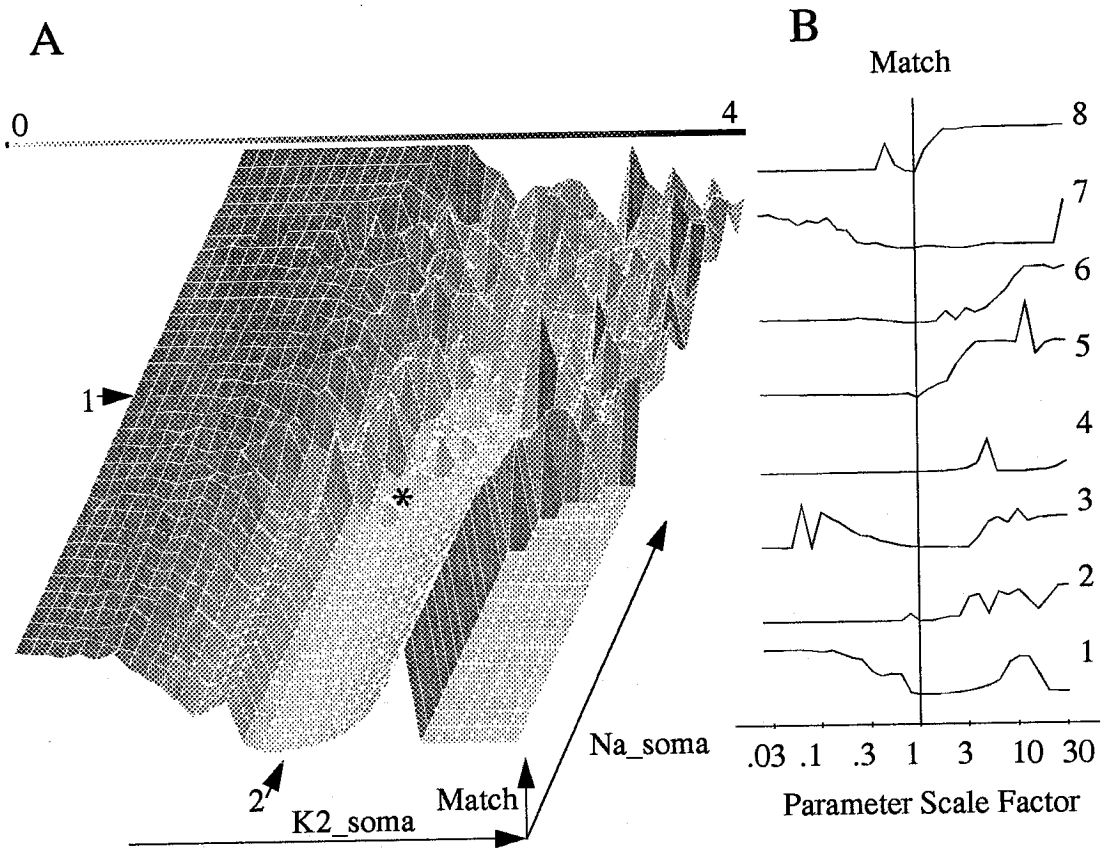

Figure 2: Parameter space for selected parameters of the mitral cell model. A: 2-dimensional plot of a plane section through parameter space. The shading and vertical axis represent the match value, which is zero for a perfect match. The X and Y axes (labelled K2_soma and Na_soma) are the scale factors for the densities of the fast potassium (Kfast) current in the soma, and the sodium (Na) current in the soma, respectively. Each grid division is a factor of $2^{1/3}$ (approx. 1.26) larger than the previous one. The range of the axes is from $2^{-16/3}$ to $2^{15/3}$. The location of the final model in parameter space (corresponding to a scale factor of 1 for all parameters) is represented by the *. The indicated lines 1 and 2 correspond to traces 1 and 2 in B. B: Variation of the match value when the density of a single channel is varied away from that of the final model. 1 to 6 are channels in the soma: Kfast, Na, Ca, K, KA, KCa. 7: Na in proximal secondary dendrites; 8: Ca in the glomerular tuft. All match values in A and B were calculated using the same set of weighting factors for the waveform matching function (Appendix A). Different weighting factors produce qualitatively very similar curves. Complete sets of parameter match values can be obtained from the authors.

Mitral cells

PASSIVE PROPERTIES. Hyperpolarizing current injections into the mitral cell produce charging curves with two time constants (Mori et al.; 1981a; Rall 1969) and provide an estimate for the cell's input resistance and electrotonic length. The model replicates these results when somatic membrane resistivity is lower than for the rest of the cell. As has been previously reported (e.g., Motoneurons: Segev et al. 1990; hippocampal granule cells: Yuen and Durand 1991), such a 'step model' for Rm is consistent with the existing experimental data. The model is tuned to replicate the 60 MΩ input resistance reported for turtle mitral cells (Mori et al. 1981a) impaled by an intracellular electrode. This input resistance is higher than obtained in intracellular recordings from other systems (e.g., cat spinal motoneurons: Rall 1977; hippocampal pyramidal cells: Schwartzkroin 1978). However, this upward revision is consistent with a trend towards higher estimates of membrane resistivity based on patch electrode recordings (Staley et al. 1992). When one removes this 'leak conductance' from the model and sets the somatic resistivity equal to that for the rest of the cell, the model predicts an input resistance of 120 MΩ. This figure is comparable to those obtained using whole-cell patch electrode recordings in salamander mitral cells (David P. Wellis, personal communication). and in the rat olfactory bulb slice preparation (Nickell 1992). The passive parameters for the final models for the mitral cell and its subclasses were: R_{axial} = 2.0 Ωm = 200Ω.cm; $R_{membrane}$ = 10.0Ω.m^2 = 100,000Ω.cm^2; $C_{membrane}$ = 0.01 F/m^2 = 1.0 μF/cm^2. Electrode damage was modeled as a leak conductance of 120 MΩ.

CHANNEL DISTRIBUTIONS. The final mitral cell model has 718 channels, on average, 2.5 channels per compartment.

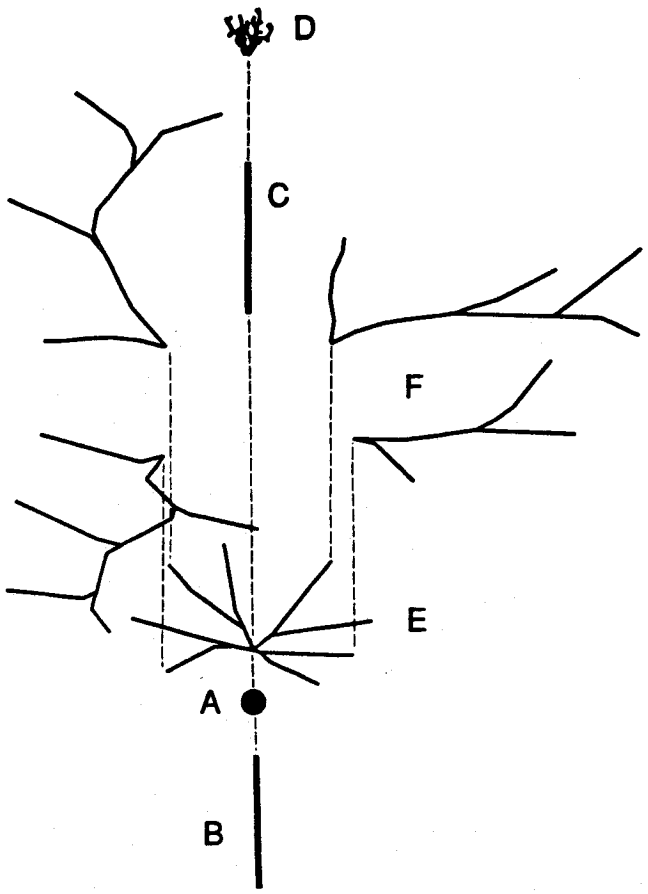

Figure 3: Regions for mitral cell parameter variations. The cell was subdivided into 6 regions, A to F. A: soma. B: axon. C: primary dendrite. D: glomerular tuft. E: proximal secondary dendrites. F: distal secondary dendrites. As described in the text, these regions were the basis for parameter variations. Within each region all channel densities are uniform, except for the axon. In the axon, the channel densites near the soma were greater, but the densities were always varied by a uniform scaling factor when doing paramter variations. The final values for channel densities are given in table 1 .

Table 1: Mitral cell channel distributions *

Region	Na	Kfast	LCa	K	KA	KCa
A:	soma	1532	1956	40	28	58.7
B:	axon †	4681	1541	20	15.5	51.5
C:	primary dendrite		13.4	12.3	22	17.4
D:	glomerular tuft		0	0	95	28
E: proximal secondary dend.	330	226	4	8.5	0	0
F: distal secondary dend.	122	128	0	0	0	0

* Channel densities are expressed as Siemens/square meter for the maximum conductance value $\bar{g}$ in the rate equation for the channel.

† The channel densities on the axon varied between compartments, the values for the most proximal are given.

Fast Na and K. These two channels are differentially distributed with the highest density occurring in the soma and axon initial segments (See Table 1). Previous modeling studies involving mitral cells (Rall and Shepherd 1968; Rall 1970) have incorporated corresponding spiking mechanisms in the axon and soma. High channel densities in these regions are in agreement with the classical description of a neuron and are required to replicate the sequence of M, A, and B spikes during antidromic activtion of the mitral cell. This spike sequence is interpreted as the successive activation of the myelinated axon (M), the axon initial segment (A), and the soma-dendritic membrane (B) (Mori et al. 1981a; Jahr and Nicoll 1982; Mori and Takagi 1975; Mori and Takagi 1978). As discussed in previous studies on olfactory bulb models (Rall and Shepherd 1968; Rall 1970), there is an impedance mismatch between the thin axon and the much larger soma which may lead to failure of antidromic spike propagation. Our study explicitly models the axon initial segment as a succession of short compartments with diameter increasing to match that of the soma, and with large Na and K channel densities. This leads to a satisfactory replication of experimental data relating to various phases of antidromic spikes. With respect to the dendrites, neither of these channels were included in the primary dendrites and glomerular tufts, but the best match to the observed spike waveforms required the inclusion of both at a lower but significant density in the secondary dendrites. Again, this is consistent with the earlier studies (Rall and Shepherd 1968; Rall 1970) where it was found that active dendritic compartments supported the rapid depolarization of the dendrites following antidromic spike invasion.

KA and KCa. The KA and KCa channels are present only in the soma and axon initial segments in our model. The simulations accurately reproduced experimental data for current injection in the presence of TEA and TTX with this simple arrangement (Figure 4 A).

Ca and slow K. The Ca and slow K channels are present everywhere except in the distal secondary dendrites. They are most concentrated in the glomerular tuft, at a lower density in the primary dendrite and soma, and still lower in the proximal secondary dendrites. This broad distribution gives a good approximation to experimental data (Figure 4 A) and also emerges from two additional considerations. First, it is known from experimental studies (Mori and Takagi 1975; Mori et al 1982; Jahr and Nicoll 1982; Wellis et al. 1989) that fast prepotentials occur when the olfactory nerve is

stimulated. This pathway synapses onto the glomerular region , which would therefore be a good candidate for the site of the prepotentials. Second, concentrating Calcium channels in the glomerular tuft alone is inconsistent with the large, sharp calcium spikes seen under current clamp in the presence of TEA and TTX (Figure 4 A,C).

Figure 4 compares experimental and simulated voltage traces obtained with this channel distribution. It can be seen that there is a good overall match between simulated and experimental results.

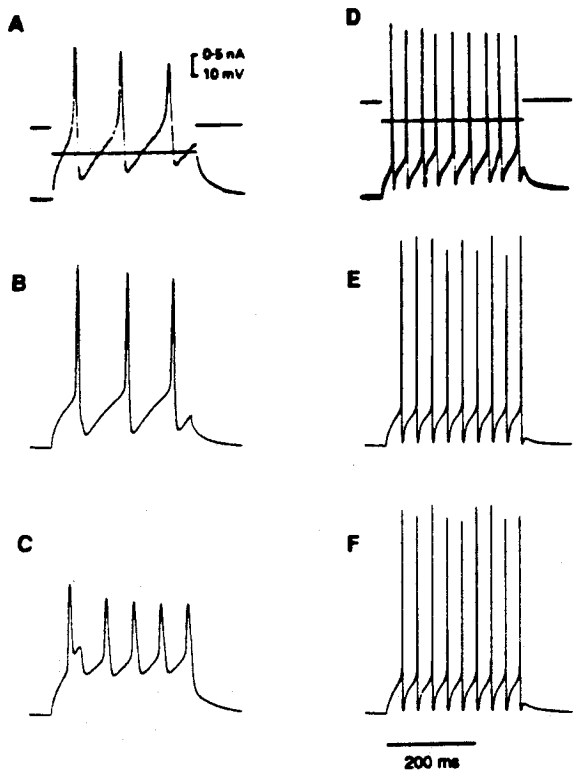

Figure 4: Experimental and simulated data for mitral cell. A: Current clamp recordings from mitral cell in the presence of 10^{-5} M TTX and $5x10^{-3}$ M TEA, injection current = 0.62 nA (reproduced with permission from Mori et al. 1981a) B: Simulated results under same conditions as A. The larger amplitude of the simulated spikes may be due to high-frequency cut-off in the recording apparatus. The model also uses a fixed Ca reversal potential of +70 mV which fails to take into account the lowered Nernst potential during the spike. C: Simulated results when model is without Ca in soma and vicinity. D: Current clamp recordings from mitral cell with injection current = 0.5 nA. (Reproduced with permission from Mori et al. 1981a) E: Simulated results under same conditions as D. The same factors as in B may affect spike height and width. F: Simulated results without modeled electrode damage. Current injection = 0.4 nA to compensate for increased input resistance of cell as compared to E.

APPLYING CELL PARAMETERS TO OTHER CLASSES OF MITRAL CELL. The passive properties and channel distributions obtained for the mitral cell model above were adapted to the other types of mitral/tufted cells studied. This process involves subdividing the cell into compartments according to their geometry, as was done for the mitral cell, and then placing similar channel densities in regions of the cells corresponding to the already calculated mitral cell model.

All four mitral cells produce similar sharp spikes with afterhyperpolarizations (Figure 5) and show similar patterns of propagation of spikes into the secondary dendrites (See Figure 11 below). This result, however, is highly dependent on the assumption of similar distributions of ion channels. One apparent difference between the cells is the latency to the first spike following current injection. This is due to the differences in passive properties of the cells (particularly input resistance and equalizing time courses), which is strongly dependent on cell geometry. The modeled data generally matches the experimental data in this regard.

There is notable similarity in spike waveform (Figure 5), passive properties (table 2) and the details of spike propagation into dendrites (Figure 11 A, turtle data is very similar) between the mitral cell and the 'turtle' mitral cell. Overall, the simulations reflect experimental findings suggesting a close correspondence between rabbit and turtle mitral cell properties.

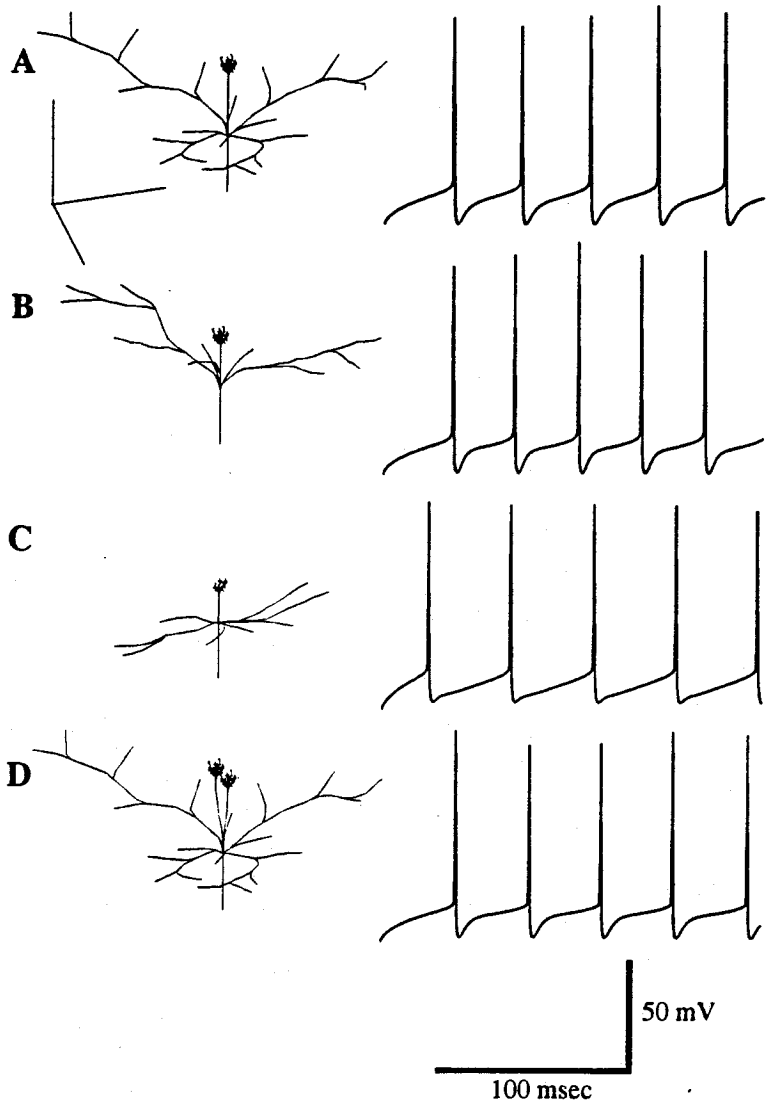

Figure 5: Different classes of modeled mitral cell. All models have assumed electrode leak at soma of 120 MΩ. Left hand column: cell geometries. Scale bars are 1 mm on each axis. Right hand column: Somatic recordings in response to current injection. A: Mitral cell, 0.5 nA current injection. B: Displaced mitral cell, 0.4 nA current injection. C: Tufted cell, 0.35 nA current injection. D: Turtle mitral cell with two primary dendrites, 0.75 nA current injection.

Table 2: mitral cell model properties *

CELL	N	NC	τ_0	τ_1	L	R_{input}
Mitral	286	718	59	6.2	1.1	60.9
Displaced Mitral	220	520	51	5.4	1.1	73.0
Tufted	133	331	36	3.6	1.0	84.6
Turtle	386	930	70	7.0	1.0	53.7

* Parameter explanations:

N: Number of compartments.

NC: Number of channels.

τ_0: First (charging) time constant of cell, in msecs.

τ_1: Second (equalizing) time constant of cell, in msecs.

L: Length of cell in length constants.

R_{input}: Input resistance of cell, in Megohms, including electrode leak.

Granule cells.

PASSIVE PROPERTIES. There is very limited information available for direct estimation of granule cell passive properties (Jahr and Nicoll 1982). Previously published data does however indicate a two-fold difference in time course between hyperpolarizing and repolarizing phases of a current pulse (Figure 8 A).

In the passive granule cell model, we have chosen to replicate the voltage trace of only the repolarizing phase because this is less likely to be contaminated by ion currents. Only one distinct time constant could be extracted from the available data. We have fitted this data using a similar assumption as for the mitral cell, that there is a constant membrane resistivity and an additional leak conductance in the soma due to the electrode. The values obtained for these parameters were 12 $\Omega.m^2$ = 120,000 $\Omega.cm^2$ and 200 MΩ respectively. The other passive properties were R_{axial} = 0.5 Ω.m = 50Ω.cm and $C_{membrane}$ = 0.01 F/m^2 = 1.0 $\mu F/cm^2$.

CHANNEL DISTRIBUTIONS. The parameter searches for the granule cells came up with three distinct sets of parameters (Figures 7 and 8) which provide a good match to experiment. It seems likely that there are many possible channel distributions which may fit the limited amount of available data. We describe the simplest set of parameters we found, in which the model has the smallest number of channels per compartment (Table 3).

The number of Hodgkin-Huxley type channels in the final model of the Type I granule cell is 162. These are distributed among 944 compartments. None of the channels are on the dendritic spines (Figure 6) in this model. The effects of including channels on the spines (Figure 8E) is dealt with in the discussion.

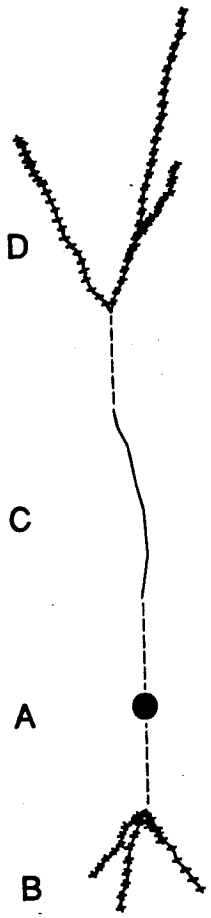

Figure 6: Regions for granule cell parameter variations. The cell was subdivided into 4 regions, A to D. A: soma. B: deep dendrites. C: trunk. D: peripheral dendrites. As described in the text, these regions were the basis for parameter variations. Within each region all channel densities are uniform. The values for channel densities are given in table 3.

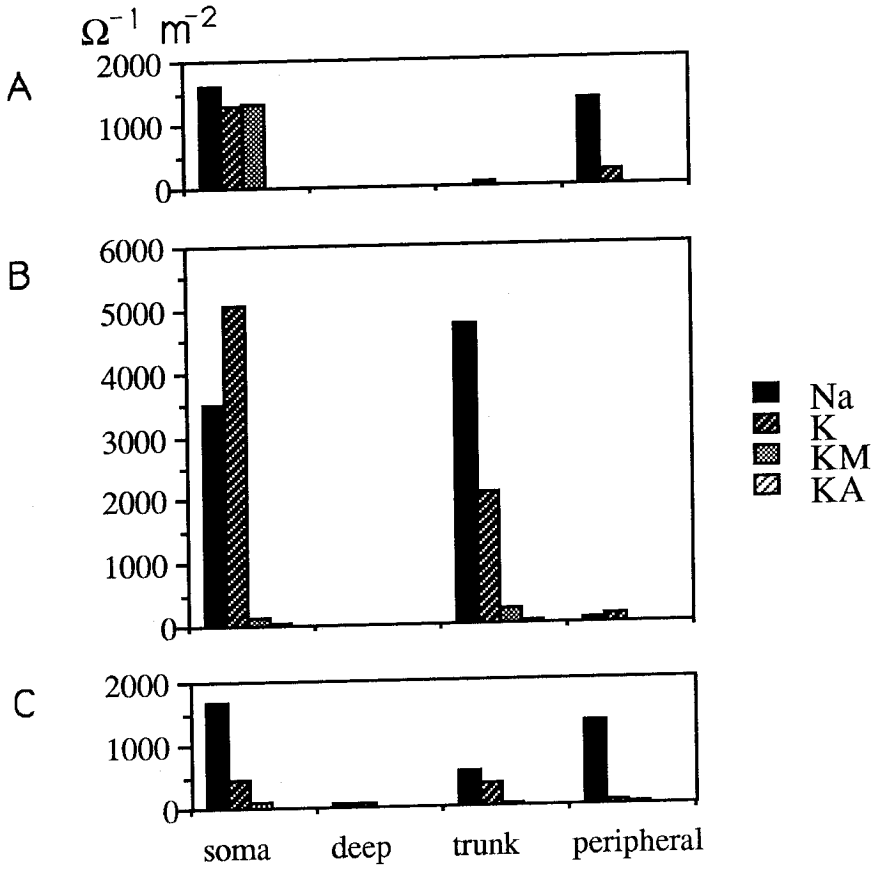

Figure 7: Channel distributions for 3 granule cell models. These all produced very close matches to experimental data (Figure 8). Each of the distributions was obtained as the result of an automated parameter search starting from a different initial set of parameters. A: Model 1. This model was selected for further analyses since it had the smallest number of channels. B: Model 2. This model is unlikely to be correct because of the very high channel densities involved; however, it gives a remarkably good match. The higher channel densities are reflected in the amplitudes and sharpness of the spikes (see Figure 8 C). C: Model 3. This had a more even distribution of Na_{gran} and K channels than the other models over the entire dendritic tree. It gives a good match to experimental data but is computationally expensive.

Table 3: Granule cell channel distributions * for model 1

Region	Na_{gran}	K	KM	KA
A: soma	1611	1313	1334	88
B: Deep dendrites	0	0	0	0
C: trunk	0	71	0	0
D: peripheral dendrites	1355	243	0	0

* Channel densities are expressed as Siemens/square meter for the maximum conductance value $\bar{g}$ in the rate equation for the channel.

Na_{gran} and K channels. These are distributed at high density in the soma and also in the peripheral dendrites. They are present at lower density in the trunk.

KM channels. This channel type is modeled in the soma alone. Their presence in the soma is clearly indicated (Yamada et al. 1989) by the increasing inter-spike interval (Figure 6A) under conditions of depolarizing current clamp. However, the relatively slow time course and the small electrotonic size of the cell as a whole combine to make it difficult to exclude the possibility that KM channels are also distributed throughout the dendritic arbor. In both cases the simulations generate similar results (Figure 7 A,C; Figure 8 B,D). It is also possible to replicate the increases in interspike interval using a combination of Ca channels, a Ca concentration pool, and Ca dependent K channels (Yamada et al. 1989). In the absence of further data on channel types and properties for these cells, we have adopted the alternative requiring fewer channel types.

KA channels. These are also modeled in the soma. Their presence is indicated by the long slow depolarizing phase of the spike waveform under current clamp (Yamada et al. 1989; Figure 8).

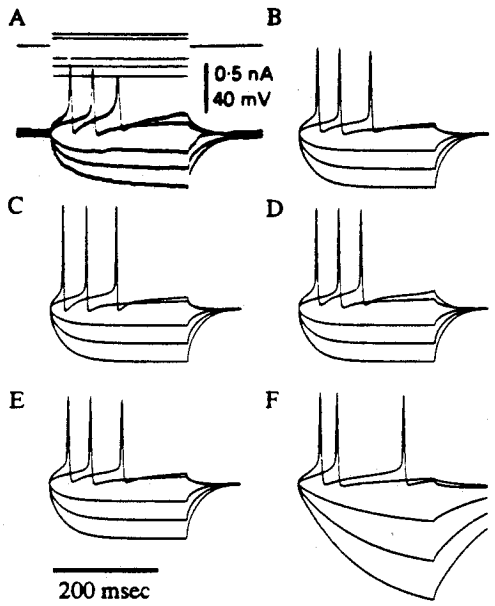

Figure 8: Experimental and simulated data for granule cell. A: Experimental data for current clamp series. (Reproduced with permission from Jahr and Nicoll, 1982.) B: Simulated data for model 1 of the granule cell, channel distribution as described in Table 3. Frequency limitations of recording apparatus may explain part of difference in spike heights. C: Simulated data for model 2 of the granule cell. D: Simulated results for modeled current clamp series for model 3 of the granule cell. E: Simulated results for model 1 with active channels modeled on spines rather than dendrites. This waveform is very similar to the waveform in B. F: Simulated results without electrode leak. All injection currents in F have been halved to compensate for the increased input resistance of the cell.

APPLYING CELL PARAMETERS TO OTHER CLASSES OF GRANULE CELLS. We generalized the model for the Type I granule cell to the other classes of granule cells, Type II and III. We assumed that the differences between the classes were purely in the morphology of the cells, and that the channels were distributed in the same way as in Type I cells. As with the mitral cells, the different geometries of the three granule cell classes led to different compartmental decompositions for the cell models.

Morphologically, different types of granule cells differ principally in the distribution of spines. Type I and II cells have spines mainly in the peripheral dendrites of the external plexiform layer, whereas type III granule cells also have spines on the deeper portions of the trunk (Greer 1987). We find that similar channel distributions produce similar spike waveforms for each of the different granule cell geometries (Figure 9). The differences in geometry and hence passive properties of the cells are reflected in the timing of the spikes.

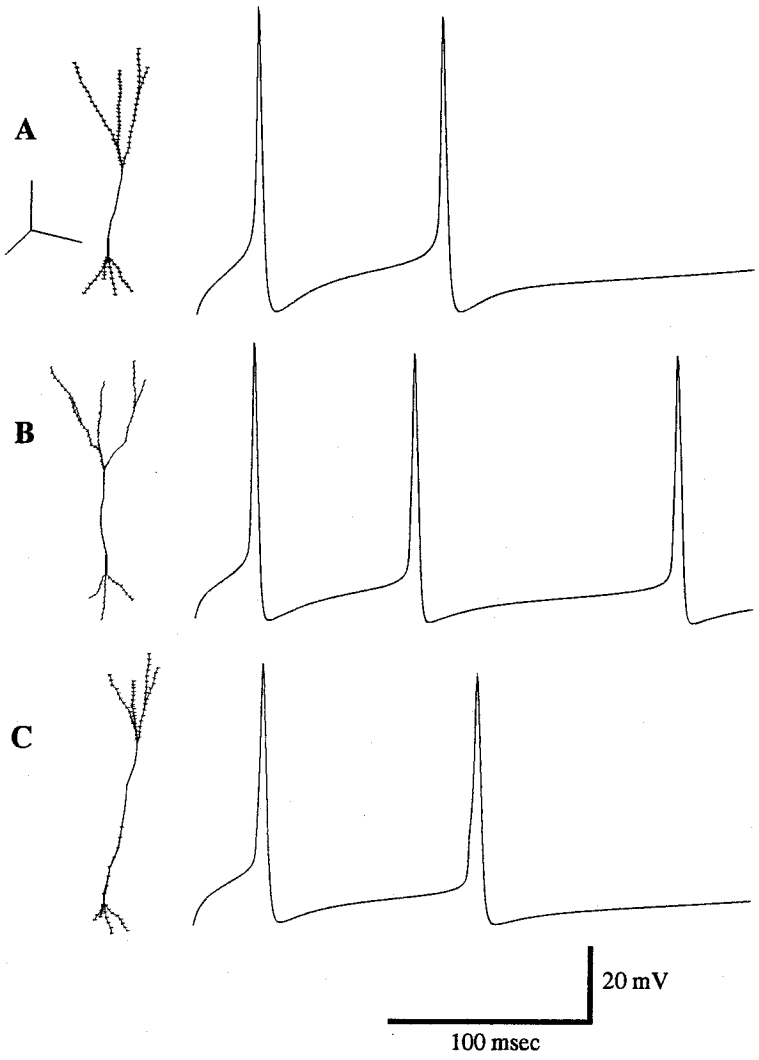

Figure 9: Different classes of modeled granule cells. Left hand column: cell geometries. Scale bars are 100 microns on each axis. Right hand column: responses to current injection of 0.125 nA. All models have assumed electrode leak at soma of 200 MW. A: Type I granule cell. B: Type II granule cell. C: Type III granule cell.

Table 4: granule cell model properties *

CELL	N	NC	τ_0	τ_1	L	
	R_{input}					
Type I	944	162	36	3.4	1.0	158.5
Type II	530	182	33	2.7	0.94	166.5
Type III	587	134	34	3.8	1.1	166.8

* The parameter names are the same as for table 2.

DISCUSSION AND MODEL PREDICTIONS

In these modeling experiments we have demonstrated that the spike waveforms generated by single neuron models are strongly dependent on channel distributions. Furthermore, the generation of physiologically realistic results requires a particular distribution of channels which may be uniquely determined if sufficient experimental information is available. We have presented a systematic approach to exploring the enourmous range of possible parameters which must be specified in any detailed neural simulation study.

The pioneering modeling studies on the olfactory bulb (Rall and Shepherd 1968; Rall 1970) showed that the details of the distribution of voltage dependent channels have a profound effect both on the behavior of individual neurons, and also on the predicted physiological properties of the bulb as a whole. More recent simulations of granule cells and spines (Shepherd and Brayton 1987; Shepherd et al. 1989; Woolf et al. 1991a) have highlighted the role that the details of single cell morphology and channel distribution may play in information processing. In this context it is clear that a more complete picture of the active properties of bulbar neurons is a prerequisite to a better understanding of the functioning of the olfactory bulb. The current modeling effort has explored the overall behavior of bulbar neurons using a full complement of active channels under a number of different experimental conditions. The results make specific predictions about the distributions of active channels and the physiological consequences of those distributions under specified experimental conditions.

Electrode leak and 'passive' properties of cells

The objective of this effort was to construct models which reflect the "natural" behavior of these neurons. Accordingly, our models have taken into account the effects of the experimental electrophysiological methods used to obtain the physiological records. While a complete description of electrode damage would almost certainly have to take into account complex factors such as changes in local ionic concentrations, diffusion, and the cytoskeleton of the cell, we have adopted the convention of

previous modeling efforts (e.g., Segev et al. 1990) and assumed that damage associated with the insertion of a recording electrode into a neuron primarily produces a lowered somatic resistance.

Based on data from current injections and input resistance (Mori et al. 1981a), we have included a leak resistance R_{leak} of 120 MΩ in the mitral cell models. A simple calculation shows that this leak resistance would be expected to give a much more depolarized value for final membrane potential than is actually observed. From Ohm's law:

$$V_{final} = E_{rest} \times (1/(1/R_{leak} + 1/R_m))/R_m = -65 \text{ mV} \times 60 \text{ MΩ} / 120 \text{ MΩ}$$

$$= -33 \text{ mV}$$

Where V_{final} is the potential produced due to the voltage divider formed by the leak and the summed membrane conductance (including the contributions due to channels). This contradiction between predicted and observed resting potentials can be resolved by postulating the presence of ion-selective channels (Pongracz et al. 1991) in addition to the non-ion selective current due to electrode damage. In our models a canditate for such a channel might be the non-inactivating voltage-dependent ion channel KM. As has been shown from comparisons of whole-cell patch recordings and conventional intracellular recordings (Staley et al. 1992), these channels produce a large inward current to compensate for the leak conductance due to electrode damage. Clearly, the approximation of a voltage-dependent channel as a linear membrane resistance is valid only if the kinetics of the compensating current are much slower than any fluctuations of membrane potential. This assumption is very likely to be good for the relatively rapid time courses of neuronal spiking which we are investigating. This condition is not met, however, when long hyperpolarizing current injection pulses are used to estimate membrane time courses. For example, in the granule cell (Figure 8 A) the time course for the hyperpolarizing phase is much longer (by a factor of 2) than the time course for repolarization back to resting potential. Thus, the granule cell data is consistent with the postulate that a K current is active at 'resting' potentials, thereby affecting the charging curve. For this reason our calculations of the passive properties of the granule cell model were based on the repolarizing phase of the current pulse, since the current is likely to be inactive at more hyperpolarized potentials (Figure 8 A).

In several simulations we have removed the electrode leakage current to estimate the response properties of cells that have not been impaled. Under these conditions we have found very little effect on the spike rates and waveforms produced by the models (Figure 4F, Figure 8F) when the injection currents are compensated for the change in input resistance. Presumably this lack of effect on cellular output is due to the fact that ionic conductances during an action potential are much larger than the leak conductance introduced by the electrode.

Active channels on mitral cell dendrites.

There is considerable experimental evidence that mitral cell dendrites have active properties. For example, fast pre-potentials are observed in mitral cell somas when the olfactory nerve is stimulated (Mori et al. 1981b; Mori and Takagi 1975; Mori et al. 1982). Further, these prepotentials persist when a hyperpolarizing current is simultaneously presented to the soma, suggesting a dendritic origin. Earlier theoretical studies of the bulb (Rall and Shepherd 1968) also proposed active dendrites in order to match the experimental data then available. Our simulations likewise predict the presence of dendritic spikes, both in the glomerulus and in the secondary dendrites (Figures 10 and 11). Thus the model supports the previous interpretations of these experimental results.

PREDICTIONS. Further exploration of the spike generating mechanism in the dendrites of mitral cells has suggested an experimental means of further testing the distribution of ion channels predicted here. Specifically, we have found that voltage clamping the model's soma at depolarizing potentials around spike threshold can reveal several properties of the mitral cell dendrites.

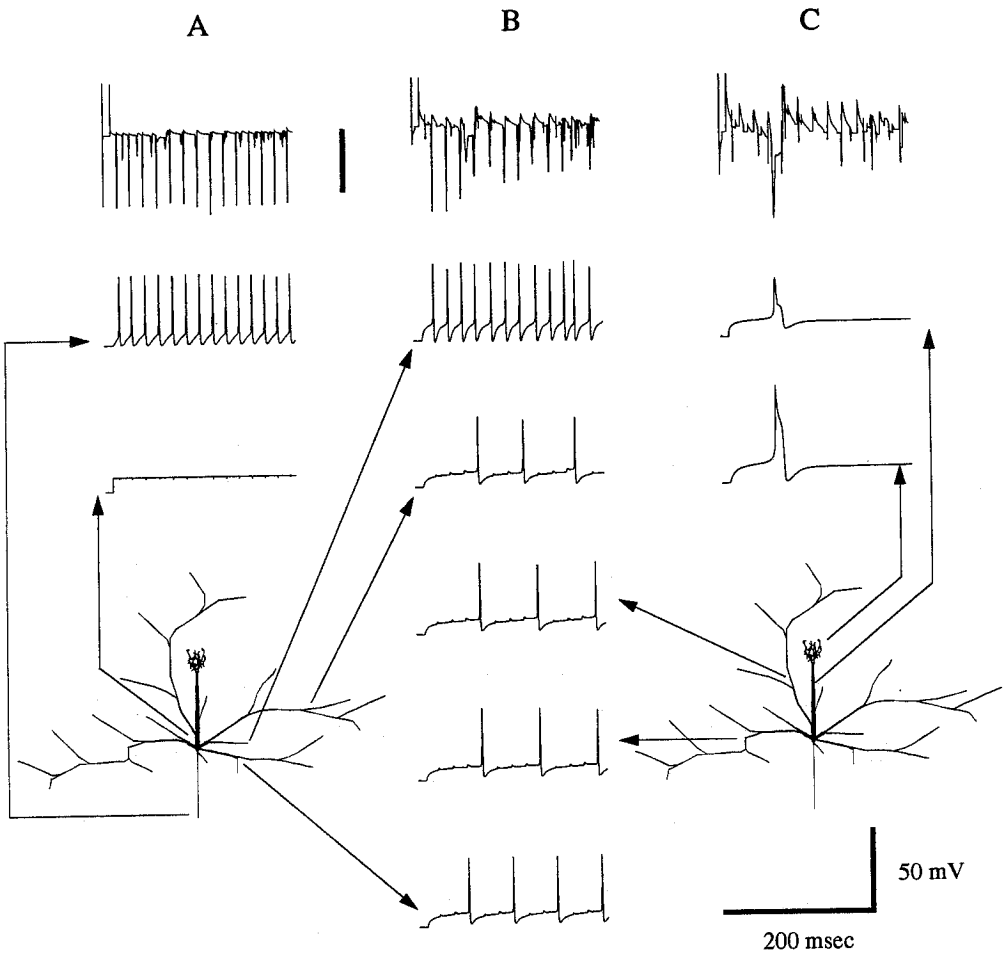

Figure 10: Voltage clamp at mitral cell soma. Recording sites are indicated on the figures of the mitral cell. A: Upper trace: Current recording from voltage clamp electrode. Scale bar is 20 nA. Middle trace: voltage recording at axon. Lower trace: Clamped voltage (-47.5 mV) recorded at soma. B: Upper trace: Current recording with large axonal spikes subtracted out. Scale bar = 5 nA. Lower traces: recordings from various locations on the secondary dendrites. The spikes are out of synchrony with each other but tend to be individually periodic. C: Upper trace: Current recording with axonal and secondary dendritic spikes removed. Scale bar = 2 nA. Middle trace: recording from primary dendrite. Lower trace: recording from glomerular tuft. The much wider Ca spike is reflected in the width of the corresponding current event.

Figure 10 A shows the current record produced by the somatic voltage clamp in the model. As can be seen in the axonal voltage recording below the current record, the large current spikes correspond to action potentials generated in the spike initiation zone modeled here in the proximal axonal compartments. However, when this contribution to the current is subtracted (Figure 10 B), a number of small current peaks occurring at different times remain. Comparison of this current record with voltage traces taken from the different dendritic branches reveals that these currents are a direct result of the local active properties of these dendrites. Closer examination of this record reveals current events with two different durations. When the secondary dendritic spikes are also removed from the current trace (Figure 10 C), a correspondence between the broader current peak and the calcium spike in the glomerular tuft and primary dendrite is evident.

If our model is correct, a single cell voltage clamp near threshold in the soma of a mitral cell should reveal all three types of current events. Our interpretation of this phenomenon is that the large physical and electrotonic size of the mitral cell makes it difficult to generate a good whole cell space clamp. Consequently, a somatic voltage clamp will only keep regions near the soma at the holding potential, while more distal regions are able to vary in potential. As shown in Figure 10, the active properties of these regions combined with the spread of depolarization from the near spike threshold somatic voltage clamp, result in the generation of dendritic electrical events which propagate back to the soma and are seen in the current trace. Further, because the soma is voltage clamped, the large dendrites are effectively decoupled from each other and generate independent events at a rate determined by their individual local properties.

In the context of the current modeling effort, the occurrence of small amplitude events in the current records of a somatic voltage clamp of a mitral cell would strongly support the existence of active properties in the dendrites of these cells. Recent results from whole-cell recordings from mitral cells (Bufler et al. 1992, David P. Wellis, personal communication) indicate that such multiple current events are indeed visible. A careful evaluation of the amplitudes and distributions of these spikes might make it possible to determine if there are differential thresholds for spiking activity in different dendrites. This,

in turn, might indicate different electrotonic distances of the dendrites from the point of voltage clamp, or different local channel distributions. Distinguishing between these possibilities, however, will require further detailed simulations of the sort described here.

FUNCTIONAL SIGNIFICANCE. On the basis of several studies demonstrating pre-potentials (Mori and Takagi 1975; Mori et al 1982; Jahr and Nicoll 1982; Wellis et al. 1989), the mitral cell glomerular tuft is believed to possess active channels. Taken in conjunction with the electrotonic distance of the tuft from the mitral cell soma, this has led to general agreement that the glomerular tuft may take part in local processing and amplification of incoming synaptic input from the olfactory nerve. (Rall and Shepherd 1968; Jahr and Nicoll 1982; Mori et al. 1982; Wellis et al. 1989). Our simulations also incorporate active channels in the primary dendrites and are consistent with this view. We also observe that, in addition to the amplification of synaptic input, the active channels in the glomerular tuft lead to interesting interactions with somatic spikes.

Figure 11: Spike propagation into mitral cell dendrites. A: Antidromic stimulation of mitral cell, shown at 1.5 msec intervals. B: Failure of spike propagation into secondary dendrite. Antidromic stimulation on axon, with hyperpolarization (0.5 nA current injection) on secondary dendrite 1 (in the first quadrant with respect to the soma). Shown at 1.5 msec intervals. C: Antidromic stimulation with glomerular tuft initially depolarized to -20 mV. The somatic spike leads to a glomerular dendritic Ca spike, which causes a second somatic spike, shown at 3.0 msec intervals.

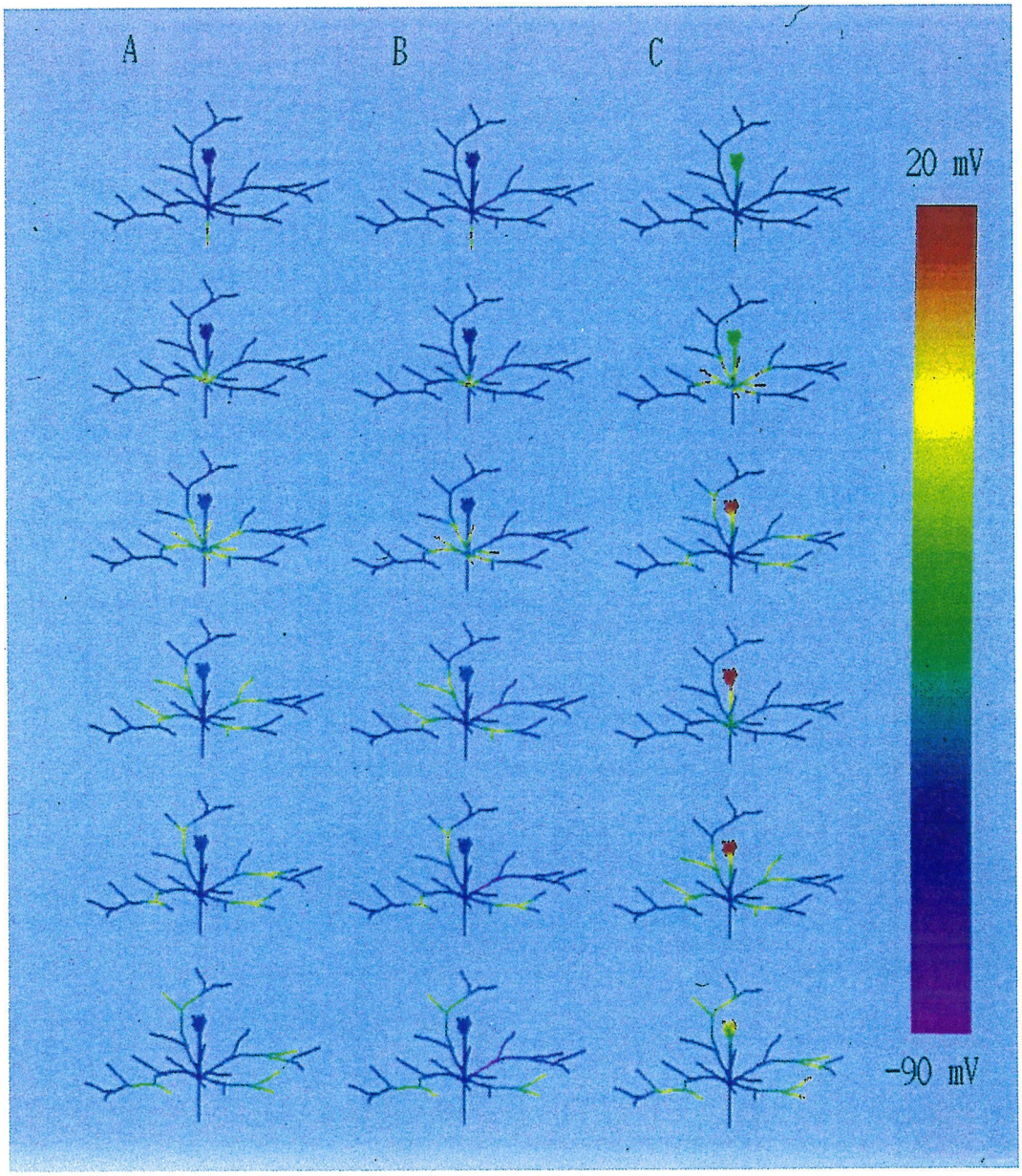
A
B
C
20 mV
-90 mV

In the non-physiological situation where spikes are being initiated at the soma by current clamp or antidromic stimuli, action potentials may propagate into the glomerulus to initiate a calcium spike (Figure 11 C). This process depends on the previous level of depolarization in the tuft. The long-lasting depolarization due to the calcium spike in the glomerular tuft may cause the initiation of a second somatic spike. Thus the model predicts a conditional propagation of spikes into the glomerulus from the soma, and vice versa, depending on the state of the cell. Similar interactions between dendritic calcium spikes and somatic action potentials has also been modeled in several other neuronal classes such as hippocampal pyramidal neurons (Traub and Llinas 1979) and Purkinje cells from the cerebellum (De Schutter and Bower 1991).

In a more physiological context, our model clearly suggests that the presence of active channels in mitral cell dendrites should support the propagation of somatic action potentials into the secondary dendrites (Figure 11 A). This propagation has been previously considered in modeling studies (Rall and Shepherd 1968) but interpretations were deferred pending additional experiments. Such dendritic spike propagation is very interesting when considered in the context of the dendro-dendritic synapses known to occur between mitral cell secondary dendrites and granule cells (e.g., Rall and Shepherd 1968; Mori 1987). In effect these dendrites may act rather like axons in conveying information in an all-or-nothing manner to the granule cells. One manifestaton of this sort of all-or-nothing behavior is seen in intracellular recordings from mitral cells with paired-pulse stimulation of the LOT (e.g., Mori and Takagi 1978). In this case the second pulse fails to elicit a somatic spike, and the ipsp at the mitral cell soma due to the second pulse is depressed. This is interpreted as a reduction in the dendrodendritic inhibition from the granule cell due to the spike blockage at the mitral cell soma (Rall and Shepherd 1968). Our model suggests that a similar, but finer control may be exerted at the level of the individual secondary dendritic branch. For example, as shown in Figure 11 A and B, action potential propagation is quite sensitive to the previous membrane potential of local regions of the dendrite. As a result, spike propagation into secondary dendrites can be blocked by a local hyperpolarization (Figure 11 B). In this way, inhibitory feedback from granule cells could block spike propagation along individual mitral cell

secondary dendrites and thereby alter the information received by granule cells in contact with those branches at points more distant from the soma. Theoretical studies (Manor et al. 1991) have investigated the computational implications of conditional failure of spike propagation in axons. Such a blockage of spikes propagating outward from the soma along individual dendrites, if correct, would be a form of information processing which has not yet been described in other parts of the mammalian CNS.

Active channels on granule cell dendrites.

As mentioned earlier, there have been many speculations on the role of active channels in granule cell dendrites, and their precise location, on the computational role of these cells (Rall and Shepherd 1968; Shepherd and Brayton 1987; Shepherd et al. 1989; Woolf et al. 1991a,b). Our present study is confined to single cell models, and therefore does not address many of these issues directly. We have used our granule cell model to test whether any predictions could be made about the exact location of active channels on the spines or on their parent dendrites. Specifically, under somatic current clamp we held the total conductance due to the respective ion channels fixed while placing channels on either the dendrites or on the spine-heads emerging from them. The results, shown in Figure 8 E, indicate that one cannot differentiate between these two possibilities using the simple somatic current clamp approach.

Whole bulb models

Ultimately, understanding the interaction of the active properties of the mitral cell on the granule cell and the consequences of this interaction on the computation performed by the olfactory bulb will require the study of network models of the entire bulb (Rall and Shepherd 1968; Rall 1970; White et al. 1992; Meredith 1992; Anton et al. 1991; Schild and Riedel 1992; Freeman et al. 1988; Li and Hopfield 1989). In this regard, the single cell modeling effort just described is a preliminary step towards the development of detailed, realistic models of the bulb as a whole. Many of the questions raised by single

cell recordings are best addressed in the context of a network, where the ramifications of active neuronal properties can be more fully explored. This effort will undoubtedly further illuminate the complexities of these cells as well as the network in which they are embedded.

CONCLUSIONS

These simulations have made both general and specific predictions about voltage dependent channel distributions in the dendrites of mitral and granule cells. The results confirm interpretations of previous experimental work as well as make specific experimental predictions which can be used to further experimentally test the accuracy of the models. Further, they suggest several functional consequences for the processing performed in these cells.

Beyond the significance of model results for function of the olfactory bulb, in this paper we have also presented a more thorough than usual search of model parameter space. The more complete mitral cell results suggest that real neurons may operate in ranges that are relatively robust with respect to physical variations. In some cases, for example, differences in channel densities of up to an order of magnitude produce relatively little change in the model output. Substantial changes in membrane properties, such as the presence or absence of electrode leak at the soma, were also shown to cause relatively small effects on the spike waveforms. Even applying the calculated channel distributions to substantially different morphologies, for different classes of mitral and granule cells, does not markedly affect the spiking properties of the cell models.

We believe these results have important implications for future modeling efforts. First, the search for the 'correct' model can only be conducted up to a certain level of precision, because members of the same class of neurons may experience variability below that level. Second, there are likely to be whole classes of models which are all equally correct as far as reproducing the data is concerned. In the absence of further experimental data constraining the model one way or another, considerations of aesthetics, efficiency, or ideas about function will continue to decide the model chosen. We believe it is the modeler's obligation to indicate, as far as possible, the range of models which might fit the data.

ACKNOWLEDGMENTS.

The authors are grateful to Dr. Erik De Schutter for many helpful discussions and valuable insights into these modeling efforts. The early phase of this work owes a great deal to the assistance of Dr. Matt Wilson and Dr. Mark Nelson. The port of GENESIS to the Delta, on which many of these simulations were performed, was carried out by Dr. Michael Speight. We would also like to thank D. Bilitch and J. Uhley for their technical assistance.

This work was supported by ONR contract number N00014-88-K-0513 and NSF grant number DIR 9017153 .

REFERENCES.

ADAMS, D. J., SMITH, S. J., AND THOMPSON, S. H. Ionic currents in molluscan soma. *Ann. Rev. Neurosci.* 3: 141-167, 1980.

ALDRICH, R.W. JR., GETTING, P.A., AND THOMPSON, S.H. Inactivation of delayed outward current in molluscan neurone somata. *J. Physiol. Lond.* 291: 507-530, 1979.

ANTON, P.S., LYNCH, G., AND GRANGER, R. Computation of frequency-to-spatial transform by olfactory bulb glomeruli. *Biol. Cybern.* 65: 407-414, 1991.

BELLUZZI, O., AND SACCHI, O. A five-conductance model of the action potential in the rat sympathetic neurone. *Prog. Biophys. molec. Biol.* 55: 1-30, 1991.

BHALLA, U. S., BILITCH, D. H., AND BOWER, J. M. Rallpacks: A set of benchmarks for neuronal simulators. *TINS* 15(11): 453-458, 1992.

BUFLER, J., ZUFALL, F., FRANKE, C., AND HATT, H. Patch-clamp recordings of spiking and nonspiking interneurons from rabbit olfactory bulb slices: Membrane properties and ionic currents. *J. Comp. Physiol. A.* 170:145-152, 1992.

CONNOR, J. A., AND STEVENS, C. F. Prediction of repetitive firing behaviour from voltage clamp data on an isolated neurone soma. *J. Physiol. Lond.* 213: 31-53, 1971.

COOLEY, J. W., AND DODGE, F. A. Digital computer solutions for excitation and propagation of the nerve impulse. *Biophys J.* 6: 583-599, 1966.

DE SCHUTTER, E., AND BOWER J. M. A computer simulation of plateau potentials and synaptic interactions in Purkinje cell spiny dendrites. *Soc. Neurosci. Abstr.* 21: 1383, 1991.

EGAN, T. M., DAGAN, D., KUPPER, J., AND LEVITAN, I. B. Properties and rundown of sodium-activated potassium channels in rat olfactory bulb neurons. *J. Neurosci.* 12 (5): 1964-1976, 1992.

ENNS, S. Free-Form curves on your micro. *Byte* 12: 225-230, 1986.

FITZHUGH, R. Impulses and physiological states in theoretical models of nerve membrane. *Biophys. J.* 1:445-466, 1961.

FREEMAN, W. J., YAO, Y., AND BURKE, B. Central pattern generating and recognizing in olfactory bulb: a corrleation learning rule. *Neural Networks* 1: 277-288, 1988

GREER, C. A. Golgi analysis of dendritic organization among denervated olfactory bulb granule cells. *J. Comp. Neurol.* 257: 442-452, 1987.

HABERLY, L., AND PRICE, J. L. The axonal projection patterns of the mitral and tufted cells of the olfactory bulb in the rat. *Brain Res.* 129: 152-157, 1977.

HINES, M. Efficient computation of branched nerve equations. *Int. J. Bio-Medical Computing.* 15: 69-76, 1984.

HIRANO, T., AND HAGIWARA, S. Kinetics and distribution of voltage-gated Ca, Na and K channels on the somata of rat cerebellar Purkinje cells. *Pflugers Arch.* 413: 463-469, 1989.

HODGKIN, A. L., AND HUXLEY, A. F. A quantitative description of membrane current and its application to conduction and excitation in nerve. *J. Physiol. Lond.* 117: 500-544, 1952.

JACK, J. J. B., NOBLE, D., AND TSIEN, R. W. Electric current flow in excitable cells. Oxford. Oxford University Press, 1983.

JAHR, C. E., AND NICOLL, R. A. An intracellular analysis of dendrodendritic inhibition in the turtle in vitro olfactory bulb. *J . Physiol. Lond.* 326: 213-234, 1982.

KOCH, C., AND BOWER, J. M. Experimentalists and modelers: can we all just get along? *TINS* 15(11): 458-461, 1992.

LI, Z, AND HOPFIELD, J.J. Modeling the olfactory bulb and its neural oscillatory processing. *Biol. Cybern* 61(5): 379-392, 1989.

MANOR, Y., GONCZAROWSKI, J., AND SEGEV, I. Propagation of action potentials along complex axonal trees. Model and implementation. *Biophys. J.* 60:1411-1423, 1991.

MASCAGNI, M. Numerical methods for neuronal modeling. In: *Methods in Neuronal Modeling: from Synapses to Networks.* Edited by C. Koch and I. Segev, Cambridge. MIT Press, 1989, p. 439-484.

MEREDITH, M. Neural circuit computation: complex patterns in the olfactory bulb. *Brain Res. Bull.* 29: 111-117, 1992.

MORI, K., AND KISHI, K. The morphology and physiology of the granule cells in the rabbit olfactory bulb revealed by intracellular recording and HRP injection. *Brain Res.* 247: 129-133, 1982.

MORI, K., KISHI, K., AND OJIMA, H. Distribution of dendrites of mitral, displaced mitral, tufted, and granule cells in the rabbit olfactory bulb. *J. Comp. Neurol.* 219: 339-355, 1983.

MORI, K., NOWYCKY, M. C., AND SHEPHERD, G. M. Electrophysiological analysis of mitral cells in the isolated turtle olfactory bulb. *J. Physiol. Lond.* 314: 281-294, 1981a.

MORI, K., NOWYCKY, M. C., AND SHEPHERD, G. M. Analysis of synaptic potentials in mitral cells in the isolated turtle olfactory bulb. *J. Physiol. Lond.* 314: 295-309, 1981b.

MORI, K., NOWYCKY, M. C., AND SHEPHERD, G. M. Impulse activity in presynaptic dendrites: analysis of mitral cells in the isolated turtle olfactory bulb. *J. Neurosci.* 2 (4): 497-502, 1982.

MORI, K., AND TAKAGI, S. F. Spike generation in the mitral cell dendrite in the rabbit olfactory bulb. *Brain Res.* 100: 685-689, 1975.

MORI, K., AND TAKAGI, S. F. An intracellular study of dendrodendritic inhibitory synapses on mitral cells in the rabbit olfactory bulb. *J. Physiol. Lond.* 279: 569-588, 1978.

MORI, K., Membrane and synaptic properties of identified neurons in the olfactory bulb. *Progress in Neurobiology.* 29: 275-320, 1987.

NICKELL, W.T., BEHBEHANI, M.M., AND SHIPLEY, M.T. *In vitro* synaptic activation of adult rat olfactory bulb mitral cells recorded by conventional and whole cell patch techniques. *Soc. Neurosci. Abstr.* 18: 1200-1200, 1992.

PONGRACZ, F., FIRESTEIN, S., AND SHEPHERD, G. M. Electrotonic structure of olfactory sensory neurons analyzed by intracellular and whole cell patch techniques. *J. Neurophysiol.* 65: 747-758, 1991.

PRESS, W. H., FLANNERY, B. P., TEUKOLSKY, S. A., AND VETTERLING, W. T. *The Art of Scientific Computing.* Cambridge, U.K. CUP, 1988.

PRICE, J. L., AND POWELL, T. P. S. The mitral and short axon cells of the olfactory bulb. *J. Cell Sci.* 7: 631-651, 1970.

PRICE, J. L., AND POWELL, T. P. S. The morphology of the granule cells of the olfactory bulb. *J. Cell Sci.* 7: 91-123, 1970.

RALL, W. Branching dendtritic trees and motoneuron membrane resistivity. *Exp. Neurol* 1: 491-527, 1959.

RALL, W. Theoretical significance of dendtritic trees for neuronal input-output relations. In: *Neural theory and modeling*. Edited by R. Reiss Stanford. Stanford University Press, 1964, p. 73-97.

RALL, W., SHEPHERD, G.M., REESE, T.S., AND BRIGHTMAN, M.W. Dendrodendritic synaptic pathway for inhibition in the olfactory bulb. *Exp. Neurol.* 14:44-56, 1966.

RALL, W., AND SHEPHERD, G. M. Theoretical reconstruction of field potentials and dendrodendritic synaptic interactions in olfactory bulb. *J. Neurophysiol.* 31: 884-915, 1968.

RALL, W. Time constants and electrotonic length of membrane cylinders and neurons. *Biophys. J.* 9: 1483-1508, 1969.

RALL, W. Dendritic neuron theory and dendrodendritic synapses in a simple cortical system. In: *The Neurosciences. Second Study Program.* Edited by F. O. Schmitt. New York. Rockefeller University Press, 1970. p. 552-565.

RALL, W., AND RINZEL, J. Branch input resistance and steady attenuation for input to one branch of a dendritic neuron model. *Biophys. J.* 13: 648-688, 1973.

RALL, W. Core conductor theory and cable properties of neurons. In: *Handbook of physiology,* sect. 1, *The Nervous System*, vol. 1. *Cellular biology of neurons*. Edited by E. R. Kandel. Bethesda. American Physiological Society, 1977, p. 39-97.

RALL, W. Perspectives on neuron modeling. In: *The Segmental Motor System.* Edited by Binder, M.D., and Mendell, L.M. New York. Oxford University Press, 1990, p. 129-149.

SCHILD, D., AND RIEDEL, H. Significance of glomerular compartmentalization for olfactory coding. *Biophys. J.* 61: 704-715.

SCHWARTZKROIN, P.A. Secondary range rhythmic spiking in hippocampal neurons. *Brain Res.* 149: 247-250.

SEGEV, I., FLESHMAN, J. W., AND BURKE, R. E. Computer simulation of group 1a EPSPs using morphologically realistic models of cat a-motoneurons. *J. Neurophysiol.* 64(2): 648-660, 1990.

SHEPHERD, G. M., AND BRAYTON, R. K. Logic operations are properties of computer-simulated interactions between excitable dendritic spines. *Neurosci.* 21(1): 151-165, 1987.

SHEPHERD, G. M. Canonical neurons and their computational organization. In: *Single Neuron Computation.* Edited by T. McKenna, J. Davis and S. F. Zornetzer. San Diego. Academic Press Inc. 1992, p. 27-60.

SHEPHERD, G. M., WOOLF, T. B., AND CARNEVALE, N. T. Comparisons between active properties of distal dendritic branches and spines: implications for neuronal computations. *J. Cog. Neurosci.* 1(3): 273-286, 1989.

STALEY, K. J., OTIS, T. S., AND MODY, I. Membrane properties of dentate gyrus granule cells: comparison of sharp microelectrode and whole-cell recordings. *J. Neurophysiol.* 67 (5): 1346-1358, 1992.

STUHMER, W., METHFESSEL, C., SAKMANN, B., NODA, M., AND NUMA, S. Patch clamp characterization of sodium channels expressed from rat brain cDNA. *Eur. Biophys. J.* 14: 131-138, 1987.

TRAUB, R.D., AND LLINAS, R. Hippocampal pyramidal cells: significance of dendritic ionic conductances for neuronal function and epileptogenesis. *J. Neurophysiol.* 42(2): 476-496, 1979.

TRAUB, R. D. Simulation of intrinsic bursting in CA3 hippocampal neurons. *Neurosci.* 7(5): 1233-1242, 1982.

TROMBLEY, P.Q., AND SHEPHERD, G.M. Noradrenergic inhibition of synpatic transmission between mitral and granule cells in mammalian olfactory bulb cultures. *J. Neurosci.* 12(10): 3985-3991, 1992.

WELLIS, D. P., AND SCOTT, J. W. Intracellular responses of identified iat olfactory bulb interneurons to electrical and odor stimulation. *J. Neurophysiol.* 64(3): 932-947, 1990.

WELLIS, D. P., SCOTT, J. W., AND HARRISON, T. A. Discrimination among odorants by single neurons of the rat olfactory bulb. *J. Neurophysiol.* 61(6): 1161-1177, 1989.

WHITE, J., HAMILTON, K. A., NEFF, S. R., AND KAUER J. S. Emergent properties of odor information coding in a representational model of the salamander olfactory bulb. *J. Neurosci.* 12(5): 1772-1780, 1992.

WILSON, M. A., BHALLA, U. S., UHLEY, J. D., AND BOWER, J. M. Genesis: A system for simulating neural networks. In: *Advances in Neural information processing systems, Vol 1.* Edited by D. Touretzky. San Mateo, Morgan Kaufman Publishers, 1989, p. 485-492.

WILSON, M., AND BOWER, J. M. Cortical oscillations and temporal interactions in a computer simulation of piriform cortex. *J. Neurophysiol.* 67(4): 981-995, 1992.

WOOLF, T. B., SHEPHERD, G. M., AND GREER C. A. Local information processing in dendritic trees: subsets of spines in granule cells of the mammalian olfactory bulb. *J. Neurosci.* 11(6): 1837-1854, 1991a.

WOOLF, T. B., SHEPHERD, G. M., AND GREER C. A. Serial reconstructions of granule cells spines in the mammalian olfactory bulb. *Synapse* 7: 181-192, 1991b.

YAMADA, W. M., KOCH C., AND ADAMS P. R. Multiple channels and calcium dynamics. In: *Methods in neuronal modeling: from synapses to networks* edited by C. Koch and I. Segev. Cambridge. MIT Press, 1989. p. 97-133.

YUEN, G.L.F., AND DURAND, D. Reconstruction of hippocampal granule cell electrophysiology by computer simulation. *Neuroscience* 41(2/3): 411-423, 1991.

APPENDIX A. QUANTITATIVE COMPARISON OF MODELED AND REAL DATA.

In order to automate the parameter search, it is necessary to quantify the similarity between simulated and experimental data for each set of parameters. The 'goodness' of our model parameters is evaluated by running a simulation using those parameters under the appropriate experimental conditions. The output from this simulation has then to be compared with intracellular voltage recordings, and some measure of similarity evaluated. The measure of match we use here is computed by comparing a number of different features of the simulated and reference waveforms. These include:

1) Shape of voltage wave forms. The non-spiking phase of each spike waveform is scaled to match on the time-axis, and directly compared using root-mean-squared difference over all the sample points. Linear interpolation is used when the sampling intervals for the two curves are different. The rms value is normalized to a typical spike amplitude of 100 mV (0.1 V in the equation since the simulation uses SI units). The additional square-root is an empirical means of keeping the scaling commensurate with the other measures.

$$Shape\_match = \sqrt{(\sqrt{(\Sigma(V_{ref} - V_{sim})^2) / (0.1 n_{points})})}$$

2) Inter-spike intervals. The time between spikes is calculated and corresponding intervals are compared. The ISIs are compared as the sum of the ratio and inverse ratio, to ensure that all changes from unity result in an increase in the measure of difference. The final sum is normalized to the number of spikes and scaled as an inverse exponential to keep the scaling commensurate with the other measures.

$$ISI\_match = 1 - \exp(-(\Sigma(ISI_{ref}/ISI_{sim} + ISI_{sim}/ISI_{ref} - 2)/n_{spikes}))$$

3) Peak-to-peak amplitudes. The amplitudes of corresponding spikes are compared using rms:

$$PTP\_match = (\sqrt{\Sigma(PTP_{ref} - PTP_{sim})^2})/n_{spikes}$$

These three measures of spike waveform similarity are combined using weighting factors determined by the user. We have also used other matching functions, which give similar results for parameter searches.

APPENDIX B. AUTOMATED SEARCHING OF PARAMETER SPACE.

There are at least three commonly used numerical methods for exploring parameter space: brute force, a systematic search based on successive approaches to the final point, and Monte Carlo methods. Our study has employed the first two.

BRUTE FORCE PARAMETER SEARCHES. If each dimension in parameter space is sampled at a fixed number of points, one can in principle exhaustively evaluate every sample point in the parameter space. However, this rapidly becomes intractable for large parameter spaces, such as in our models. For example, in the mitral cell, we use 6 channel types and subdivide the cell into 6 regions, giving a total of 36 parameters. In order to search such a parameter space even at a very coarse sampling of 6 values per dimension, we would require 6^{36} (approx. 10^{28}) simulations. In order to reduce the number of simulations to a more tractable value, we have adopted the following simplifications:

1. Intrinsic model constraints. Experimental information often enables one to eliminate large numbers of parameters from consideration. For example, in the mitral cell model under conditions of TEA and TTX application, two classes of channel (Na and fast K) were assumed to be completely blocked. This reduces the number of free parameters from 36 to 24.

2. Lumping regions together. For the purposes of searching, one can choose to lump certain regions of the cell together and vary the channel densities uniformly within the lumped regions. We were able to perform searches of 6 parameters at 6 sample points per parameter, or 10 parameters at 3 sample points per parameter (approx. 50,000 simulations each). This method is intrinsically crude and is only useful for roughly localizing regions of interest in parameter space.

3. Plane sections through parameter space. This method involves searches of pairs of parameters to generate plane sections of parameter space. Typical numbers for this case are 32 samples for each parameter, and around 50 combinations of parameter pairs (again, approx. 50,000 simulations). This method is only useful when one is already in the vicinity of the expected minimum and wishes to obtain an estimate of the robustness of the solution.

SYSTEMATIC SEARCHES USING CONJUGATE GRADIENTS. Conjugate gradient methods involve successive computations of local gradients followed by exploration of the space along a vector determined from that gradient. A number of variations of this approach exist. We have developed a modification of the Fletcher-Reeves-Polack-Ribiere method (Press et al. 1988) which is suited to parallelization. Gradients are evaluated for each dimension using two sample points to smooth out the slopes. Based on the gradient, the algorithm selects a vector in parameter space, passing through the initial point. The best value of match along this selected vector is evaluated based on a fixed number of sample points and B-spline interpolation. This match point becomes the starting point for another cycle of the gradient method.

Each of these cycles involves many independent calculations of match based on parameters determined at the outset of the stage. This allows one to compute each iteration in the same amount of time as required for a single simulation, by farming out the desired parameters to a large number of independent nodes on a parallel computer. Conjugate gradient methods are extremely efficient, usually converging within 5 or so cycles as described above (typically 200-300 simulations).

COMBINATION OF PARAMETER SEARCHING METHODS. Basic conjugate gradient methods assume that there is a unique solution to the problem, and that the energy (matching) function is smooth. Neither of these conditions is met for our neuronal parameter searching problem. We have therefore combined conjugate gradient with brute force methods to obtain solutions which are very likely to be reliable. Initial parameter searches are usually done using brute force methods. When an approximate idea of the correct region of parameter space is available, one can use the gradient scheme. This is typically done using different weighting functions and starting points, to check if there is a common solution to which all these converge. Finally, plane sections of parameter space are used to determine the smoothness of nearby parameter space and to estimate the robustness of the solution.

APPENDIX C. CHANNEL PARAMETERS.

The Hodgkin-Huxley formalism is used for all channels. Two alternative forms, the α-β form (equation 2) and the τ-m_∞ form (equation 3) are used to describe the channel kinetics. For three channels: Na_{gran}, Kfast and K, the kinetics have not been reduced to analytical form and are therefore described by plots of the voltage dependencies of their kinetics (Figure 12).

Voltage units: mV, with respect to extracellular potential. The resting potential is -65 mV for all cells. Time units: msecs; Resistance units: mΩ; concentration units: mmol/liter.

1: Compartment equation. i refers to the index of the present compartment, j is the index for the ionic conductance g_j with reversal potential E_j. The remaining terms have been defined in the text.

$$Cm_i \, {dV_i}/{dt} = (Em_i - V_i)/Rm_i + (V_{i+1} - V_i)/(Ra_{i,i+1}) + (V_{i-1} - V_i)/(Ra_{i,i-1}) + \Sigma g_j(E_j - V_i)$$

2: Dependence of gating parameter m on rate constants α and β.

$$dm/dt = \alpha_m(1-m) - \beta_m m$$

3: Dependence of gating parameter m on rate constants τ and m_∞.

$$dm/dt = (m_\infty - m)/\tau_m$$

4: Mitral Na channel.

$$g_{Na} = \bar{g}_{Na} m^3 h$$
$$\alpha_m = 0.32(V+42)/(1-\exp(-(V+42)/4))$$
$$\beta_m = 0.28(V+15)/(\exp((V+15)/5)-1)$$
$$\alpha_h = 0.128/\exp((V+38)/18)$$
$$\beta_h = 4/(1+\exp(-(V+15)/5))$$

5: Granule Na channel. See Figure 12 A,B.

$$g_{Nagran} = \bar{g}_{Nagran} m^3 h$$

6: Mitral Ca channel.

$$g_{Ca} = \bar{g}_{Ca} sr$$
$$\alpha_s = 7.5/(1+\exp((13-V)/7))$$
$$\beta_s = 1.65/(1+\exp((V-14)/4))$$
$$\alpha_r = 6.8\times10^{-3}/(1+\exp((V+30)/12))$$
$$\beta_r = 0.06/(1+\exp(-V/11))$$

7: Mitral Kfast (Kfast) channel. See Figure 12 C,D.

$$g_{Kfast} = \overline{g}_{Kfast} n^2 k$$

8: Mitral and granule cell K channel. See Figure 12 C,D. The τ parameters are slower (larger) by a factor of 4 from the values in the figure.

$$g_K = \overline{g}_K n^2 k$$

9: Mitral and granule cell KA channel.

$$g_{KA} = \overline{g}_{KA} pq$$
$$\tau_p = 1.38$$
$$p_\infty = 1/(1+\exp(-(V+42)/13))$$
$$\tau_q = 150$$
$$q_\infty = 1/(1+\exp((V+110)/18))$$

10: Granule cell KM channel.

$$g_{KM} = \overline{g}_{KM} x$$
$$\tau_x = 1000/(3.3\exp((V+35)/40)+\exp(-(V+35)/20))$$
$$x_\infty = 1/(1+\exp(-(V+35)/5))$$

11: Mitral K_{Ca} channel. χ represents Calcium ion concentration.

$$g_{KCa} = \overline{g}_{KCa} y$$
$$\alpha_y = \exp((V-65)/27)\times(500(0.015-\chi)/(\exp((0.015-\chi)/0.0013)-1)$$
$$\beta_y = 0.05$$

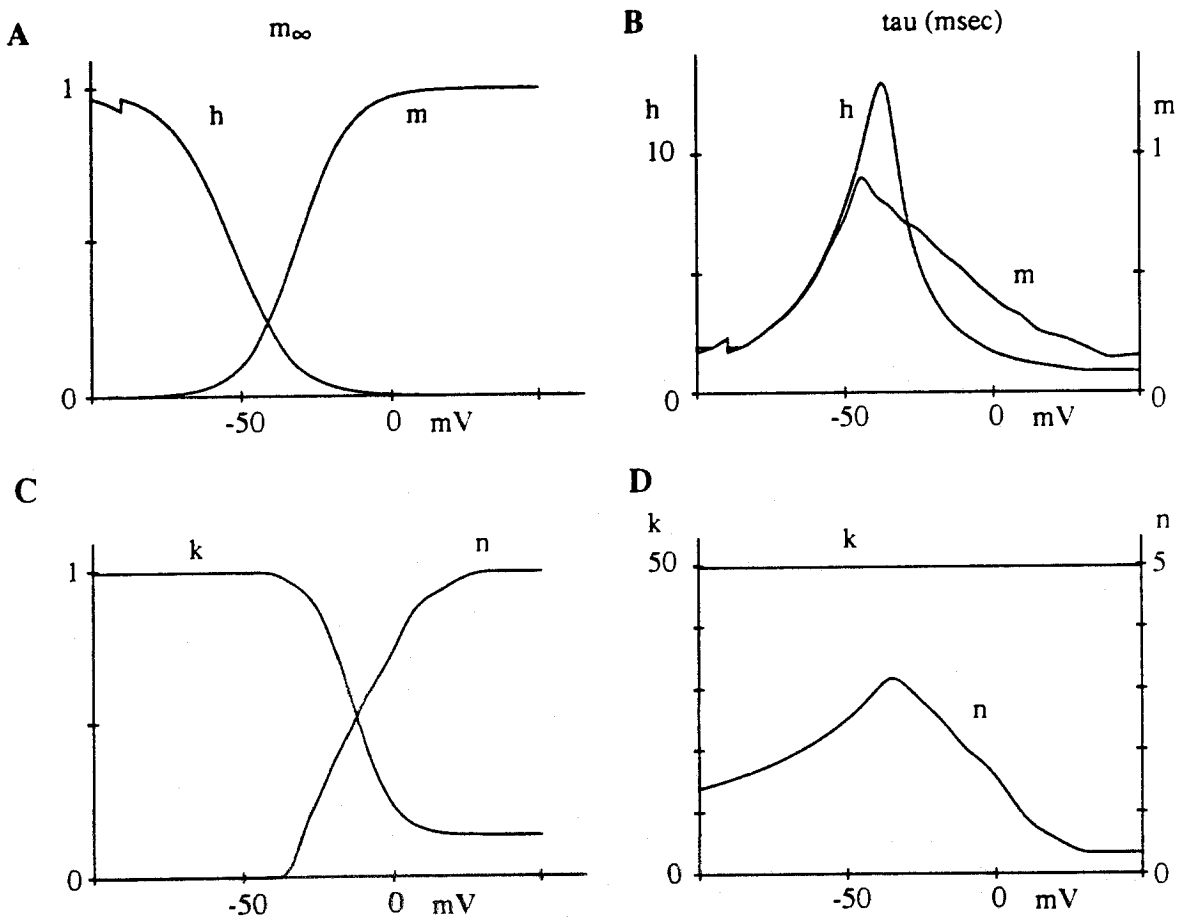

Figure 12: Channel parameters. A: m_∞ and h_∞ curves for Na_{gran} channel. B: Tau curves for Na_{gran} channel. C: n_∞ and k_∞ curves for Kfast and K channels. The small jump in the curves at -90 mV is due to an error in the scaling routines for the kinetics. The cells almost never encounter values in this range. D: Tau curves for Kfast and K channels. The K channel has slower kinetics but the shape of the curves are identical to Kfast. The tau values for K are scaled up by a factor of 4 from the graph. For all calculations outside the tabulated voltage range, the values for the extreme points are used.

SECTION 2. EXPERIMENTS.

The previous section describes the development of simulation techniques and models which incorporate a large amount of experimental data. The previous models were tuned using intracellular recordings. Such data does not provide much information about the dynamics of network activity. In order to develop the simulations to the level of the bulb as a whole, we required additional data. This was provided in part by the experiments described in this section.

A number of techniques were developed in order to carry out these experiments. These include the development of microdrives for recording from awake behaving rats, the development of the behavioral setup and paradigms, and the analysis software. All these techniques were used in the experiments and analysis described in Chapter 4. This chapter is to be submitted to the Journal of Neurophysiology.

Multi-day recordings from olfactory bulb neurons in awake freely moving rats: Spatial and temporal patterns in odorant responses.

Upinder S. Bhalla and James M. Bower

Division of Biology,

California Institute of Technology, Pasadena, CA 91125

SUMMARY AND CONCLUSIONS

1. Chronic single-unit as well as multi-unit extracellular recordings were carried out in the olfactory bulb of awake freely moving rats placed in an odorant stream. Twisted-pair stereo electrodes were positioned in the mitral cell layer based on cellular activity patterns and later verified histologically. Single units were discriminated using eight different parameters of the waveforms. Discrimination was verified using inter-spike interval histograms.

2. Three odors: citral, isoamyl acetate, and methyl salicylate were presented at low (nanomolar) concentrations to avoid habituation. The ability of rats to detect and discriminate between the three odors at these low concentrations was behaviorally verified. During neural recording sessions, odors were presented in a cyclical sequence, with purge and clean air periods interspersed. Each cycle lasted 40-60 seconds. Each run consisted of approx. 10 repetitions of this cycle. Two to six runs were carried out per day, on a daily basis.

3. A total of 186 single neurons were isolated, 121 of which were held for more than one run. The longest duration recordings of 5 days were achieved in 5 neurons. In 166 runs more than one neuron was isolated and recorded simultaneously. The largest number of neurons recorded simultaneously was 6. Single unit data analysis was based on a total of 618 single unit records taken during 369 individual runs. Analysis of multiple-unit traces in which all spike activity was pooled, was based on 512 recordings taken over the same 369 runs.

4. Neuronal responses were characterized in terms of three features: the mean firing rate, the phasic response to odor onset, and the respiration-coupled response. The mean firing rate showed statistically significant odor-related changes in 12% of runs. There was a significant odor-onset response to one or more odors 27% of the time. In 46% of recordings the baseline firing of the neuron showed respiration-related periodicity, but this periodicity showed odor-dependent differences only 23% of the time. A large percentage (56%) of neurons showed significant variability in firing rate between cycles within a run.

5. Similar characterizations were performed on a subset of the data recorded during periods when the rat was actively sniffing, and therefore presumably attending to the odor stimuli. The sniff dataset had even more (84%) neurons where the baseline firing rate showed respiration-coupled periodicity, but the number where the periodicity was odor-dependent was very similar (25%) to the main dataset.

6. The same three measures when used to compare responses of the same neuron recorded during different recording runs revealed significant differences (Chi-squared test) in odorant specific response patterns in 11% of cases.

7. A scalar measure of differences in response (R) was devised to compare response patterns between recordings. When comparing individual neurons recorded at different times, R was found to follow a normal distribution, with a mean between completely consistent and completely random levels. This implies that in this population of neurons, some responded very consistently, and others very inconsistently, but most showed an intermediate level of variability in response. Furthermore, R did not show much time dependence whether comparing recordings from successive runs or from several days apart. Therefore, the response of an individual neuron does not drift indefinitely, but varies within well defined bounds, and the time scale for this variability is less than the 10 minutes between runs. We propose that the response of a neuron can be represented as a combination of a consistent component, and a variable component.

8. Using the same measure R, comparisons were made between the same neuron on different runs on the same day (ss) and multiple days (sm); adjacent neurons compared on the same day (as) and multiple days (am); and distant neurons compared on the same day (ds) and multiple days (dm). As a control, comparisons were also made between unrelated neurons recorded from different rats (c). In order of increasing variability, R was found to follow the sequence:

$$ss \leq sm < as \approx am < dm \approx c < ds$$

This would be consistent with a spatial distribution of responses, where adjacent neurons respond more similarly than chance, but less so than an individual neuron over time. Distant neurons show complementary responses when compared at short time intervals, but at intervals of days this is not

significant. This sequence was very robust, remaining unchanged when considering only one odor at a time, or only one of the response measures (mean rate, odor onset, or respiration coupled).

9. When the same comparisons were made for recordings from the sniff dataset, a different sequence emerged:

$$as < am \approx ss \approx sm < dm \approx c < ds$$

This implies that the variability in single neuron responses is elevated when the animal is actively sampling odorants. Furthermore, adjacent neurons continue to respond similarly even when individual neuron responses change substantially. At a more fundamental level, the difference between sniffing and resting situations indicates that the olfactory bulb may operate in more than one processing mode. We propose that the resting state corresponds to an unbiased sampling of odorants, while during sniffing the bulb actively suppresses responses to familiar odorants to improve discrimination of novel ones.

INTRODUCTION

It is clear that olfactory information is represented in the olfactory bulb in a complex manner. Two major aspects of olfactory encoding have been analyzed: temporal spike codes in the firing patterns of individual neurons (Hamilton and Kauer 1985; Harrison and Scott 1986; Chaput 1986) and spatial mapping of odorants onto the surface of the bulb (reviewed in Shepherd 1993; Scott et al. 1993). In each case there are a number of lines of evidence which appear to be difficult to reconcile, and which can broadly be described as supporting a specific or a distributed representation, respectively.

The presence of a specific representation in the temporal domain is indicated by experiments on mitral cell tuning specificities (Mori et al. 1992; Harrison and Scott 1986), which imply that these responses are a consistent property of the cell. The odor related information is therefore available from a short sample of the neuronal firing pattern. In the spatial domain a variety of experiments have pointed towards some form of topographic representation of olfactory stimuli on the bulb. These include 2-deoxyglucose studies (Lancet et al. 1982; Jourdan et al. 1980) where individual glomeruli, or small groups of them, are specifically labeled under conditions of odorant stimulation. Electrophysiological studies (Freeman and Grajski 1987; Buonviso and Chaput 1990; Buonviso et al. 1992) are beginning to define the functional aspects of olfactory bulb spatial organization. A number of anatomical studies (Astic et al. 1987; Fujita et al. 1985) also imply that there is a stable, specific spatial representation of odors across the surface of the bulb.

Evidence for a distributed representation in the temporal domain is provided by a number of experiments where mitral cell response tuning has been found to display a degree of variability (Chaput and Holley 1985; Chaput and Lankheet 1987; Macrides and Chorover 1972). In this case the information relating to the odorant is distributed over time, since one would need to sample from the neuron over a long period to determine its response. In the spatial domain, ablation experiments (Slotnick et al. 1987) indicate that the presence of these odor-specific glomeruli is not an absolute requirement for discrimination and recognition of the relevant odors. Furthermore, the apparent broad tuning of individual

receptors (Sicard and Holley 1984) and mitral cells (Jiang and Holley 1992; Duchamp-Viret et al. 1990) raises questions about the degree to which a specific spatial representation of odorants can be sustained by the underlying network.

The encoding of olfactory information in the bulb has a direct bearing on the function of further stages of olfactory processing, to which it provides the sole source of olfactory input. For the last several years we have been studying information processing in the piriform cortex, using a combination of experimental (Hasselmo and Bower 1992) and simulation (Wilson and Bower 1992; Hasselmo et al. 1992) techniques. In order to further relate these studies to the biological system, we have sought in the study reported here to characterize the encoding of olfactory information in the mitral cells of the olfactory bulb.

This study addresses both the temporal and the spatial aspects of encoding in the olfactory bulb and reveals some important relationships between them. By quantifying such relationships, it provides a means for beginning to address a number of apparent conflicts in the literature and to build a unified picture of olfactory processing in the bulb.

METHODS

General Procedures.

These experiments involved multiple single-neuron recordings in awake behaving animals. During recording, animals were confined to a Plexiglas box into which three different odors were cyclically introduced using a computer controlled olfactometer. Nanomolar concentrations, calibrated using a Gas Chromatograph/Mass Spectrograph, were used to minimize habituation. The ability of the rats to detect and discriminate between the odorants at these concentrations was verified through behavioral testing using operant conditioning. Chronic neuronal recordings were made with stereo electrodes with up to eight electrodes inserted in any one animal. Amplified signals were digitized and recorded directly to disk for further analysis.

SURGICAL PROCEDURES.

Chronic recordings were made from 15 adult (over 5 months in age) female Sprague-Dawley rats (250-300 gm). Preparations for chronic recordings were performed in a separate, initial surgical procedure using full anesthetic conditions. Specifically, experimental animals were anesthetized using chloral hydrate (4.2gm/kg i.p.) and maintained under anesthesia with supplemental doses. Local anesthetic (Xylocaine hydrochloride) was topically applied during the later phases of the surgery. The skin overlying the skull was retracted and a dental cement foundation for the implant was laid down over the anterior 2/3 of the skull. The foundation was anchored by several self-tapping miniature stainless-steel bone screws (FST 19010) placed anterior and posterior to the olfactory bulb (Figure 2). Following construction of the foundation, an exposure of approx. 2mm x 1.5 mm was made in the bone overlying the left olfactory bulb, and the dura was slit and folded aside to facilitate electrode penetration. The microdrive was then cemented to the foundation and the electrodes inserted a small distance (approx. 500 microns) into the olfactory bulb under visual inspection. The exposure was covered with silicone grease (Dow Corning High Vacuum Grease) and sealed in with dental cement. Sutures and/or wound clips were used to fold together flaps of skin over the base of the foundation. The rats were given at least five days to recover from surgery before recordings commenced. Implants were usually very stable and had a typical lifetime of two or more months.

ODORANT STIMULUS PROCEDURES.

Odorant Chamber. All experiments were conducted with animals placed in an odorant chamber with a continuous flow of pure or odorized air. This chamber consisted of a 7"x 8"x 8" Plexiglas box with baffles at the odorant delivery end and an exhaust fan at the far end. A W131 in-line air flow meter placed in the center of the chamber showed a flow rate of approx. 0.2 meters/sec, and approx. 0.1 meters/sec at its edges. The total air flow rate was 3.2 liters/sec. At this rate the air in the box was completely replaced in approx. 2 sec. Therefore, 2 sec represents an upper limit for odorant permeation

through the entire box. However, when sampling the air in the box, the experimenter was unable to detect any lag between the opening of the odorant valves and the arrival of odor in the box.

Stimulus sequence. A cyclical paradigm of odorant presentation was used. Pure air was presented for a 5 sec period, followed by odor 1 for 5 sec, then the odor lines were purged for 3 sec (the 5-5-3 sec sequence). Following this the second and third odors were presented in the same sequence. This cycle of three odors was then repeated numerous times in each run. In this way, each recording run consisted of approx. 12 cycles lasting a total of approx. 8 minutes. In the initial 70% of the recordings, this basic stimulus sequence was alternated with another sequence intended to determine the dependence of responses on the particular timing of the odorant deliveries. This alternative timing pattern consisted of 10 sec (air), 7 sec (odor) , 3 sec (purge). As no marked difference in neuronal responses between these two patterns were observed, the results presented here represent data pooled over both sequences.

Control of odor delivery. The odorant stimulus was generated using an automated olfactometer (Figure 1) based on a modification of the design by Slotnick and Nigrosh 1974. Briefly, compressed air (10 psi) was filtered through charcoal, dessicant and distilled water. Three odorant streams were generated by continuously bubbling the filtered air through the a glass bubbler containing one of these odorants. The odors used in these experiments were: Odor 1 - citral (CIT); Odor 2 - isoamyl acetate (ISO); Odor 3 - methyl salicylate (MSAL). 3 mm. glass beads were placed in the bubblers to improve mixing and retard aerosol formation. The flow of each odorized stream was then directed to either the exhaust or the odor chamber by solenoid valves. A purge line vented purified air at a high flow rate (>2500ml/min) through the common air pathway leading to the odor chamber. All air streams were continually monitored using calibrated flow meters (Cole-Parmer Instrument Company).

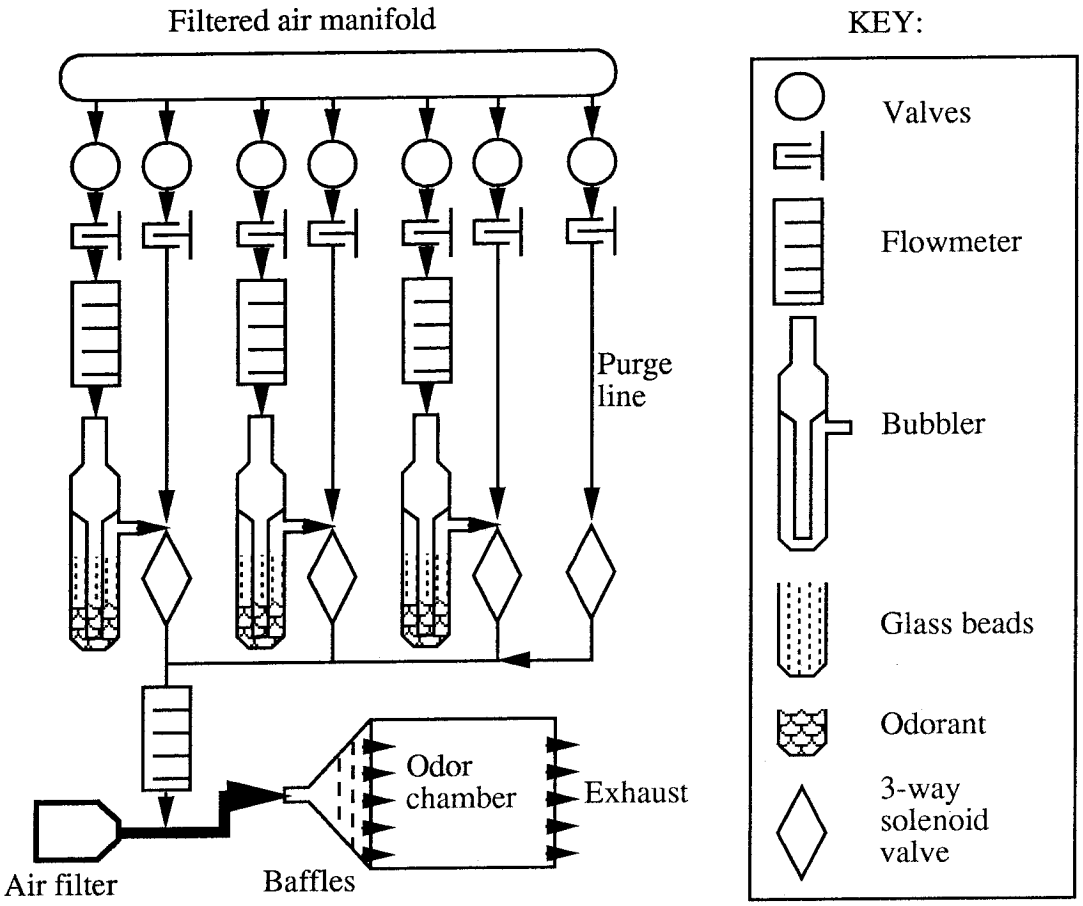

Figure 1. Odorant delivery setup. This was based on a design by Slotnick et al. Filtered air at 10 psi was regulated by a series of flow valves and monitored using a flow meter. Each odorant channel consisted of two lines, one going through a glass bubbler which contained the odorant, and the other diluting the odorant line. The bubbler was packed with glass beads well beyond the level of the odorants. This served two functions. First, the beads increased the surface area and improved consistency of vaporization of the odorant. Second, the beads reduced the amount of odor aerosol by providing a large capture area above the odorant level. The diluted odorant stream was switched using a solenoid valve between the exhaust and the odorant outlet, which was also monitored using a flow meter. A further stage of dilution was provided near the entry to the odorant chamber where the odorant stream was diluted in a high volume air stream.

A final stage of air dilution was provided by a high flow rate (3.2 liters/sec) air stream leading into the odor chamber, regulated by a Watts 26A pressure regulator. This air stream was filtered using Koby Junior activated charcoal filters replaced at 1-month intervals, except for the initial 20% of recordings, which used unfiltered air. The odor streams emerging from the olfactometer were mixed with this air stream in a narrow (15 mm) tube, and then passed through two baffles, to ensure complete mixing.

Brass solenoid valves were employed for all odorant switching, and the odorants were carried in Teflon tubing except at joints, which involved nylon couplings and, in some cases, short lengths of Tygon tubing. However, the same odorants always flowed through the same section of the olfactometer to minimize contamination. The whole olfactometer was washed out with 95% ethyl alcohol every 2 to 6 weeks. The sequence of odor delivery was controlled by an IBM PC using custom designed hardware and software.

The temperature of the olfactometer was held consistent between 26 and 28 degrees Celsius during all odor runs and during calibration, to insure that the vapor pressures of the odorants did not change significantly.

Quantifying odor concentrations.

The very low (nanomolar) odor concentrations used in these experiments were calibrated using an HP model 5890 gas chromatograph with a HP 5970 mass selective detector (GCMS). Samples of the odorant streams were obtained using a dry-ice/acetone trap at the output of the olfactometer, prior to the final dilution. Once obtained, the condensed odorant was extracted from the trap using two washes of 5 ml hexane each, which were subsequently mixed. Known concentrations of Benzophenone were added to this solution as reference, and 2 ml of the final mixture were analyzed on the gas chromatograph. Odorant samples were taken on two different days to test variability, which was found to be less than 10%. The measured concentrations for isoamyl acetate, for which saturated vapor values are available, correspond to approx. 90% saturated vapor at the bubbler, which is in the expected range (Duchamp-Viret et al. 1990). Once the concentration at the output of the olfactometer was determined, the final odor concentrations in the actually recording chamber was calculated from the dilution due to the known air flow rates. The

values for odor concentration in the recording chamber are listed in Table 1. At these concentrations all the odorants are distinct and pleasant to the experimentor. As described in the appendix, we verified that rats are able to detect and to discriminate between the odorants at these concentrations.

Table 1. Olfactometer calibration.

Odor	Concentration (nM at rat)	Coeff. of variation (%)
Citral (CIT)†	5.4	20
Isoamyl Acetate (ISO)	64.5	6
Methyl Salicylate (MSAL)	16.4	14

†Citral exists as 2 stereoisomers. Their sum is given.

Recording electrodes

Electrode Manufacture. In order to obtain the maximum number of neuronal recordings with the best possible single neuron isolation and stability, the majority of these experiments used stereo electrodes ("stereotrodes") as described by McNaughton et al. (McNaughton et al. 1983). These electrodes consisted of two insulated wires twisted tightly together. Two kinds of electrode wire were used: Platinum Iridium wire of 0.8 mil (20 micron) diameter, insulated with isonel, and Nichrome wire of 1 mil (25 micron) diameter, insulated with formvar and further coated with epoxylite. Epoxylite coating was also used in some cases for the PtIr wires to increase mechanical strength. Electrode impedances were in the 500 KΩ to 2 MΩ range and were relatively stable for a particular electrode, as determined by measuring resistances before the implant and after the microdrive had been removed after some months of being implanted.

Microdrive Design. Two basic designs of microdrive were developed for these experiments (Figure 2). Each of these carried up to eight independently adjustable stereo electrodes. One allowed full adjustment over a range of 3 mm with an accuracy around 30 microns corresponding to a 30 degree rotation of the drive screws. The other, simpler design required adjustment of the electrodes by moving the guide tubes by hand using a metal tube or tweezers. In general, the first design was able to give better unit isolation due to the finer adjustability, but the second design was more reliable. The second design also had an advantage in that it was simpler to make.

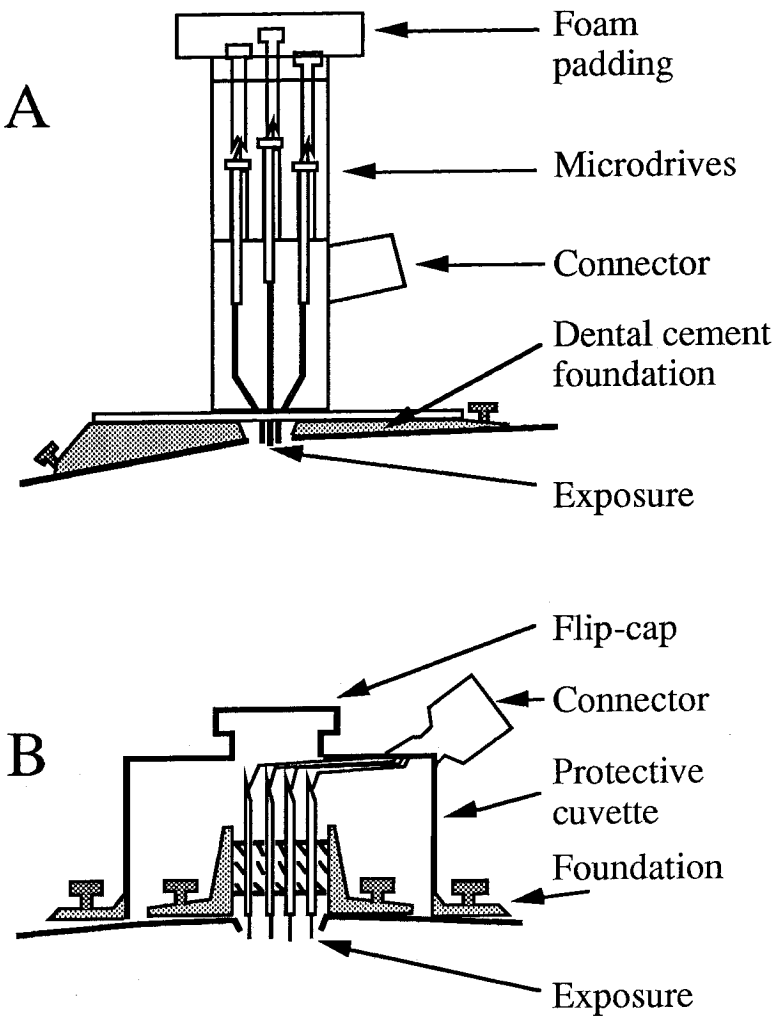

Figure 2. Microdrive design and attachment to rat. A. Screw-adjustable microdrive. The electrode wire is threaded through an outer and an inner guide tube. The outer guide tube is pushed down by a screw to advance the electrode. The inner guide tubes converge to approx. 400 micron spacing over the exposure. The screws can be advanced on the awake rat to approx. 30 micron precision, corresponding to 30 degrees rotation. B. Hand-adjustable microdrive. Each electrode wire is threaded through a 30 gauge needle, which is supported in a layer of silicone or wax sandwiched between two stainless steel grids. The electrode wire protrudes through the bottom of the needle into the exposure. The electrode assembly is protected by a modified plastic cuvette, which is mounted separately on the skull for mechanical isolation. Access to the electrode assembly is through a flip-cap on the cuvette. Adjustment is done using a pusher rod or a pair of tweezers, on rats briefly immobilized by wrapping in a towel and/or using halothane.

Electrode leads. Connections to the amplifier were made through a connector-preamplifier assembly weighing under 5 gm. The preamplifier was a 25 channel unity gain FET array (Micro Probe Inc.) of which 16 channels were used (8 stereo electrodes). The assembly attached directly to a miniature connector (Microtech, Inc.) on the headstage in order to further minimize electrical noise. The preamplifier cable was electrically shielded with a metallic spring which also protected the cable from mechanical damage. In both microdrive designs, a ground electrode constructed of 50u stainless steel was placed over the exposure and connected to the preamplifier to minimize electrical noise due to rat movements.

Monitoring respiration. The connector-preamplifier assembly also carried a glass bead thermistor (Fenwal Electronics) mounted on the end of an adjustable stainless steel wire, for respiration monitoring. In use this was moved near the left naris of the rat, ipsilateral to the site of the implant. This arrangement did not interfere with the breathing of the rat. The thermistor arrangement was capable of following temperature fluctuations as fast as 10 Hz. Transients due to contacting the cage surfaces and displacement during grooming behavior were detected and removed in software. Thermistor signals were converted to a TTL pulse for data analysis by a circuit detecting rate of change of resistance. Analog thermistor signals were digitized at 700 Hz and stored to computer disk in a subset of recordings.

Recording procedures

Electrode tuning. The use of adjustable microelectrodes enabled the tuning of electrodes to improve recording quality. At the time of implant, the electrodes were placed above the dorsal mitral cell layer. With the screw microdrives (Figure 2 A), it was possible to gradually (approx. 25-100 microns a day) advance the electrode till it reached a region of high activity corresponding to the mitral cell layer (see below). Electrodes in this layer were adjusted very sparingly, and typically picked up one or more neurons while they remained in the mitral cell layer. With the less accurately adjustable 'grid' microdrives (Figure 2 B), electrode adjustment was carried out using a stainless steel tube to push the needles. In this case, the rats were sometimes lightly anesthetized using halothane to reduce movement during the adjustment procedure. In general, recordings were more stable if electrode adjustments were kept small and infrequent.

Unit waveforms tended to drift immediately following electrode adjustment but generally became stable within an hour.

Data acquisition. Recorded waveforms were sampled at 18 Khz per channel and recorded directly to disk using Brainwave systems software and hardware. For each spike above a selected threshold, 32 voltage samples were recorded to disk for later analysis. The system simultaneously evaluated 8 parameters (see below) of each spike waveform and recorded them. All the odorant control signals from the olfactometer were also recorded to disk to provide accurate timing information for analysis. All data was transferred to workstations via ethernet for tape backup and subsequent analysis. A typical recording run of 9 minutes generated 5 to 15 Megabytes of data, up to 6 such recording runs were carried out every session for every rat.

Neuronal waveform discrimination

Basic Spike Classification. All single unit discrimination was carried out using spike classification software. We used this approach because our electrodes frequently encountered signals from multiple neurons and the software allowed us to separate such signals. This increases the number of neurons recorded, and also permits us to record simultaneously from adjacent neurons, which play an important role in the analysis. Classifying neuronal signals based on a large number of features of the spike waveform also provided a means for uniquely identifying spikes on successive runs and days. This was very important for analysis of recordings over a long period of time.

Waveform discrimination was based on the evaluation of eight different parameters for every spike recorded using the stereo electrodes (channels x and y). These parameters were: peak on x channel, peak on y channel, peak phase angle ($\arctan(peak_y/peak_x)$), valley phase angle ($\arctan(valley_y/valley_x)$), max peak-to-peak, spike width, $valley_x$ and $valley_y$. Conventional window discrimination methods usually only take into account the first of these parameters, the peak amplitude. Recorded spikes were first manually classified on the basis of each of these parameters using cluster cutting (McNaughton et al. 1983) employing custom written graphical software on workstations. Once the cluster classifications had been

established by the experimentor, the software automatically identified individual spikes and recorded their time of occurrence. During and after data acquisition, interspike intervals where constructed for each identified neuron and evaluated for intervals occurring too rapidly, i.e., spikes occurring within the refractory period of the neuron (Figure 3). All recordings which lacked a clear refractory period were rejected.

Particular care was taken in separating two waveforms recorded on the same stereotrode. In this case, inter-neuron inter spike interval histograms (spike intervals for one unit triggered with respect to the other) were generated for each putative pair. Any histogram revealing a refractory period resulted in a reevaluation of the cluster boundaries, and the exclusion of one or both units from analysis as a refractory period between two recordings would have indicated that the neurons were not fully isolated (Buonviso and Chaput 1990) .

As described above, and shown in figure 3, we adopted a conservative measure of spike isolation for this data. However, cluster cutting methods, especially when used conservatively, are susceptible to type II errors, i.e., they can exclude legitimate spike events. In the current case we opted for a conservative measure of positive spike classification on the assumption that any excluded events would occur completely randomly with respect to the stimulus conditions. Since all our analysis is based on comparisons within a data run, during which period the cluster boundaries are held fixed, the exclusion of valid spikes should be unbiased with no effect other than reducing the total number of events recorded.

Figure 3. Spike Classification. A. Isolation of two units from a single recording. Left: one second of recorded waveform data for x and y channels of the stereo electrode. Each spike waveform contains 32 samples at 18 KHz. The period between spikes is not sampled. Center: Cluster plot of 2 of the 8 parameters used in the cluster classification. The parameters displayed here are: X axis: peak height of upper (x) trace, Y axis: peak height of lower (y) trace. The boxes represent the windows for acceptable spike peaks. The cluster at the lower right consists of lower amplitude spikes which were not classified. The cut-off at the lower left-hand represents the thresholds for recording spike waveforms for the two channels. Right: ISI histograms corresponding to two neurons discriminated from the digitized waveforms. The upper histogram is of the faster firing neuron represented by the denser upper cluster. Note the differences in histogram shapes, which provides a further criterion for unit identification.

B, C. A single neuron isolated on two successive days. Note the close correspondence between the cluster locations and the shapes of the ISI histograms for the two days.

Scale bars: 250 msec time axis, 200 μV voltage axis.

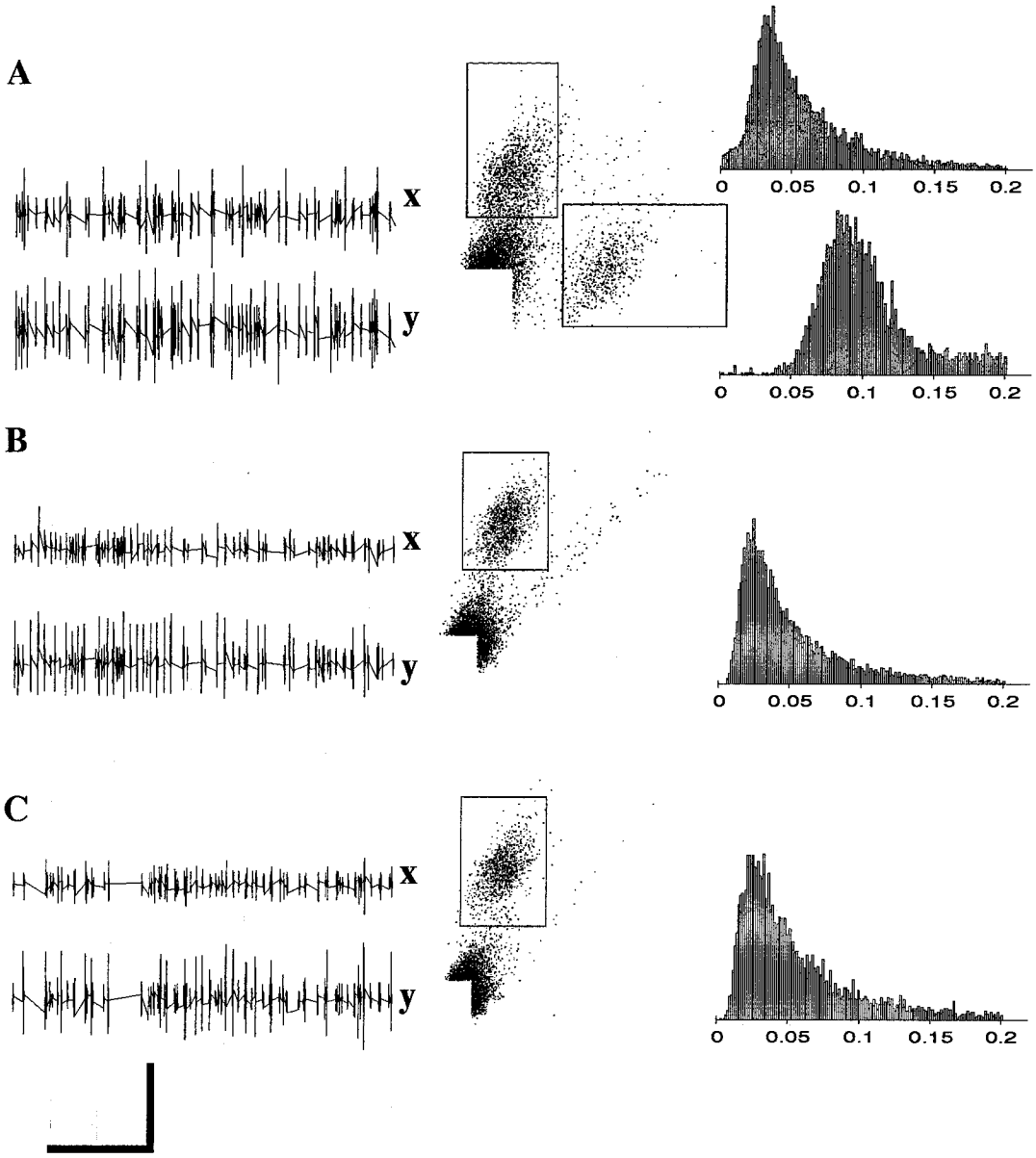
A
x
y
0
0.05
0.1
0.15
0.2
B
x
y
0
0.05
0.1
0.15
0.2
C
x
y
0
0.05
0.1
0.15
0.2

Unit identification between recording sessions.

Within a recording session units were continually monitored. Variability in spike shape was usually very small, typically only present when the electrodes had been recently adjusted. Between the daily recording sessions units were not continually monitored. In these cases, spike waveforms were recognized as likely to be from the same neuron if the values of the same eight parameters used for cluster cutting on the first recording day still yielded a "clean" interspike interval histogram. In addition, the often unique shape of the ISI (Figure 3 A) was used as a measure of identity. However, in the interest of conservativeness, units were not classified as being the same if there was a gap of more than a day between recordings even if they met all of the other criteria.

Data analysis

General.

The data analysis was carried out in two parts. First, a relatively conventional analysis was applied, where individual neuronal responses were tested for significance according to three measures of response. Each of these measures (mean rate, phasic response to odor onset, and odor-dependent respiration related response) have been previously utilized to measure single neuron responses to odorant stimulation (mean: Meredith 1986; odor onset: Hamilton and Kauer 1985; Harrison and Scott 1986; Meredith 1986; Kauer and Shepherd 1977; respiration related: Chaput et al. 1992). Second, we performed comparisons on responses from different recordings: between the same neuron at different times as well as between different neurons. These comparisons were performed using a distance measure which is insensitive to differences in baseline firing rates, and selectively estimates differences in response properties.

INDIVIDUAL NEURON RESPONSES.

Each of the following analyses was carried out on a recording run, consisting of at least eight complete odor-delivery cycles, as previously discussed. The 95% confidence level was used for all tests.

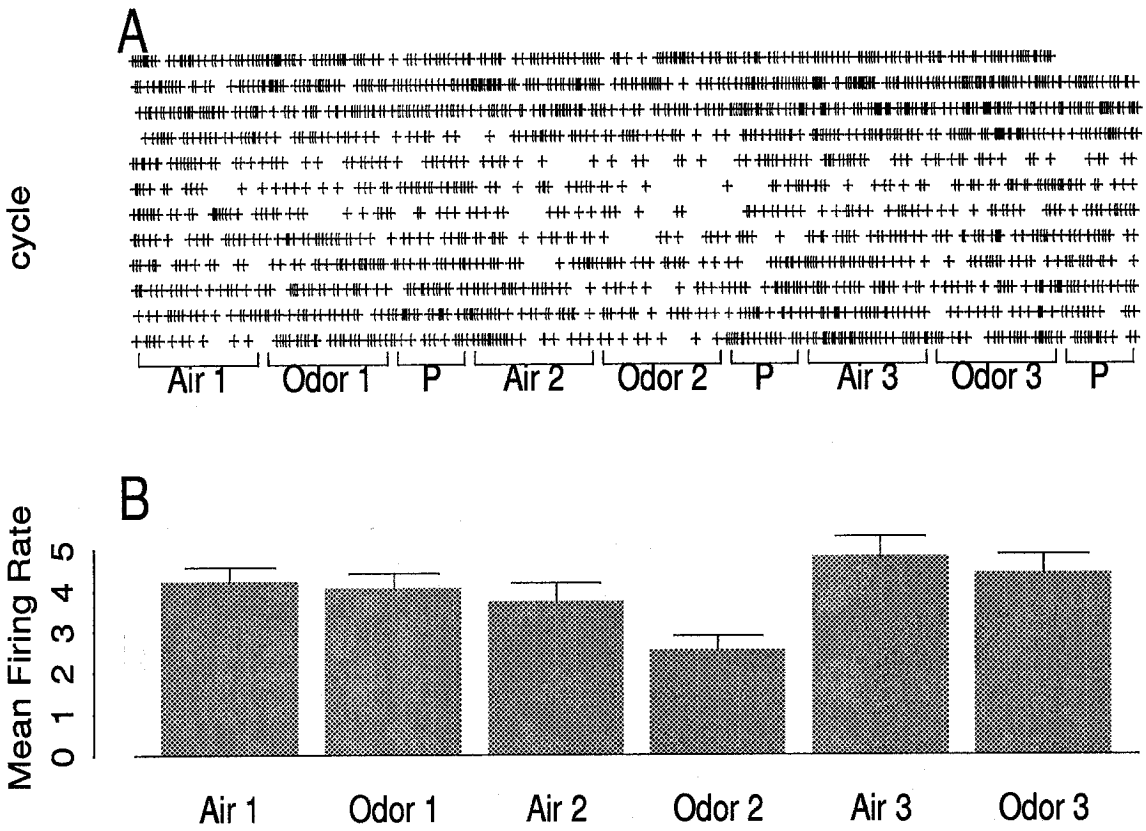

Figure 4. Analysis of changes in mean firing rates.

A. Dot raster of entire trial (10 cycles). The timings of the odor delivery periods are indicated below the raster.

B. Histogram of mean firing rates for each of the indicated odor/clean air periods in the run. The neuron has a suppressive response to odor 2. Two statistical tests are carried out on the components of this histogram: Test 1 checks if the overall histogram is significantly different from a flat distribution. Test 2 checks odor periods against their immediately preceding pure air periods to see if the difference in mean rates is significant. The Fisher's Protected Least Significant Difference test used here requires that test 1 be significant before test 2 can be applied.

1. Mean firing rates. The data for this analysis consisted of spike rates in the six periods of the odor delivery cycle: Odor 1, 2 and 3, and each of the immediately preceding pure air periods (Figure 4). The purge periods were not used. A two-factor Analysis of Variance (ANOVA) (Keppel 1982) was performed between these six rates and all the cycles within a run.

If the analysis demonstrated a significant variability in the rates, the mean rate for each odor period was compared with the mean rate for the preceding pure air period (Fisher's Protected Least Significant difference test).

2. Phasic responses to odor onset. Each odor period was compared with the preceding pure air period to determine if there was a change in firing pattern (Figure 5). A peri-stimulus histogram was constructed starting at the onset of the odor period. Spike counts during the odor period were binned over all cycles. Bin widths of 1.0 seconds were used, giving a total of 5 bins. A similar histogram was constructed for the air period. The shapes of the two histograms were compared by using the chi-squared analysis to compare the bin totals for odor and air periods. If the test revealed a significant difference between the histogram shapes, it was counted as a response to that odorant.

The same procedure was carried out for each of the three odorants.

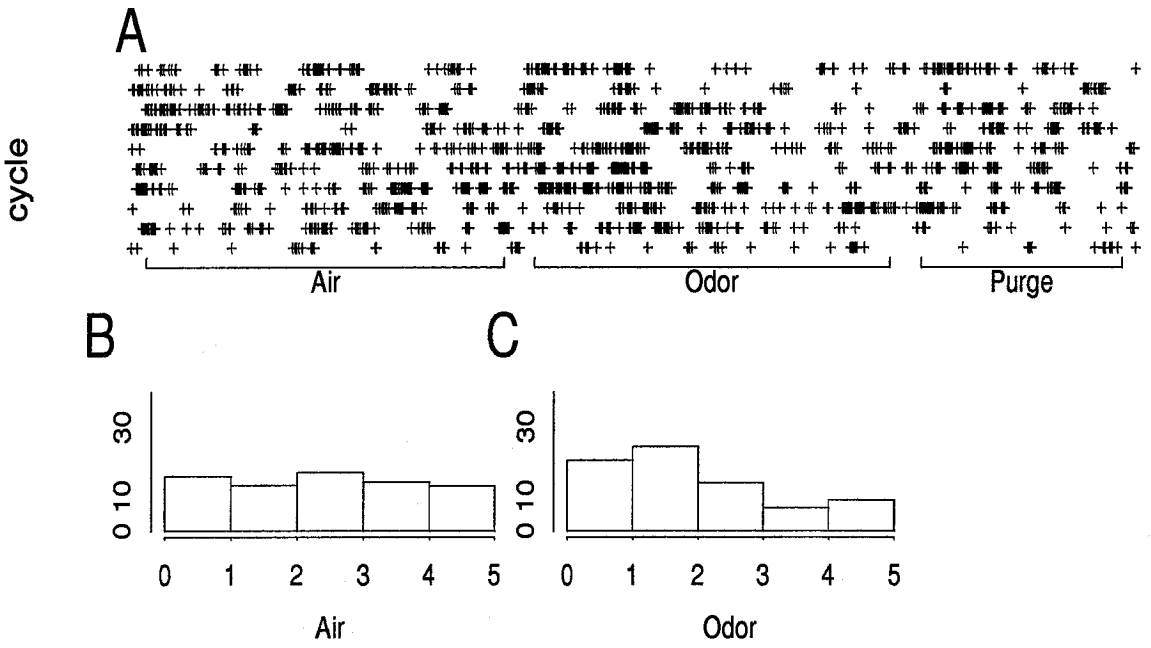

Figure 5. Analysis of odor-onset responses.

A. Dot raster corresponding to the delivery of odor 2, and the air and purge periods surrounding it. The variability in firing rates between cycles was typical.

B. Histograms of spike counts during the air period. Each bin is 1 second wide.

C. Histogram of spike counts during the odor delivery period. Each bin is 1 second wide. The chi-squared test between histograms B and C determines whether there is a significant response to this odor.

3. Odor-dependent phasic responses to respiration. Each odor was compared with its preceding pure air period (Figure 6). A phase-triggered histogram was constructed for the spikes within the odor period, as described in previous studies (Buonviso et al. 1992). Briefly, each respiration cycle was subdivided into 5 bins, and the phase of each spike with respect to the respiration cycle determined which bin it was summed into. A phase of zero corresponded to the transition from exhalation to inhalation There were typically at least 5 such respiration cycles within each odor delivery period. Bin counts were accumulated over all the presentations of the odor within a run.

A similar histogram was constructed for the air period preceding the odor. The shapes of the histograms were compared using the chi-squared analysis to determine if there was a respiration related response to the odorant.

The same procedure was carried out for each of the three odorants.

Supplemental analyses. The following supplementary analyses were carried out to further characterize individual neuron behavior:

Variability within a run. Given the availability of spike counts for each cycle within a run, it was possible to test if the mean firing rate changed between cycles. This was done using the Analysis of Variance (Keppel 1982).

Baseline dependence on respiration cycle. Phase-triggered histograms were constructed as before, with respect to the respiration cycle, using the data from each run as a whole. The chi-squared test was applied to test for significant difference from a flat firing rate.

A large number of additional comparisons could, in principle, be carried out (e.g., the response to odor 1 compared to any of the two other air delivery periods). However, it was judged that the most relevant comparison was to the immediately preceding air period. In addition, performing large numbers of comparisons potentially introduces statistical artifacts (Keppel 1982).

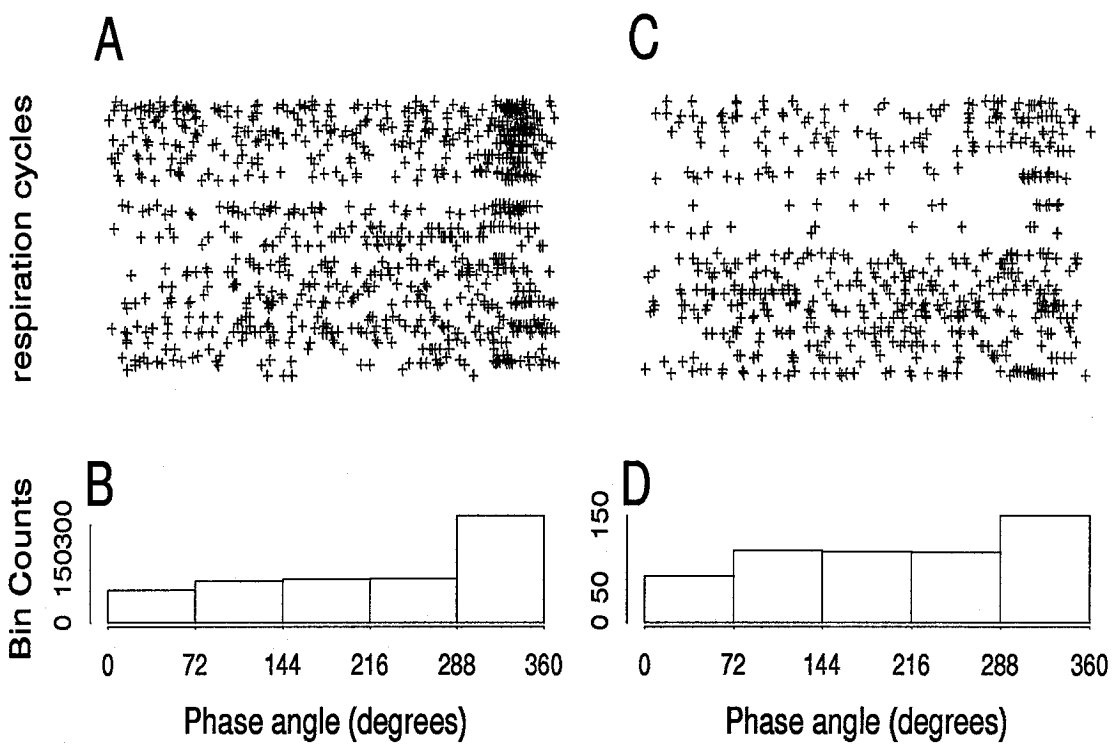

Figure 6. Analysis of respiration-phasic responses.

A. Dot rasters for the phase of spikes with respect to the respiration signal. All spikes in this histogram were collected from the air period preceding the delivery of odorant 2. The transition from exhalation to inhalation corresponds to a phase of 0. Since there were multiple respiratory cycles in each air period, there are multiple spike traces for each odor delivery cycle.

B. Histograms derived from the dot raster in A. Two tests are applied to this data.

C. Similar dot raster for spikes during the delivery of odor 2. Note that the overall number of spikes was considerably less than during the air period.

D. Histogram derived from dot raster in C. The shape of this histogram is significantly different from that in B. The difference in total number of spikes does not contribute to this estimate of difference.

Comparison of neuronal responses.

Previous measures of response difference of olfactory neurons have usually involved classification of responses into a number of categories, and then comparing the number of responses that fall into each category (Buonviso et al. 1990, 1992). In order to facilitate comparisons, a scalar measure of difference is preferable. As a simple measure of response difference, chi-squared comparisons were performed for each pair of histograms to which the distance measure had been applied. The number of significantly different pairs were summed. This sum not a very sensitive measure of difference, and lacks a way of estimating variance. However, it does provide an independent measure for reference purposes.

In order to more accurately compare the response properties of cells, we have developed a scalar measure of the difference between two cell responses. We will refer to this quantity as R in following sections. The derivation of R is discussed in Appendix B. A brief outline of the process is presented here.

R is used to compare the shapes of response histograms from two different neurons, or from the same neuron recorded at the same time. For example, when comparing the odor onset responses to odor 1, we obtain a 5-bin histograms described above, for each neuron. These histograms are normalized to a mean of 1 so that the comparison measures only the shape of the histograms, not differences in their mean firing rates. The 5 bins of each histogram define a point in 5-dimensional space. R is the geometrical distance between these two points. The variability between cycles within a run provides us with an estimate of the error in R. R is averaged across all response histograms (see individual neuronal response calculations above) and over all pairs of neurons in a given category (e.g., adjacent neurons recorded simultaneously) to obtain an estimate for response difference for neurons in that category.

R is normalized with respect to control pairs of neurons, which are comparisons of neurons from different rats. These are clearly unrelated to each other. The resulting measure of R has the following properties:

$R = 0$ implies identical responses.

$0 < R < 1$ indicates similarity in responses as compared to control neurons.

$R = 1$ indicates that responses are unrelated to each other.

$R > 1$ shows that the responses are more dissimilar than control neurons.

Testing analysis sensitivity. As a check on our analysis methods, and as a way of calibrating the sensitivity of the tests with datasets of known variability, we generated synthetic data sets and subjected them to the analysis procedures described above. The synthesized data was generated in accordance with the hypothesis that each neuronal response consisted of a consistent component and a variable component. The consistent component contained mean firing rate, odor-onset, and respiration-phasic responses in the same proportions as seen in the experiments. The random component was generated as gaussian noise and summed onto the consistent component. The analyses described above were then carried out on this synthetic dataset.

Analysis combinations. As described in the results section, these response comparison techniques were used to make several different comparisons including: 1. the same neuron recorded at different times; 2. Adjacent neurons recorded simultaneously; 3. Adjacent neurons recorded at different times; 4. Distant neurons recorded simultaneously; 5. Distant neurons recorded at different times; and 6. Unrelated neurons (from different rats), as a control and normalization factor for the other comparisons. These comparisons were made using the distance measure just described.

Analysis software and hardware. Preliminary statistical calculations were performed using routines slightly adapted from Numerical Recipes in C (Press et al. 1988), and incorporated into custom-written analysis code (nextbda). The ANOVA analysis was carried out based on the procedure described by

Keppel (Keppel 1986). Subsequent and more detailed analyses were performed using the statistical analysis language S-plus (Statistical Sciences Inc.). Bulk data analysis was performed on Sun workstations.

RESULTS

The results presented represent data obtained from a total of 186 distinct single neurons. In total, 618 recording runs were completed in which each of 3 odors were presented in at least 8 stimulus cycles. The mean firing rate of neurons in this dataset was 8 Hz (Figure 7). Most neurons (90%) lay between 3 and 20 Hz. A small number of units (4) had background firing rates as high as 40 Hz over a period of several hours.

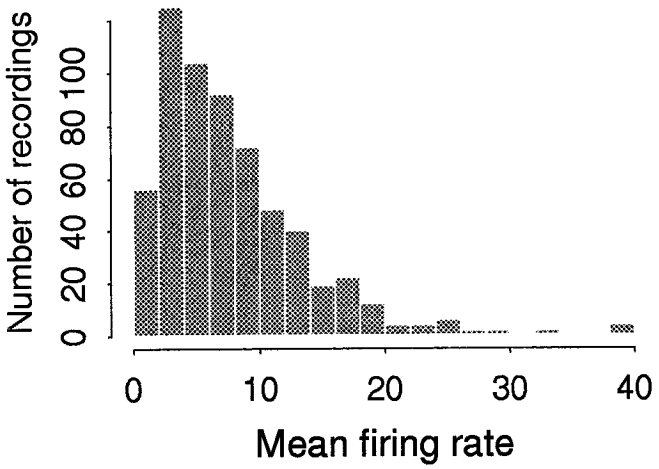

Figure 7.

Distribution of firing rates. The mean was around 8 Hz. 4 different neurons had a firing rate in the region of 40 Hz. Most neurons fired relatively slowly, between 3 and 10 Hz.

Unit characterization. Most of our recordings are expected to have been from mitral cells. We base this conclusion on the following factors: First, the recording electrodes are made out of large, low impedance (approx. 1 MegOhm) wires and would only be expected to pick up signals from large neurons such as the mitral cells. Second, strong background activity was usually seen when the electrode was able to pick up isolated neurons. This background activity is most likely to correspond to the activity of the other cells in the mitral cell layer. Third, electrolytic lesions were performed in 3 animals (2 chronically implanted, 1 acute) on electrodes that had been picking up neuronal signals satisfying the first two criteria. Histological analysis (Figure 8) using Cresyl violet stained sections of the olfactory bulb show that the identified lesions were within the mitral cell layer. Taken together, these criteria have commonly been used to identify mitral cells (e.g., Buonviso and Chaput 1990). Most electrode sites were found to have been located near the anterior dorsal aspect of the olfactory bulb.

Figure 8. Coronal section through olfactory bulb of implanted rat. Left: Low magnification (50x) view of the bulb. An electrode track and the lesion site are visible. Right: Higher magnification (140x) view of lesion site. The region around the lesion is displaced due to a sectioning artifact. The lesion site itself is in the mitral cell layer. Cresyl violet staining was used.

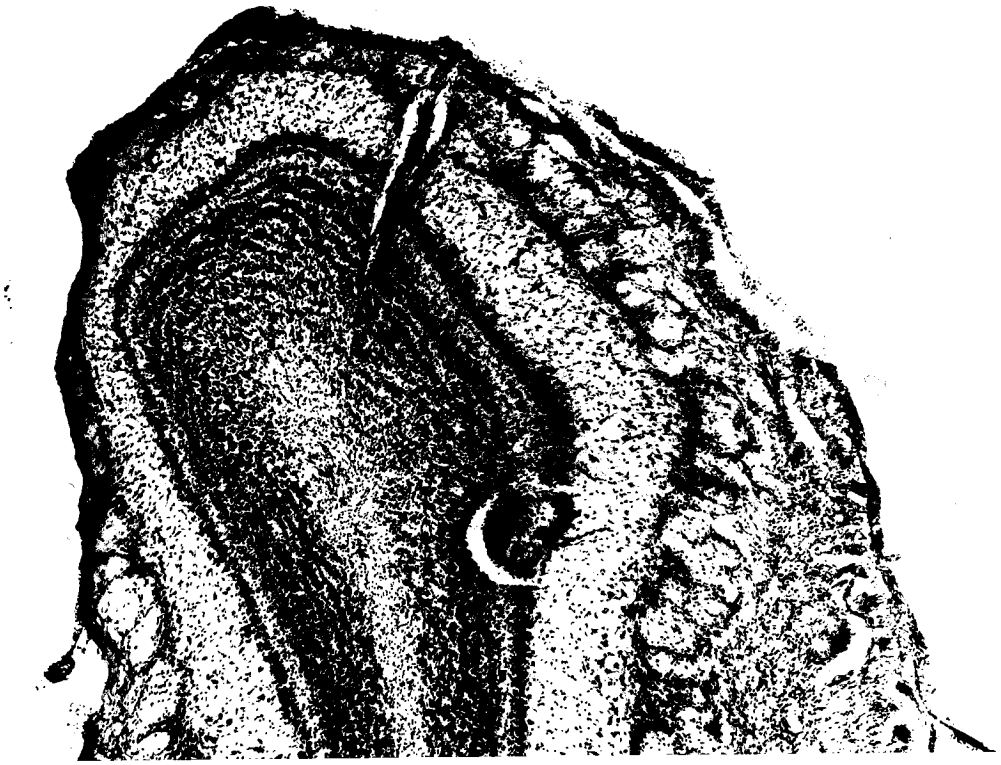

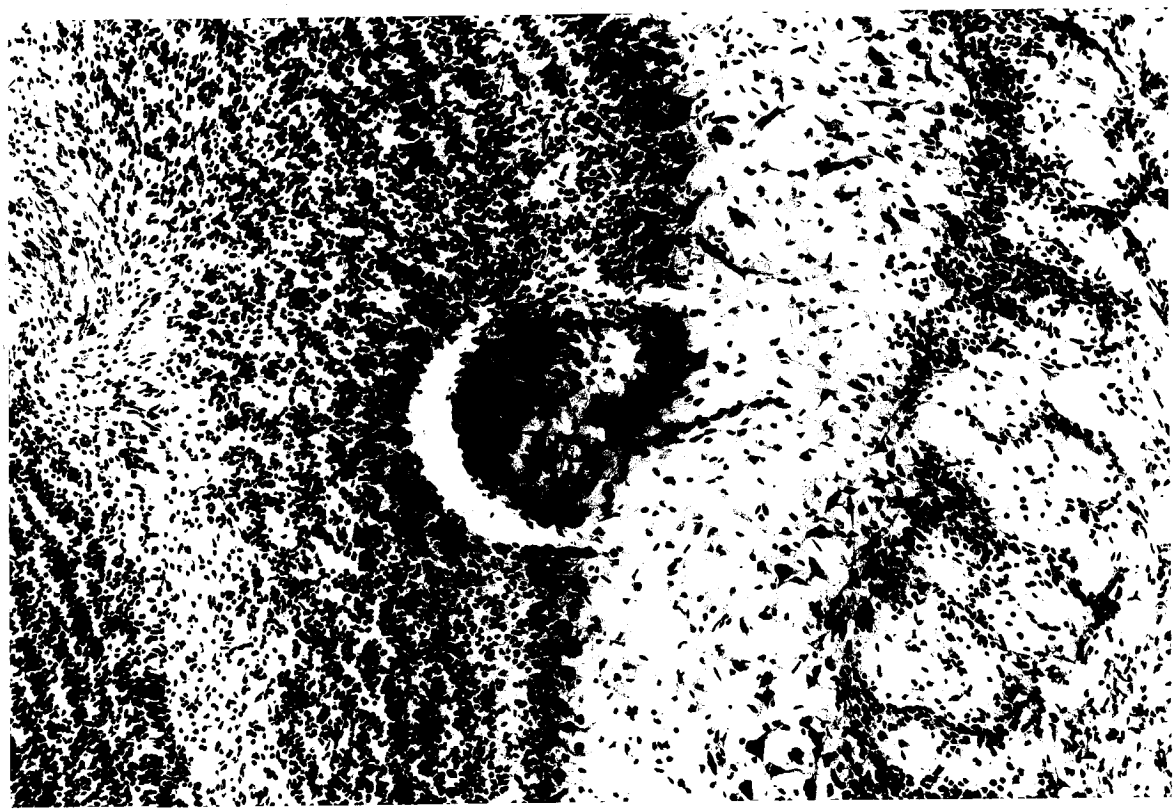

BASIC CELLULAR RESPONSE PROPERTIES

The first stage of data analysis involved performing measurements similar to those that have been used previously to characterize mitral cell responses. As described in the methods section, we characterized a neuron's response to a particular odor in terms of three properties: mean rate, odor-onset, and respiration-phasic effects. This analysis was applied to each of the three odorants. The number of significant responses to each odor in each category is displayed in Table 2. In general, odorant responses were difficult to detect in the mean firing rate but were seen in roughly equal amounts at 10% for each odor, in both the phasic measures (Table 2). Several neurons responded to more than one odorant for each measure.

Mean firing rate responses. Of the three features of odorant response analyzed, odor-dependent changes in mean firing rate were clearly the least prominent. The ANOVA analysis of the overall datasets indicates that in 12% of the cases the firing patterns were significantly different from uniform. When comparisons were made between the three individual odors and their immediately preceding pure air periods, < 5% showed a significant difference (by Fishers Protected Least Significant Difference test, 95% criterion) for each comparison (Figure 9 A, B). The number of significant responses to each odor is given in table 2.

Responses following odor onset. A wide variety of histogram shapes were observed during odorant presentations (Figure 9 C, D). Previous studies (e.g., Hamilton and Kauer 1985; Harrison and Scott 1986) have also shown a very wide variety of single-unit responses to odorants. As discussed in the methods section, we compared histogram shapes between the odor and air periods to determine response. Roughly 10% of the neurons showed a statistically significant response (Chi-squared test, 95% criterion) for each odor (table 2). In general, however, there were no consistent patterns to the odor-presentation responses, though for Citral and isoamyl acetate (Odors 1 and 2) there is some tendency for a slightly elevated spiking rate during the first second after odor presentation (Figure 13 A, B).

Table 2. Odor response percentages *.

	Any odor	Odor 1	Odor 2	Odor 3
Main Dataset				
Mean**	7.6 (12)	2.8	3.2	3.5
POH†	27	11	12	9
PRH‡	23	10	9	7
Sniff Dataset ***				
PRH‡	28	9	9	10
Multiunit Dataset				
Mean**	7.2 (10)	3.5	3.3	2.0
POH†	72	43	45	45
PRH‡	63	40	25	20

* Percent with significance greater than 95%. Only those recordings with a firing rate of > 0.5 Hz are included.

** Means: Percent responding with a change in the mean firing rate. The percentage of significant ANOVA tests over the whole set of odors is given in brackets. The significance of the individual odors was found according to Fisher's Protected Least Significant Difference test.

†POH: Percent showing a phasic response to odor onset. In some cases a neuron responded to more than one odor, therefore the first column is less than the sum of the last three.

‡PRH: Percent showing a respiration tuning in response.

*** Only the PRH percentages could be found for the sniff dataset. See Methods section.

Respiration related responses. A large proportion (46%) of neurons showed a significant tendency for firing rates to depend on the respiration phase, when considering the entire recording run. However, only 10% of the recorded neurons showed clearly different respiration related responses during odor presentation as compared to pure air (Table 2) for each odor. As with the odor-onset responses, many different combinations of respiratory triggered responses were observed (Figure 9 E,F). The bulk of the responses were either excitatory or inhibitory at onset of inspiration (phase=0 deg), as seen in the tendency for the corresponding bins to have elevated or depressed spike counts. Both these results are comparable to previous results in awake (Chaput and Lankheet 1987) and anesthetized (Chaput et al. 1992) preparations.

Elevated respiration rates, referred to as sniffing, occur when rats are actively exploring their olfactory environment and presumably have heightened responsiveness to olfactory stimuli (Youngentob et al. 1987). For this reason, we separately analyzed the subset of data obtained during periods of sniffing activity, defined as at least 3 successive respiration intervals of less than 0.5 sec. This contained 30% the total recording time, and also about a third of the number of spikes in the complete dataset. Despite the smaller numbers, a much larger proportion of neurons (84%, a nearly two-fold increase) showed significant respiration tuning than for the main dataset (Table 2). However, the number of odor specific differences in respiration-phasic responses was almost the same (10% per odor).

Dependence on the duration of odor presentation. In order to test for the possible dependence of our results on the length of odor presentation, we compared cellular response properties using two slightly different odor-exposure cycles: 5 sec air, 5 sec odor, and 3 sec purge (N=435) and 10 sec air, 7 sec odor, 3 sec purge (N=183). Analysis using the chi-squared test revealed no significant difference in any of the cellular response measures listed above. One implication of this result is that no substantial changes in habituation effects were detectable in the 5- to 10-second range of inter-odor periods.

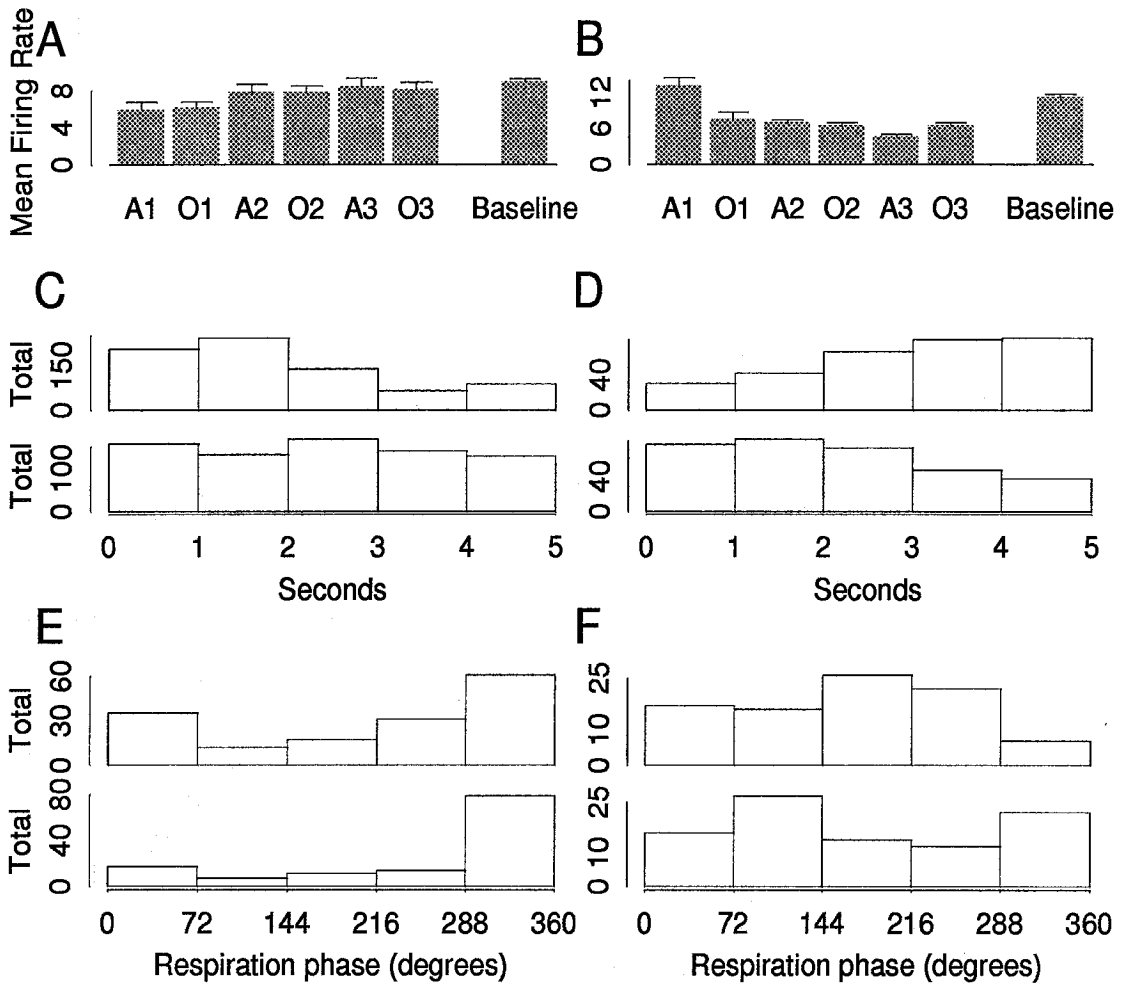

Figure 9.

A, B. Examples of responses in the mean firing rate. Error bars are standard errors of the mean. Bin names are: A1, A2, A3: air periods preceding odors 1, 2, 3, respectively. O1, O2, O3: odor periods 1, 2, and 3, respectively. Baseline firing rates are derived from an initial run in the absence of the odorants. This was carried out before any odorant trials had occurred.

C, D. Examples of odor-onset responses. The upper histograms are from the odor periods, the lower histograms from the air delivery periods as described in figure 5. The baseline bins are found as for the means. The chi-squared test is carried out between the upper and lower histograms to determine if the response is significant. In histogram D we have an example of a suppressive response to the odor which is delayed for approx. three seconds following odor onset.

E, F. Comparisons of respiration-phasic response between odor periods (Upper histograms) and their immediately preceding air periods (Lower histograms). The differences are significant in each case.

Dependence on binning. We repeated the above analysis using twice the number of bins (10) and half the bin width, to test for binning artifacts. The distribution of responses using 10 bins numbers were very similar to those using only 5 bins, showing that there are unlikely to be binning artifacts in the analysis.

Multi-unit data. The analysis described above was all performed on well isolated single units. However, we also recorded a large amount of multi-unit data in which single units could not be reliably isolated. The numbers of spikes in this dataset was much larger (4 fold) than in the main dataset, since the strict criteria for single-unit selection were no longer being applied. We have also analyzed this data, for comparison with the main dataset. Results indicate that the proportion of neurons responding to odorants by changes in the mean firing rate was similar to that in the isolated single unit dataset. Responses linked to odor-onset, however, were seen four times as often for each odor: 40% of the recordings. Respiration phasic responses were also significant in a larger proportion of cases (Table 2).

ANALYSIS OF VARIABILITY IN RESPONSES OF SINGLE CELLS

In performing the more classical analysis of mitral cell responsiveness just described, it became apparent that there was considerable variability in the responses of a particular neuron both within individual runs and between different recording sessions. As described in the methods section, we developed analysis techniques to look at this issue directly.

Variability within a run. The strongest effect seen in these statistical tests was not variation between odorants, but between cycles within a run (e.g., figures 5A, 6A). According to the ANOVA test, firing rate changes were significant in 56% of runs. This variability between trials was even more apparent in the multi-unit data analysis, occurring in 70% of recordings.

Variability between runs. In 121 neurons (65% of total), discrimination was maintained long enough to perform multiple stimulus runs. In 41 neurons (22% of total) discrimination was maintained over at least two days allowing a comparison of response properties on successive days. Our ability to

record the same neurons on multiple runs allowed us to examine the considerable response variability seen on successive runs, and even over several days.

We have made this comparison for all possible pairs of recordings from the same neuron at all available time intervals. These comparisons have been made based on the sum of significant Chi-squared differences as well as the distance measure R as described in the methods section.

Same neuron, Same day. Comparisons between recordings separated by intervals of 1 to 5 runs (time intervals of 10 min to 50 min) show a significant degree of change in responses as measured by the chi-squared test, in approx. 11% of cases. As described in the methods section, the number of cases with a significant chi-squared difference was summed and normalized for purposes of comparison with other datasets (Figure 10 B. Table 3). The measure R was also utilized for performing these comparisons (Figure 10A, Table 3). It is apparent that both measures of response difference remain approximately constant over time. As a check of these calculations, comparisons of recordings were also made against themselves, corresponding to an interval of 0 runs. As expected, the zero time interval comparisons show zero difference.

Same neuron, Successive days. In this case the interval was the number of days between recordings. R is similar to that for within-day comparisons (Table 3, Figure 10 A,B). The number of recordings available for the longer time intervals (3 to 5 days) is small, and therefore the error bars on those comparisons are larger. As previously, a check on the calculations was performed by comparing recordings made on the same day which corresponded to an interval of 0 days (self-comparisons excluded). These calculations correctly resulted in the same average as the within-day values of R .

Figure 10. Response variability over time.

A value of 1 corresponds to completely unrelated responses; and a value of 0 corresponds to identical responses. The x axis represents time. The first 6 points (Run interval) are for runs within the same day. Each run took approximately 10 minutes. The next 6 points (Day interval) compare runs separated by intervals of 0 to 5 days. Error bars are standard errors of the means.

A. Normalized distance measure R for the main, sniff and multiunit datasets. For all times greater than zero, R is significantly different both from zero (identical responses) and from 1 (unrelated responses). R is zero for times equal to zero. The error in R tends to increase with larger intervals because of decreasing sample size. The values of R for each dataset (main, sniff and multiunit) are significantly different from each other. The main dataset has the most consistent responses, followed by the multiunit dataset, and finally the sniff dataset.

B. Sum of significant chi-squared comparisons as a measure of response difference. This is a poorer measure of difference, as only approx. 11% of the responses which showed significant differences over time could contribute to the measure. However, it too falls cleanly between a difference of 0 and 1. The differences between the datasets cannot be resolved by this measure.

C. Normalized R for responses of individual odorants. All the odorants have essentially identical values of R over all times. This shows that the effects are not odor dependent.

D. Normalized R based on the three measures of response (mean rate, odor-onset and respiration related). It is clear that the different response measures have different degrees of variability. Respiration-related responses are the most stable, while odor onset responses, the least. Odor-onset and mean responses appear to become more variable when compared at intervals of more than 2 days, but this may be an artifact due to small sample size.

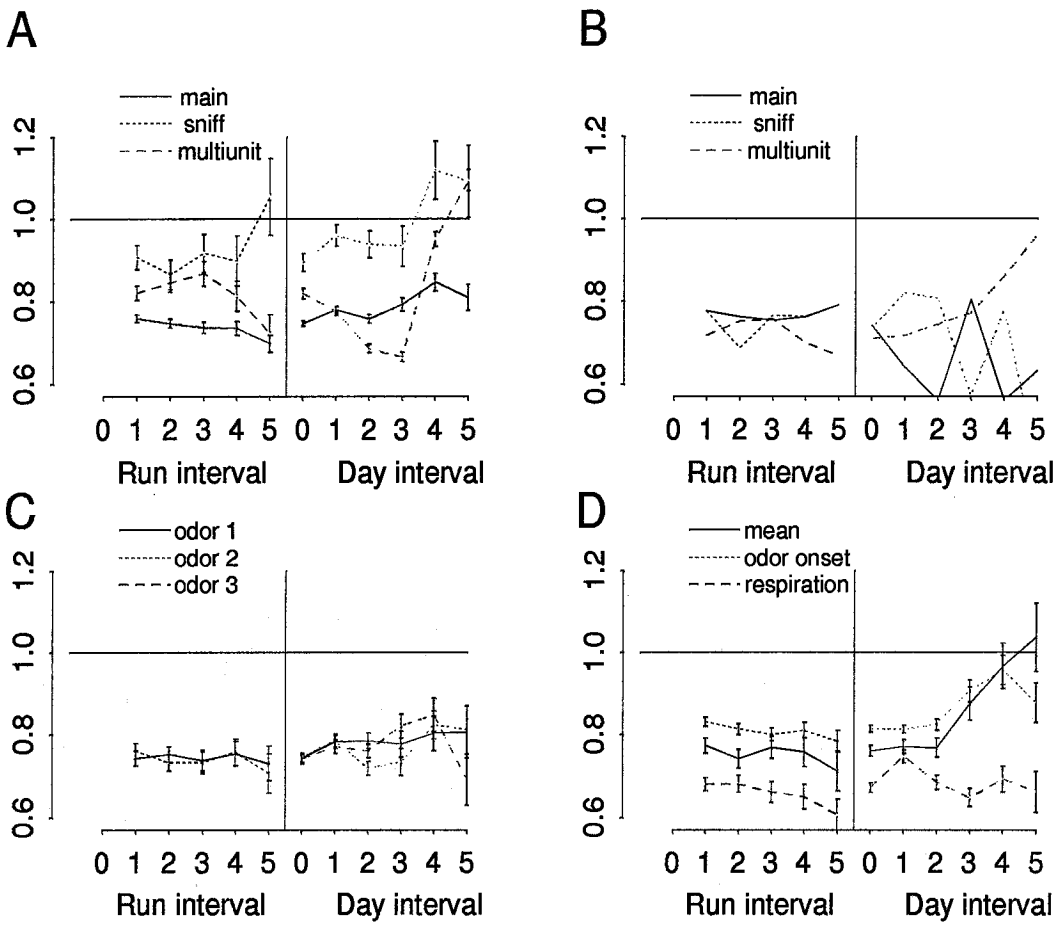
A
main
sniff
multiunit
0.6
0.8
1.0
1.2
0 1 2 3 4 5 0 1 2 3 4 5
Run interval
Day interval
B
main
sniff
multiunit
0.6
0.8
1.0
1.2
0 1 2 3 4 5 0 1 2 3 4 5
Run interval
Day interval
C
odor 1
odor 2
odor 3
0.6
0.8
1.0
1.2
0 1 2 3 4 5 0 1 2 3 4 5
Run interval
Day interval
D
mean
odor onset
respiration
0.6
0.8
1.0
1.2
0 1 2 3 4 5 0 1 2 3 4 5
Run interval
Day interval

Table 3. Distance measures* for different datasets†

	ss	sm	ns	nm	ds	dm
main	.73±.008	.76±.005	.84±.008	.83±.006	1.06±.007	.99±.007
sniff	.89±.03	.93±.02	.81±.03	.92±.02	1.06±.02	1.02±.02
multiunit‡	.82±.02	.82±.006	-	-	1.11±.01	
large	.70±.01	.69±.01	.77±.02	.81±.01	1.01±.02	.85±.02
odor 1	.74±.01	.76±.01	.86±.02	.83±.01	1.10±.01	1.01±.02
odor 2	.73±.02	.76±.01	.84±.02	.83±.01	1.10±.01	1.03±.01
odor 3	.74±.01	.76±.01	.82±.01	.84±.01	1.04±.01	.97±.01
means	.75±.02	.78±.01	.84±.02	.84±.01	.97±.01	.93±.01
POH	.80±.01	.82±.006	90±.01	.88±.007	1.02±.01	.98±.01
PRH	.66±.01	.70±.01	.78±.01	.78±.01	1.14±.01	.98±.01
chi main	.74	.68	.85	.76	1.09	1.07
chi sniff	.73	.75	.48	.74	.98	1.03

* Distance measures are defined in the methods section. They are expressed here as normalized means ± standard error of mean.

† Datasets: main = recordings during normal respiration; sniff = recordings during sniffing; multiunit = multiunit recordings; large = high amplitude neurons; odor 1, 2, 3: subset of data taken during presentation of specified odor; means = comparisons using only mean firing rate responses; POH = comparisons using only phasic responses to odor onset; PRH = comparisons using only respiration-tuned responses; chi main = main dataset using counts of significant chi-squared differences rather than distance measure (see methods); chi sniff = sniff dataset chi counts.

‡ The multiunit dataset did not have any near-neuron comparisons, since all recordings from a given stereo electrode were combined in this dataset.

Variability during sniffing. For both same day and different days, the observed variability (R = 0.89 and 0.93, respectively) is much greater during sniffing, i.e., much closer to chance levels than the main dataset (Figure 10A, Table 3). R for the sniffing dataset was constructed using only the respiration-related responses, and is therefore more appropriately compared with the respiration response variability of the main dataset (Figure 10 D, Table 3, last line). In this case the contrast is even more striking, since in the main dataset the respiration responses are the least variable (R = 0.66 and 0.70, respectively). This finding is especially interesting in the context of the spatial relationships discussed below.

Types of response changes. The preceding measures of change in response only reveal total change. We have also analyzed the details of changes underlying these measures. This was assessed by considering the response transitions seen when comparing the significant responses on successive trials. As described in the methods section, there are seven possible categories of response. We also include transitions to and from the null response condition (Table 4). Overall, there is no clear pattern to the response transitions. The most common transitions was from response to non-response. There was no particular tendency for responses to remain consistent.

Table 4. Response transitions*

	M†	POH1	POH2	POH3	PRH1	PRH2	PRH3	NONE
M	6	6	6	9	2	4	4	23
POH1	7	8	10	7	4	7	8	10
POH2	4	9	17	5	6	10	9	12
POH3	5	4	6	1	4	3	1	17
PRH1	6	6	8	6	5	5	4	12
PRH2	6	6	8	3	11	6	3	9
PRH3	3	9	4	3	2	3	5	10
NONE	25	17	16	16	22	15	4	116

* Number of cases where significant responses in the named rows were followed by significant responses in the named columns, on successive runs.

† Abbreviations for significant response categories are as follows: M: mean rate; POH1: phasic response to odor 1 onset; POH2: odor 2; POH3: odor 3; PRH1: phasic response in respiration tuning for odor 1; PRH2: odor 2; PRH3: odor 3.

Distribution of R. In order to quantify the range of response variability seen in this experiment, we estimated R for each neuron individually. We find that the population of neurons follows a normal distribution with respect to R (Figure 11). In other words, some neurons are more variable, some less so, but the population as a whole has a roughly normal spread of such neurons. The significance of this finding with respect to the mechanisms of response variability is dealt with in the discussion.

Additional comparisons.

As noted in the methods section, comparisons involving only one response measure (means, odor-onset and respiration-phasic responses) must be treated as separate distributions. Individually, each of these comparisons behaved much the same as the combined responses (Figure 10 D, Table 3). The respiration-phasic response was more consistent over time than the other two, both according to R and the chi-squared test. For multi-day comparisons the mean and odor-phasic responses showed a remarkable increase in variability (to levels approaching unrelated recordings, R = 1) when comparing recordings 4 or more days apart (Figure 10 D). This was not the case for the respiration-phasic response.

In general, the tendency of a neuron recorded at different times to respond more similarly than chance levels was a robust phenomenon. Subsets of the main data set, such as high-amplitude neurons, comparisons made one rat at a time (data not shown), comparisons restricted to one odorant at a time, and comparisons using different bin sizes, behaved in the same way as the main dataset (Table 4). In multi-unit data (Figure 10) there appeared to be greater variability in individual responses (difference measures of 0.82 for same as well as multi-day comparisons), but again the difference measures were stable over time.

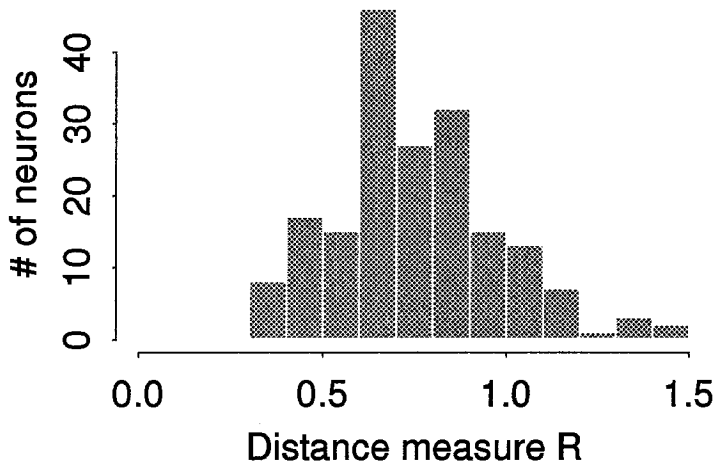

Figure 11. Distribution of R over the entire set of neurons. Note that it is reasonably close to a normal distribution. Some neurons appear to respond fairly consistently, while at the other extreme there appear to be a few neurons whose responses at different times are complementary.

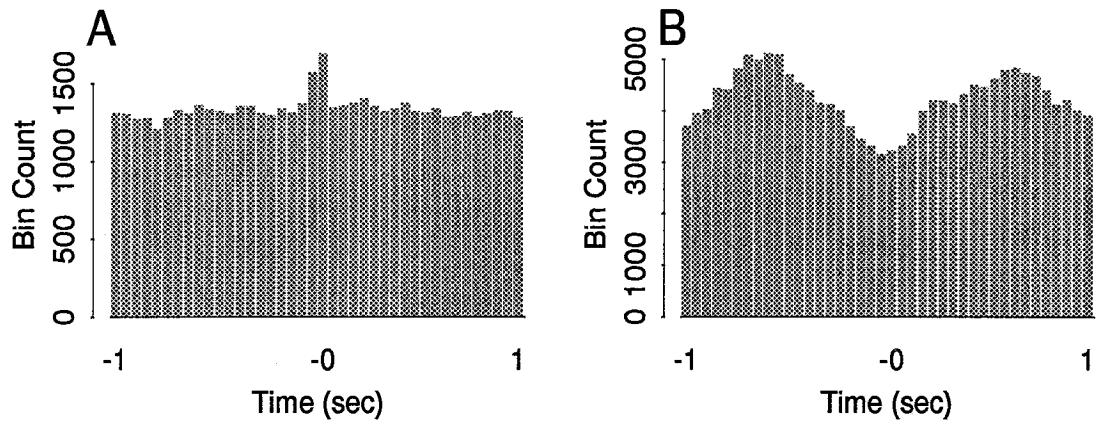

Figure 12. Cross correlation histograms for simultaneously recorded neurons.

A. An adjacent pair of neurons. There is some correlation in activity at intervals of less than 50 msec. Such responses were rather rare.

B. A distant pair of neurons. Each neuron had strong baseline respiratory tuning, which is reflected in the cross correlogram. Such relationships were observed between adjacent as well as distant neurons, but were also rather rare.

RESPONSES OF SIMULTANEOUSLY RECORDED NEURONS

A total of 404 pairs of simultaneous neuronal recordings were obtained, 127 from adjacent neurons and 277 from distant neurons. While techniques for evaluating data from multiple simultaneously recorded neurons are being developed (Gerstein and Aertsen 1985) the relative complexity of our stimulus scheme in addition to the complications due to the variability in respiratory cycle make these difficult to apply. We therefore carried out basic cross correlation studies on simultaneously recorded neuronal pairs, in addition to the spatial response analysis discussed below. Large cross-correlation effects were uncommon, but were observed both in adjacent (Figure 12 A) and distant (Figure 12 B) pairs of neurons. As might be expected, strong cross correlations were frequently related to respiration tuning of neuronal responses. (Figure 12 B) (Buonviso et al. 1992). Unfortunately, the irregular nature of the respiratory cycle limits the use of cross correlograms as a measure of relatedness of response in the analysis of this multiunit data.

In the following sections, we use the previously described difference measure R to contrast the response properties of nearby and distant cells recorded at a range of time intervals.

Adjacent neurons (recorded from the same stereo electrode). All pairs of neurons recorded from the same electrode on a given day (including simultaneous recordings), and multiple days, were compared. The geometry of the stereo electrodes is such that the separation of these neurons is unlikely to be more than 40 microns. The time interval between the recordings was noted, and the resultant values for R are shown in Figure 13 A. Also see Table 3. Two features of this comparison are notable: the value of R (0.84 for same day; 0.83 for multi-day), which is significantly smaller than chance levels, and the consistency of R over time. This consistency extended to multiple day comparisons. Similar, though less precise conclusions may be drawn from the summation of significant chi-squared differences (Table 3).

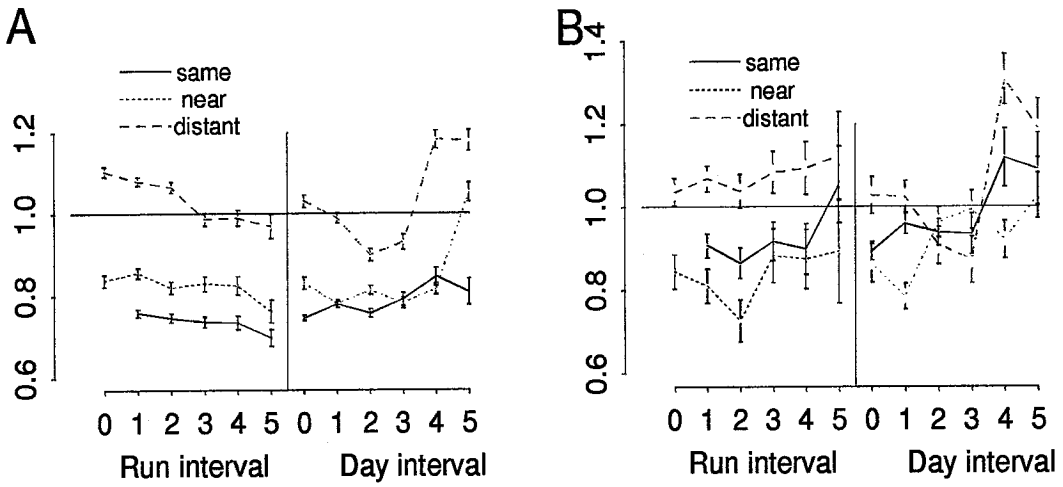

Figure 13. Normalized R for different comparisons between neurons, at different time intervals.

A. Main dataset. The responses of the same neuron at different time intervals (same); adjacent neurons (near); and distant neurons (distant); are compared. R for same-neuron comparisons is smaller than for near-neuron comparisons, which are in turn smaller than chance. Both these effects seem to be consistent over all times studied. The 'distant' responses appear to start out more dissimilar than chance levels, but drop to nearly chance levels for intervals of more than 3 runs. The smaller numbers available for comparison at longer time intervals make it difficult to assess the significance of R for longer time intervals.

B. Sniff dataset. In this case the 'near' responses and 'distant' responses behave quite similarly to the main dataset, but R for the 'same' comparisons increases to a level between 'near' and chance. At intervals of more than a day, however, both 'same' and 'near' cases have a large R. The small sample size reduces the precision of the estimates for large time intervals.

Distant neurons (recorded from different electrodes). Comparisons were made between all possible pairs of neurons recorded on the same day and the same rat, on different electrodes (Figure 13 A). The electrode spacing was at least 400 mm (Figure 2, microdrive design). Again, the time interval between the recordings was noted in order to evaluate how R changes for recordings made at different times. In this case the value of R is significantly greater than chance (1.06), i.e., the responses are more dissimilar than chance levels. The same conclusion may be drawn from the chi-squared comparisons (Table 3).

When the corresponding comparisons were made over multiple days, the resulting difference measure (R = 0.99) was at chance levels. The production of dissimilar responses at large distances appears to be a short-term effect. However, the chi-squared comparisons continue to indicate an increased difference measure (1.07). In the absence of confidence limits for the latter case, we cannot say whether this is a real effect.

Data during sniff periods. The same comparisons were carried out on the subset of data recorded during sniff periods.

1. Adjacent neurons. Comparisons were carried out on all possible pairs at known time intervals, as for the main dataset (Figure 13, Table 3). We obtained a value of R = 0.81 for same-day comparisons, which was consistent over runs carried out within the same day. However, the multi-day comparisons resulted in a larger value of R = 0.92. The chi-squared counts agree with this trend (Table 3).

2. Distant neurons. The same-day R was 1.06, significantly greater than chance. Over multiple days R was not significantly different from chance levels. The chi-squared counts do not appear to be different from chance levels in either case.

Comparison of variability over time and space.

The use of a single, normalized scalar measure of similarity/difference of responses enables direct comparison between the cases listed above (Figure 14 A, Table 4). Using the summary data in table 3, we obtain the following sequence of increasing R for neurons from the main dataset:

$$ss(0.73) \leq sm(0.76) < as(0.84) \approx am(0.83) < dm(0.99) \approx c(1) < ds(1.06)$$ where ss = same neuron, same day; sm = same neuron, multiple days, as = adjacent neurons, same day, am = adjacent neurons, multiple days, ds = distant neurons, same day, dm = distant neurons, multiple days, and c = control. Basically, a particular neuron responds fairly consistently, its neighbors tend to respond similarly to it, and distant neurons tend to respond in a complementary manner. Essentially this same sequence is also seen for subsets of the main dataset, whether comparisons are restricted to a single odor, or to a single response measure. The chi-squared counts agree well with this sequence.

The sequence of R for the sniff dataset differs from the main dataset:

$$as(0.81) < am(0.92) \approx ss(0.89) \approx sm(0.93) < dm(1.02) \approx c(1) < ds(1.06)$$ In this case a neuron is more likely to respond in a similar manner to its neighbor recorded at the same time, than to itself at subsequent times (Figure 14 B). At longer times neighboring cells respond about as differently as do the individual cells. Distant neurons recorded at small intervals respond differently, and at long intervals their responses are unrelated. The chi-squared counts measure is inconclusive about distant neurons, but is consistent with trend for the remainder of the sequence.

As discussed below, these two sequences suggest quite different processing modes during normal respiration and sniffing.

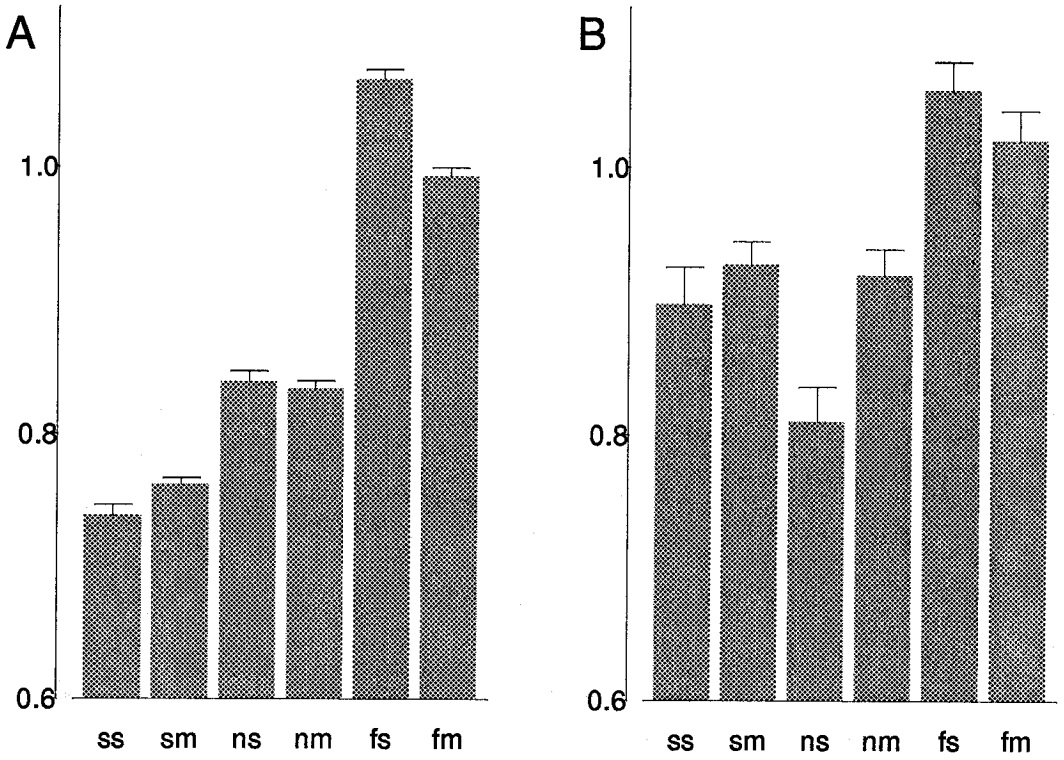

Figure 14. Normalized R, combined over time.

Bin labels: ss = Same neuron, Same day. sm = Same neuron, Multiple days. ns = Near neurons, Same day. nm = Near neurons, Multiple days. fs = Far neurons, Same day. fm = Far neurons, Multiple days. Error bars are standard errors of means.

A. Comparisons from the main dataset. There are significant differences between all bins, except 'ns' and 'nm.' Furthermore, all bins except 'fm' are significantly different from the chance level, 1.0. The intuitively obvious sequence of differences is apparent here: the same neuron responds fairly consistently, adjacent neurons less so, and distant neurons are even more different than chance, at least for short times.

B. Comparisons from the sniff dataset. Since the number of spike events in this dataset was smaller, the error bars are larger. The only significant differences are between 'ns' and the other bins, and between 'fs' and 'fm' and the other bins. Again, all bins except 'fm' are significantly different from chance levels. In this dataset, R is smallest for adjacent neurons recorded on the same day. Even the responses of an individual neuron are more variable, i.e., have a larger R.

DISCUSSION

Recording conditions.

To assure that the responses recorded were as "natural" as possible, these experiments were performed in awake freely moving animals. While there is a large body of literature on mitral cell response properties in the anesthetized preparation (e.g., Harrison and Scott 1986) there are relatively few in awake animals (e.g., Chaput 1985; Pager 1985). Further, previous reports have been limited to recording responses over relatively short periods of time (minutes to hours) where we have recorded responses up to several days. In addition, our study involves a relatively large sample of neurons. As discussed below, the ability of the animals to display changes in behavioral state, such as sniffing, provided additional insights into the processes taking place in the olfactory bulb.

One of the difficulties in performing olfactory stimulus experiments, in contrast to other modalities, is the long time course over which olfactory neuron responses frequently occur (e.g., Harrison and Scott 1986; Chaput and Panhuber 1982). This complicates the use of multiple stimulus cycles, since one cannot be sure that there will not be dependencies on previously delivered stimuli. This effect is reduced at low odor concentrations (Harrison and Scott 1986), and this was a major reason for using nanomolar odorant concentrations in this study. Second, naturally occurring odorant stimuli are often present at low concentrations and we wished to observe responses in as natural a context as possible. Third, we wished to avoid causing aversive responses in the rats which might be induced by high odor concentrations. Fourth, there are suggestions in the literature that odorant responses at high concentrations may be complicated by the recruitment of additional receptor neurons and glomeruli (Lancet et al. 1982) which do not normally respond to them at lower concentrations.

The concentrations used here are well above levels reported for single receptor cell discrimination and olfactory bulb neuron discrimination (Duchamp-Viret et al. 1990). As described in the Appendix, we have verified that animals can readily detect our set of odors at these concentrations, and can discriminate between them.

Temporal aspects of olfactory information encoding.

In this study we estimated three temporal features of mitral cell firing which have been suggested to encode olfactory information: mean rates, phasic responses related to odor onset, and respiration-related responses.

In particular, the mean firing rate is shown to be a relatively poor measure of neuronal response to an odor, while the phasic components of response appear to encode more odor related information. Based on the number of neurons which show odor-onset and respiration-phasic response, these two features of the firing patterns appear to carry roughly equal amounts of information. Each of these categories of response has been suggested in previous studies to be relevant to olfactory information encoding (mean rates: Meredith 1986; odor onset: Kauer and Shepherd 1977; respiration-phasic: Chaput et al. 1992). It has been accepted for some time that mean rates are less likely to be a good measure of odorant response (Meredith 1986), but to our knowledge a comparative estimate of all three measures has not been previously carried out.

The types of response to odorants seen in this study are in generally good agreement with many previous investigations both in anesthetized animals (e.g., Chaput et al. 1992; Harrison and Scott 1986) and unanesthetized (Chaput 1985; Chaput and Lankheet 1987). It is interesting that there is qualitative agreement between the two, since this indicates that the responses are a fundamental property of the network which is not greatly affected by the animal being conscious. Awake and anesthetized responses have previously been directly compared (Chaput and Holley 1979) and shown not to differ with respect to cell classification, though the firing patterns did change. Awake recordings are more likely to reveal aspects of behaviorally relevant information processing in the system, as we discuss later.

The somewhat low response probabilities we observe are consistent with experiments that indicate that low odorant concentrations reduce the number of readily observed responses (Wellis et al. 1989; Harrison and Scott 1986; Chaput and Lankheet 1987). This is also consistent with results from 2-deoxyglucose studies showing that at low odorant concentrations the number of glomeruli which display a significant degree of labeling is considerably reduced (Lancet et al. 1982).

Variability in single cell responses.

We have found a remarkable degree of variability in single cell responses to odors. This is a very robust result. It is evident in two different tests (summing chi-squared responses as well as from the distance measure), and is present in all subsets of data from the main dataset. Response variability has previously been reported on short time scales (minutes to hours) in anesthetized (Harrison and Scott 1986; Macrides and Chorover 1972) and awake (Chaput and Holley 1983) preparations. Our study has dealt with a greater range of times, with a larger sample of neurons, and has quantified the extent of this variability. We have shown that a) the degree of variability is smaller than chance levels, b) response variability is consistent over time, and c) that the distribution of variability resembles a normal distribution.

The observation of variability in neuronal response could be interpreted in a number of ways. First, there could be a fixed fraction of neurons whose responses are always consistent, and the remainder of neurons be completely changeable. Second, individual neurons could maintain their responses for a fixed period, and then change to another steady response. This might occur, for example, as a result of changing peripheral connectivity due to a rapid regrowth of peripheral receptors (Graziadei and Monti Graziadei 1979). Third, individual neurons could have two components to their responses, a consistent response component and a variable component, in such a ratio as to give rise to the observed degree of variability.

Not all of these possibilities, of course, are mutually exclusive. However, we have found it possible to weight the likelihood of several by a closer examination of the data. For example, if we were seeing variability in a sub population of neurons with others remaining stable, it seems reasonable to assume that the first possibility was correct. When the data is examined, however, we find that the neurons fell into a continuous distribution (Figure 11) rather than two classes of neurons with small and large amounts of change. If the second alternative is correct, then we would expect less variability in response at short time intervals compared to longer intervals. Figure 10 A indicates that this is not the case. Instead the same degree of variability is seen regardless of the length of time between the samples.

We therefore are inclined to accept the third alternative as the model for individual neuronal response variability.

Our hypothesis is that individual neurons have both a consistent and a variable component to their response, and that the relative sizes of the two components varies according to a normal distribution. In terms of information encoding, this implies that an individual mitral cell could potentially respond differently at different times, but over time, or over a large population of cells, there would be a clearly identifiable consistent response. Thus the specificity of responses and perceptual stability could be maintained over a population of neurons. A distributed representation of this sort would also explain observations on the resilience of olfactory memories after ablation of substantial portions of the olfactory bulb (Slotnick et al. 1987).

This idea provides a way of reconciling some of the previous, apparently contradictory observations on consistency or variability in mitral cell responses to odorants. In a sample from the mitral cell population, one would have examples of consistent or variable cells. The proportions of each would depend strongly on the exact experimental conditions. For example, stably anesthetized preparations might be expected to show somewhat more consistent responses, especially if the respiration and other variables were carefully controlled. Several of the studies which have reported variability have indeed been performed in awake animals (e.g., Chaput and Holley 1983). We have direct evidence that attentional states affect the degree of variability, in that neuronal responses during sniff cycles are much more variable than during normal respiration (Table 4). Odor concentration is another factor which may affect the relative degree of consistency and variability in observed responses. It is also likely that the consistency of mitral cells in different parts of the bulb may intrinsically vary over a wide range, perhaps in a manner related to narrowness of tuning or topography of projections (Astic et al. 1987).

Confounding learning paradigms. One important consequence of our results concerns the examination of possible learning effects in the olfactory bulb (Goldberg and Moulton 1987; Freeman and Grajski 1987; Wilson and Leon 1988). In fact, the experiments described here were originally intended as controls for experiments in which we were recording from mitral cells during the acquisition of an odor

discrimination task. Having found considerable variability in response, we followed this up to establish baseline levels of variability. As already discussed, we found a consistent level of variability in responses over time.

Previous experiments on behavioral aspects of odor presentation (Goldberg and Moulton 1987) have reported an evolution of multiunit responses over days. This was interpreted as being related to the behavioral learning as these experiments involved a training sequence over the same time. Some degree of variability in the multiunit burst patterns was also observed. The present data indicate that a substantial fraction of such variation may arise spontaneously in the absence of any explicit learning. Such variability would have to be taken into account in interpreting learning experiments such as those of Goldberg and Moulton.

Spatial aspects of olfactory information encoding.

We have obtained a rather precise estimate of the degree of spatial relationships of responses of neurons separated by two distances (< 40 m, and ~ 400 m), and have observed the evolution of this relationship over time. In particular, adjacent neurons respond more similarly than chance levels, and distant neurons more differently. This effect is different from simple center-surround inhibition in that the measures of neuronal response are much more complex than simple changes in firing rate. Shorter term comparisons in acute preparations have come up with a qualitatively similar picture. Previous studies differ in their estimates of the range of maximal inhibition (e.g., 100-200 microns: Buonviso and Chaput 1990; Wilson and Leon 1987; 400-600 microns: Meredith 1986). Since our measurements only cover two separations, we are not in a position to address this question in detail. The complexity of the responses we have seen force us to raise the question whether the concept of center surround inhibition is really appropriate in this case. We would prefer to think of the effects of distance as contributing to computation in a way quite different from classical notions of center surround (see below). It is possible that the 'dissimilarity' effect is general and extends throughout the extent of the bulb. Such extensive interactions are most likely to be due to the dendro-dendritic interactions between mitral and granule cells in the external plexiform layer (Rall and Shepherd 1968; Price and Powell 1970). Our recent modeling

work (Bhalla and Bower 1993), as well as several experimental studies (Mori et al. 1982; Cinelli and Salzberg 1992) suggest that mitral cell secondary dendrites may be capable of active action potential propagation, which could play a major role in these interactions. Of course, glomerular layer cells (Pinching and Powell 1971 a,b; Meredith 1992) might play a role in closer range interactions, which would be at a smaller scale than the >= 400 microns length scale of the observations in the current study.

The dissimilarity of distant neurons in this study ceases to be significant at periods of over a day. This may simply be due to a reduced sample size. However, adjacent neurons continue to show essentially the same levels of similarity over days. It seems possible, therefore, that the processes involved in producing dissimilar responses are different and more dynamic than those resulting in similarity of responses of adjacent neurons. This dissimilarity may be interpreted as part of an active mechanism to assure a range of responses. In this way mitral cell responses at a distance may be being manipulated or controlled to assure a very broad sample of the stimulus space, while mitral cells locally are being tuned to look closely at one aspect. This idea fits with the apparent broad tuning (Sicard and Holley 1984) and diversity of receptors (Buck and Axel 1991) reported in the literature.

The same spatial relationships are apparent from the data collected during periods of sniffing. Within a day, the levels of similarity/dissimilarity are nearly the same as for the main dataset. At longer intervals both the adjacent and distant neurons show changes in the estimates of difference, again suggesting the presence of shorter-term mechanisms for spatial responses under these conditions.

Relationships between variability, spatial response and tuning

The properties of variability in response, response tuning, and spatial organization of responses might seem at first glance to be mutually exclusive. Our analysis demonstrates that all three emerge from the same set of data, and quantification of the degree of difference between responses reveals how they can coexist. Each of the properties is more a matter of degree than an absolute. Tuning of responses, which is implicit in labeled-line theories of olfaction, can clearly only be present to the extent that variability in response is absent. We find that response consistency lies on a continuum. This suggests that tuning properties are also a matter of degree. It has been proposed (Kauer 1987) that olfactory encoding may involve both a specific, highly tuned aspect, and a broader, distributed aspect. Our results would indicate

that rather than two distinct aspects, the tuned and distributed representations are just extremes among a range of encoding mechanisms.

Similarly, a spatial organization of responses may seem to imply consistent and well tuned responses of individual neurons. In fact, we observe a situation (during sniffing) where the spatial organization is even more stable than individual neuron response. It has been noted that a strict labeled line view of olfaction is likely to be incomplete (Shepherd 1993). Our results take this a step further and suggest that any theory of olfactory bulb function which relies on strict constancy of responses at the mitral cell level may also be too limited.

Modes of information processing in the olfactory bulb

As previously mentioned, our results indicate that comparisons between different combinations of neurons over time and spatial separation reveal a clear sequence. For normal respiration this sequence is:

$$ss \leq sm < as \approx am < dm \approx c < ds$$

and for sniffing the sequence is:

$$as < am \approx ss \approx sm < dm \approx c < ds$$

where ss = same neuron, same day; sm = same neuron, multiple days, as = adjacent neurons, same day, am = adjacent neurons, multiple days, ds = distant neurons, same day, dm = distant neurons, multiple days, and c = control. These results have strong implications for the information processing taking place in the olfactory bulb. The first sequence of difference in response is fairly intuitive: Individual neurons respond fairly consistently, adjacent neurons somewhat less similarly, and distant neurons respond in a complementary manner. The second sequence is remarkable in two ways. First, the variability in individual neuronal responses rises from its non-sniffing value to the point where it is significantly greater than the difference between adjacent responses. This implies that adjacent neurons are tracking each others responses, even while each individual response is varying considerably. Second, and more fundamentally, it represents a different organization of responses in the bulb, which takes place within the fraction of a second it takes for sniffing to be initiated. In other words, the bulb is functioning in a different mode during sniffing as compared to the 'resting' state.

Our interpretation of the altered state of response during sniffing is that responses to familiar odors are selectively suppressed in order to focus attention onto novel stimuli. The familiar odors in this case would be the three odors delivered in the cycle. Since the usual responses to these odors are suppressed, an increased variability in response becomes apparent.

The mitral-to-granule synapses offer a possible mechanism for this process. Each granule cell receives excitatory input from many mitral cells. NMDA receptors have been shown to be present at these synapses (Cotman et al. 1987). If these synapses were to be modifiable in an activity-dependent manner, then groups of mitral cells firing together (for example, in response to a common excitatory odorant) could lead to a strengthening of the synapses associated with those cells. However, these synapses are reciprocal. Therefore a strengthened connection onto a granule cell is likely to result in greater excitation of the local granule cell dendrite, which in turn will increase the inhibition on the original mitral cell (Shepherd and Brayton 1979). Consequently, if the granule cell activity were to be raised by centrifugal input, the responses to that particular odorant could be suppressed in a large number of mitral cells. This mechanism offers a way of quickly suppressing responses to a selected subset of odorants. There are a number of centrifugal inputs which terminate specifically on granule cells (e.g., HLDB, LOT. Reviewed in Mori 1987), which may serve this function.

We have proposed a model of mitral cell responses as a sum of a consistent component and a more variable component. However, we do not mean to imply that the variability is simply due to some random noise. In fact, it is interesting to consider the possibility that the variability in response may itself be a coordinated mechanism. It is striking that the reorganization of the bulb during sniffing may act as precisely such a mechanism. The dissimilarity of responses of distant neurons (above) may also be an example of this sort of coordinated response change. Further possible examples are provided by several studies which have demonstrated differences in response properties of olfactory bulb neurons related to behavioral states (Pager 1978; Freeman and Grajski 1987; Bressler 1988; Gray and Skinner 1988). It seems plausible that there may be several such 'modes of operation' of the olfactory bulb, each optimized for a specific task. From this perspective, the 'resting state' would correspond to a broad sampling of odor

space, sniffing would correspond to a selective search for new odors, hungry rats may specifically tune their olfactory responses to be sensitive to food odors (Pager 1978), and so on. The operation of a single network in a number of distinct states subserving different functions has been found to be a common feature of many invertebrate networks (reviewed in Harriswarrick and Marder 1991). Applying the idea in its extreme form, one could suggest that the variable component of neuronal response is continually regulated by feedback from higher centers as part of an ongoing, unconscious strategy for extracting maximal information from the odorant signal.

ACKNOWLEDGMENTS

We are grateful to Hemant Keny and Markus Djaputra who assisted with some of the experiments, and to Dr. Matthew Wilson who participated in the development of the microdrives. Kraig Anderson provided a great deal of help with the GCMS used for calibrating the olfactometer. The Eckoustic enclosure was a gift from Dr. Mark Konishi. The olfactometer and behavioral setup were built with the assistance of Tim Heitzman, Mike Walsh, and Herb Adams. Peirre Baldi, Jack Gallant, and Mike Lewicki were involved in many stimulating and valuable discussions on the work. The suggestions of John Kauer and Lewis Haberly are also deeply appreciated.

This investigation was supported by ONR contract number N00014-88-K-0513.

REFERENCES

ALBERTS, J.R., AND GALEF, B. G., JR. Acute anosmia in the rat: a behavioral test of a peripherally induced olfactory deficit. *Physiol. Behav.* 6:619-621, 1971.

ASTIC, L., SAUCIER, D., AND HOLLEY, A. Topgraphical relationships between olfactory receptor cells and glomerular foci in the rat olfactory bulb. *Brain Res.* 424:144-152, 1987.

BRESSLER, S. L. Changes in electrical activity of rabbit olfactory bulb and cortex to conditioned odor stimulation. *Behav. Neurosci.* 102: 740-747, 1988.

BUCK, L., AND AXEL, R. A novel multigene family may encode odorant receptors: a molecular basis for odor recognition. *Cell* 65: 175-187, 1991.

BUONVISO, N. AND CHAPUT, M. A. Response similarity to odors in olfactory bulb output cells presumed to be connected to the same glomerulus: Electrophysiological study using simultaneous single-unit recordings. *J. Neurophysiol.* 63: 447-454, 1990.

BUONVISO, N., CHAPUT, M. A. AND BERTHOMMIER, F. Temporal pattern analyses in pairs of neighboring mitral cells. *J. Neurophysiol.* 68: 417-424, 1992.

CHAPUT, M. A. Respiratory-phase-related coding of olfactory information in the olfactory bulb of awake freely-breathing rabbits. *Physiology and Behavior* 36: 319-324, 1986.

CHAPUT, M. A. AND PANHUBER, H. Effects of long duration odor exposure on the unit activity of olfactory bulb cells in awake rabbits. *Brain Res. Paris* 250: 41-52, 1982.

CHAPUT, M. A. AND HOLLEY, A. Spontaneous activity of olfactory bulb neurons in awake rabbits with some observations on the effects of pentobarbitol anesthesia. *J. Physiol. Paris* 75: 939-948, 1979.

CHAPUT, M. A. AND HOLLEY, A. Responses of olfactory bulb neurons to repeated odor stimulations in awake freely-breathing rabbits. *Physiol. and Behav.* 34: 249-258, 1983.

CHAPUT, M. A. AND LANKHEET, M.J. Influence of stimulus intensity on the categories of single-unit responses recorded from olfactory bulb neurons in awake freely-breathing rabbits. *Physiology and Behavior* 40: 453-462, 1987.

CHAPUT, M. A., BUONVISO, N. AND BERTHOMMIER, F. Temporal patterns in spontaneous and odour-evoked mitral cell discharges recorded in anaesthetized freely breathing animals *Eur. J. Neuroscience* 4: 813-822, 1992.

CINELLI, A. R. AND SALZBERG, B. M. Dendritic origin of late events in optical recordings from salamander olfactory bulb. *J. Neurophysiol.* 68: 786-806, 1992.

COTMAN, C.W., MONAGHAN, D.T., OTTERSEN, O.P., AND STORMMATHISEN, J. Anatomical organization of excitatory amino-acid receptors and their pathways. *TINS* 10:273-280, 1987.

DUCHAMP-VIRET, P., DUCHAMP, A., AND SICARD, G. Olfactory discrimination over a wide concentration range. Comparison of receptor cell and bulb neuron properties. *Brain Res.* 517: 256-262, 1990.

FREEMAN, W.J., AND GRAJSKI, K.A. Relation of olfactory EEG to behavior: Factor Analysis *Behav. Neurosci.* 101: 766-777, 1987.

FUJITA, S.C., MORI, K.R., IMAMURA, D., AND OBATA, K. Subclasses of olfactory receptor cells and their segregated central projections demonstrated by a monclonal antibody. *Brain Res.* 326:192-196, 1985.

GERSTEIN, G.L., AND AERTSEN, A.M.H.J. Representation of cooperative firing among simultaneously recorded neurons. *J. Neurophys.* 54:1513-1528, 1985.

GOLDBERG, S.J., AND MOULTON, D.G. Olfactory Bulb responses telemetered during an odor discrimination task in rats. *Experimental Neurology* 96: 430-442, 1987.

GRAY, C.M., AND SKINNER, J.E. Centrifugal regulation of neuronal activity in the olfactory bulb of the waking rabbit as revealed by cryogenic blockade *Exp. Brain Res.* 69: 378-386, 1988.

GRAY, C.M., AND SKINNER, J.E. Field potential response changes in the rabbit olfactory bulb accompany behavioral habituation during the repeated presentation of unreinforced odors. *Exp. Brain Res.* 73: 189-197, 1988.

GRAZIADEI, P.P.C., AND MONTI GRAZIADEI, G.A. Neurogenesis and neuron regeneration in the olfactory system of mammals. I. Morphological aspects of differentiation and structural organization of the olfactory sensory neurons. *J. Neurocytol.*, 8:1-18, 1979.

HAMILTON, K.A., AND KAUER, J. S. Intracellular potentials of salamander mitral/tufted neurons in response to odor stimulation. *Brain Res.* 338: 181-185, 1985.

HARRISON, T.A., AND SCOTT, J.W. Olfactory bulb responses to odor stimulation: Analysis of response pattern and intensity relationships. *J. Neurophysiol.* 56: 1571-1589, 1986.

HARRISWARRICK, R.M., AND MARDER, E. Modulation of neural networks for behavior. *Ann. Rev. Neur.* 14:39-57, 1991.

HASSELMO, M.E., AND BOWER, J.M. Cholinergic suppression specific to intrinsic not afferent fiber synapses in rat piriform (olfactory) cortex. *J. Neurophysiol.* 67:1222-1229, 1992.

HASSELMO, M.E., ANDERSON, B.P., AND BOWER, J.M. Cholinergic modulation of associative memory function. *J. Neurophysiol.* 67:1230-1246, 1992.

JIANG, T., AND HOLLEY, A. Some properties of receptive fields of olfactory mitral/tufted cells in the frog. *J. Neurophysiol.* 68:726-733, 1992.

JOURDAN, F., DUVEAU, A., ASTIC, L., AND HOLLEY A. Spatial distribution of 2-deoxyglucose uptake in the olfactory bulbs of rats stimulated with two different odors. *Brain Res.* 188: 139-154, 1980.

KAUER, J. S. *Coding in the olfactory system.* In: Neurobiology of taste and smell. Edited by T.E. Finger and W.L. Silver. John Wiley, New York. 1987.

KAUER, J. S., AND SHEPHERD, G.M. Analysis of the onset phase of olfactory bulb unit responses to odour pulses in the salamander. *J. Physiol. Lond.* 272:495-516, 1977.

KEPPPEL, G. *Design and analysis. A researcher' s handbook.* Second edition. New Jersey: Prentice-Hall, Inc., 1982.

LANCET, D., GREER, C.A., KAUER, J. S. AND SHEPHERD, G. M. Mapping of odor-related neuronal activity in the olfactory bulb by high-resolution 2-deoxyglucose autoradiography *Proc. Natl. Acad. Sci.* 79: 670-674, 1982.

MACRIDES, F. AND CHOROVER, S.L. Olfactory bulb units: activity correlated with inhalation cycles and odor quality. *Science* 175: 84-87, 1972.

MCNAUGHTON B.L., O'KEEFE, J., AND BARNES, C.A. The stereotrode: a new technique for simultaneous isolation of several single units in the central nervous system from multiple unit records. *J. Neurosci. Meth.* 8:391-397, 1983.

MEREDITH, M. Neural circuit computation: Complex patterns in the olfactory bulb. *Brain Res. Bull.* 29: 111-117, 1992.

MEREDITH, M. Patterned response to odor in mammalian olfactory bulb: the influence of intensity. *J. Neurophysiol.* 56: 572-597, 1986.

MORI, K. Membrane and synaptic properties of identified neurons in the olfactory bulb. *Progress in Neurobio.* 29: 275-320, 1987.

MORI, K., MATAGA, N., AND IMAMURA, K. Differential specificities of single mitral cells in rabbit olfactory bulb from a homologous series of fatty acid odor molecules. *J. Neurophysiol.* 67: 786-789,1992.

MORI, K., NOWYCKY, M.C., AND SHEPHERD, G. M. Impulse activity in presynaptic dendrites: analysis of mitral cells in the isolated turtle olfactory bulb. *J. Neurosci.* 2:497-502, 1982.

PAGER, J. Ascending olfactory information and centrifugal influxes contributing to a nutritional modulation of the rat mitral cell responses. *Brain Res.* 140: 251-269, 1978.

PAGER, J. Unit responses changing with behavioral outcome in the olfactory bulb of unrestrained rats. *Brain Res.* 289: 87-98, 1983.

PAGER, J. Respiration and olfactory bulb unit activity in the unrestrained rat: statements and reappraisals. *Behav. Brain Res.* 16: 81-94, 1985.

PINCHING, A.J., AND POWELL, T.P.S. The neuropil of the glomeruli of the olfactory bulb. *J. Cell Sci.* 9: 347-377, 1971a.

PINCHING, A.J., AND POWELL, T.P.S. The neuropil of the periglomerular region of the olfactory bulb. *J. Cell Sci.* 9: 379-409, 1971b.

PRESS, W. H., FLANNERY, B. P., TEUKOLSKY, S. A. AND VETTERLING, W. T. *The Art of Scientific Computing.* Cambridge, U.K. CUP, 1988.

RALL, W., AND SHEPHERD, G.M. Theoretical reconstruction of field potentials and dendrodendritic synaptic interactions in olfactory bulb. *J. Neurophysiol.* 31:884-915, 1968.

SCOTT, J.W., WELLIS, D.P., RIGGOTT, M.J., AND BUONVISO, N. Functional organization of the main olfactory bulb. *Micr. Res. and Tech.* 24:142-156, 1993.

SHEPHERD, G. M. AND BRAYTON, R. K. Computer Simulation of a dendrodendritic synaptic circuit for self and lateral inhibition in the olfactory bulb. *Brain Res.* 175: 377-382, 1979.

SHEPHERD, G. M. Principles of specificity and redundancy underlying the organization of the olfactory system. *Micr. Res. and Tech.* 24:106-112, 1993.

SICARD, G., AND HOLLEY, A. Receptor cell responses to odorants: similarities and differences among odorants. *Brain Res.* 292: 283-296, 1984.

SLOTNICK, B.M., GRAHAM, S. LAING, D.G., AND BELL, G.A. Detection of propionic acid vapor by rats with lesions of olfactory bulb areas associated with high 2-DG uptake. *Brain Res.* 417: 343-346, 1987.

SLOTNICK, B.M., KUFERA, A., AND SILBERBERG, A.M. Olfactory learning and odor memory in the rat. *Physiol. and Behav.* 50: 555-561, 1991.

SLOTNICK, B.M., AND NIGROSH, B.J. Olfactory stimulus control evaluated in a small animal olfactometer. *Perceptual and motor skills*. 39:583-597, 1974.

WELLIS D. P., SCOTT, J. W. AND HARRISON, T. A. Discrimination among odorants by single neurons of the rat olfactory bulb. *J. Neurophysiol.* 61: 1161-1177, 1989.

WILSON, D. A. AND LEON, M. Evidence of lateral synaptic interactions in olfactory bulb output cell responses to odors. *Brain Res.* 417: 175-180, 1987.

WILSON, D. A. AND LEON, M. Spatial patterns of olfactory bulb single-unit responses to learned olfactory cues in young rats *J. Neurophysiol.* 59: 1770-1782, 1988.

WILSON, M., AND BOWER, J.M. Cortical oscillations and temporal interactions in a computer simulation of piriform cortex. *J. Neurophysiol.* 67:981-995, 1992.

YOUNGENTOB, S. L., MOZELL, M.M., SHEEHE, P.R. AND HORNUNG, D.E. A quantitative analysis of sniffing strategies in rats performing odor detection tasks. *Physiol. and Behav.* 41: 59-69, 1987.

APPENDIX A - Behavioral controls for odor concentrations

BEHAVIORAL CONTROL.

These experiments have intentionally made use of very low odor concentrations. These low concentrations were chosen in order to reduce the possibility that neural signals would be seriously influenced by habituation during the relatively prolonged periods of odor presentation. As described in this appendix, a series of behavioral tests were performed in order to make sure that the odorants and concentrations used during neural recordings were detectable and discriminable by the rats.

Behavioral tests were carried out in a sound-proof box (eckoustic enclosure) with continual air circulation. Within this sound-proof box were the rat chamber and the odorant chamber (Figure 15 A), which was supplied with the odorized air. The settings on the Watts 26A pressure regulator attached to the air filter were the same in these behavioral experiments as in the recording sessions assuring that the same flow rates and odorant concentrations were used in each case. The odorant chamber used for the behavioral work (Figure 15 A) was smaller than the recording chamber (Figure 1) and therefore had an even shorter air replacement time.

Three female Sprague-Dawley (6 months) rats were trained in a series of go- no-go operant conditioning tasks, using water as a positive reinforcement (after Slotnick and Nigrosh, 1974). The rats were water deprived to not less than 80% of initial body weight, which was monitored daily. The rats were tested on a set of 6 odor discrimination tasks, proceeding to each after the previous task had been learnt to criterion (80% correct responses over a day's run of at least 80 trials). Each training trial consisted of an intertrial period of 3 sec, followed by an odor discrimination period signaled by the opening of a door to the odor chamber (Figure 15 A). An infrared beam detected the presence of the rat at the door. Touch sensitive paddles were used to monitor the response of the rat. The reinforcement was delivered at the paddle when it was correctly pressed according to the paradigm. Each rat underwent one training run (at least 80 trials) every day, following which the rats were returned to animal facilities.

Figure 15. Behavioral control. A. Behavioral setup. As described in the text, the door to the odor chamber is closed except during stimulus presentation. The odor chamber is shown displaced from the rat chamber for clarity; actually, they were tightly attached. The water reward is delivered though the tubes in the paddles. The odor chamber contains two paddles; however, there was no distinction between them in this paradigm. B. Performance of one of the rats on the odor tasks. The criterion level is 80%; 50% corresponds to chance. Stimulus pairs are labeled along the top of the graph. Alternate stimulus pairs are shaded for clarity. The first item in each stimulus pair is reinforced. Note the consistent responses following sham anosmia treatments with saline, and the abrupt fall to chance levels when the ZnSO4 treatment was carried out. The other two rats had very similar curves.

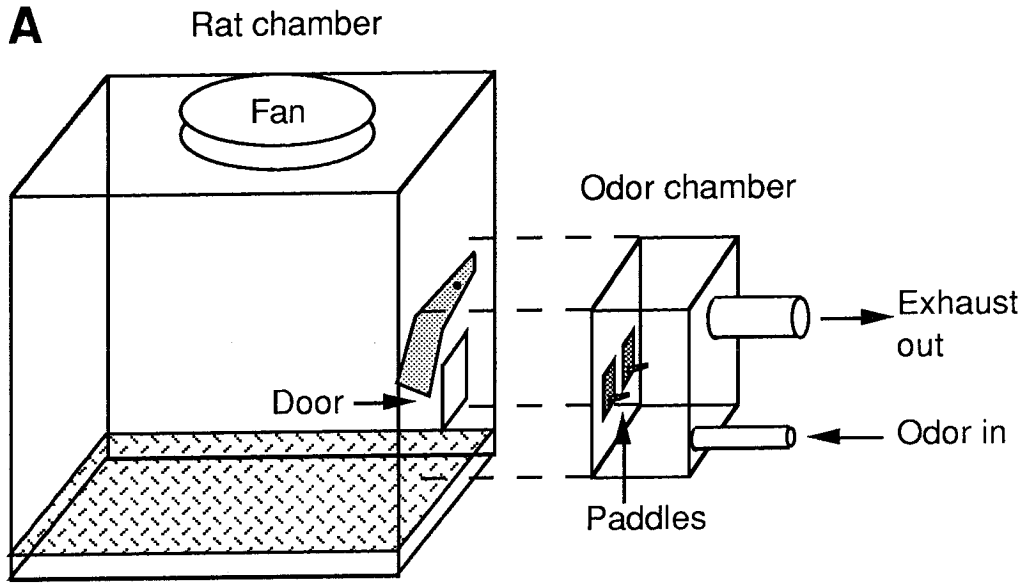
A
Rat chamber
Fan
Odor chamber
Exhaust
out
Door
Odor in
Paddles

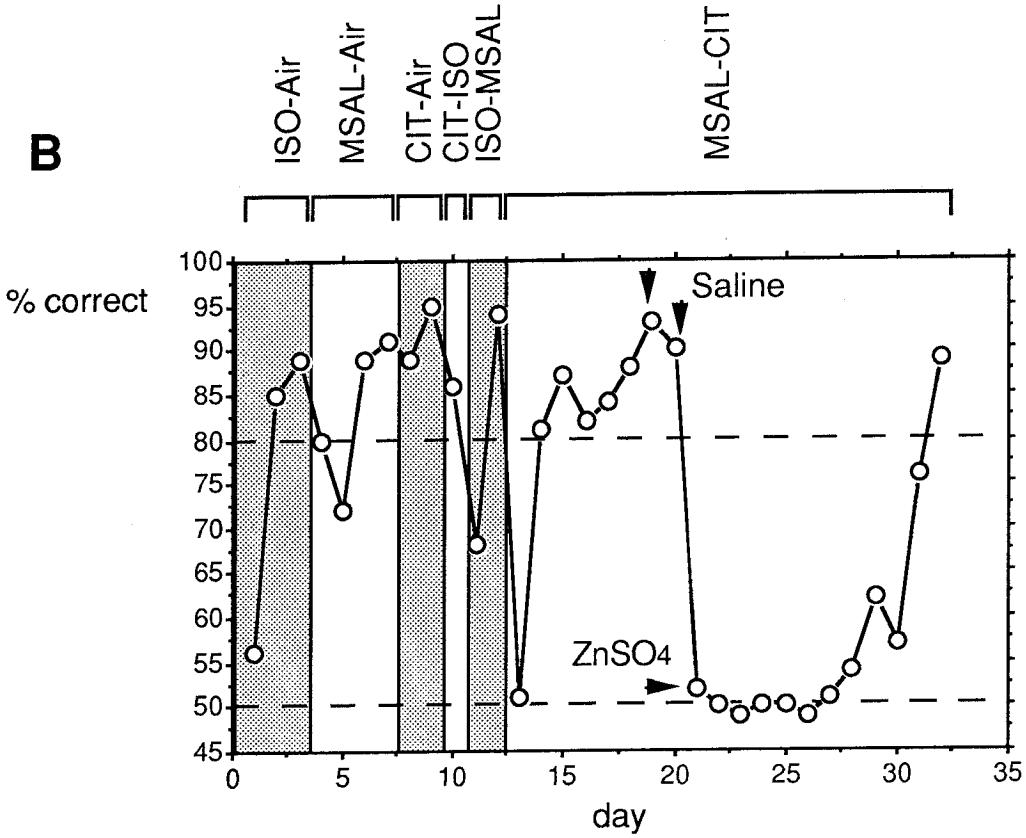
B
ISO-Air
MSAL-Air
CIT-Air
CIT-ISO
ISO-MSAL
MSAL-CIT
% correct
100
95
90
85
80
75
70
65
60
55
50
45
Saline
ZnSO4
0
5
10
15
20
25
30
35
day

Initial training was conducted with shaping and a simple paradigm which rewarded the rats for every paddle push. After the rats grew familiar with the setup and the mechanics of paddle pushing, they were introduced to the full odor discrimination paradigm. The initial set of three odor discrimination tests involved a discrimination between pure air and odorant. A go-no-go reward paradigm was used, where the odorant stimulus was associated with the reward. The rats were initially trained on ISO, and displayed the very quick learning expected of olfactory cues (Slotnick et al. 1991), performing to the 80% criterion within 2 runs (Figure 15 B). This demonstrates that the odorant concentrations used were well within the range detectable by the rats. When the rats had satisfied the criterion, they were switched to MSAL. This led to initially poor scores on the test, but within a day they were again performing to criterion. The final switch to CIT led to an even briefer period of erroneous responses, so that the total score for the day of the switch itself was above criterion in two out of the three rats. The third rat attained criteria on the following day. This formation of learning set for odorant cues is typical of rat behavioral learning on olfactory discrimination tasks (Slotnick et al. 1991).

Having established the ability of the rats to discriminate between each odor and air, the paradigm was changed to study discrimination between pairs of odorants. In this paradigm, one odor was the signal for the reward, and the other did not have any associated reward. In order to avoid bias to any particular odorant, the sequence of odor pairs was CIT-ISO, ISO-MSAL, MSAL-CIT, where the first member of each pair was reinforced. Learning of the odor-odor discrimination tasks took a little longer, because the reinforcement status of one of the odors was always the reverse of the previous pair of odors. This arrangement avoided the problem of the rats always associating the reward with a particular odorant. Despite the difficulty of this task, the rats typically performed to criterion within two training sessions.

The final phase of the behavioral tests was to verify that the rats were responding to odorants and not any other possible stimulus. The previous pair of odorants (MSAL-CIT) was retained for these tests. A sham infusion of saline through the nasal cavity was performed, and discrimination tested on the subsequent day. Having verified that performance was not impaired, anosmia was induced using infusion of 5% Zinc Sulphate (Alberts and Galef 1971). The performance immediately dropped to chance levels

(Figure 15 B). This demonstrates that the rats were performing the discriminations purely on the basis of odorant cues. During this final phase, it was necessary to run the rats for longer periods and/or supplement their water intake in order to maintain body weight. After 12, 14 and 19 days respectively, the rats recovered odorant discrimination capability. This is a somewhat longer recovery period than the 3 to 7 days that has been previously reported (Alberts and Galef 1971) and may be related to the use of relatively low odorant concentrations.

These behavioral controls establish the following points pertinent to the recordings. First, the rats are easily capable of discriminating between odorants and air; and between different odorants at the concentrations used in the experiment. Second, there are no signs of any impairment of discriminatory ability over the period of the behavioral tests (except for the anosmia test). This makes it unlikely that endemic nasal infections would be a significant factor in the recording results. Third, habituation effects, if any, do not impair odorant detection or discrimination on similar time-scales to those used in the recording experiments.

APPENDIX B. Calculation of R.

The measure R is used to compare responses of different neurons or of the same neuron at different times. The calculation of R involves several stages.

1. Comparison of two histograms, x and y. The histograms are first normalized so that each has a mean of one. Each histogram represents a point in space, whose components are given by the bin totals x_i and y_i respectively. The geometrical distance between the two bins is R_{raw}:

$$R_{raw} = \text{sqrt}(\Sigma(x_i - y_i)^2)$$

2. Estimation of error in R_{raw}. Since each histogram is constructed from multiple cycles, we can estimate the standard deviation of each bin i:

$$\sigma x_i$$

from the variance between cycles.

In order to obtain the standard deviation along the direction of R_{raw}, we take the component of σx_i and σy_i along R_{raw}:

$$sdev_x = \Sigma\ (\sigma x_i * (x_i - y_i)/dist)$$

$$sdev_y = \Sigma\ (\sigma y_i * (x_i - y_i)/dist)$$

The standard deviation in R_{raw}, $sdev_{raw}$, is estimated to be the sum of these two components.

$$sdev_{raw} = sdev_x + sdev_y$$

Note that this is likely to be on the large (conservative) side. When estimating the standard deviation of a difference it is more usual to take

$$sdev_{difference} = \text{sqrt}(sdev_x^2 + sdev_y^2)$$

However, we are using vector differences in this situation, and therefore it seemed more appropriate to use a conservative measure.

3. Combining R_{raw} for a pair of neurons. Each comparison between two neurons (or the same neuron at different times) involves seven individual comparisons between histograms. The corresponding histograms compared were:

Mean rate histograms. These have six bins each, i.e., O1, O2, O3 and A1, A2, A3. The comparison yields one value for R: R_M.

Odor Onset Histograms. These have 5 bins each, for the 5 seconds following odor onset. A response histogram is generated for each of the three odorants. Corresponding histograms are compared between the two neurons. Therefore we obtain three values for R: R_{O1}, R_{O2}, R_{O3}.

Respiration Histograms. These also have 5 bins each, but the bins represent 72 degrees of phase in the respiration cycle. Again, there are three odorants and therefore three comparisons are carried out to obtain: R_{R1}, R_{R2}, R_{R3}.

In general, the distributions of R_M, R_O, and R_R differ (Figure 10 D). This means that they need to be normalized separately, as discussed below. The three values for R_O: R_{O1}, R_{O2}, R_{O3} have the same distribution, and therefore can be combined. The same applies for R_M. The process of combining R and estimating the combined standard error are discussed below.

4. Combining R_{raw} over all possible pairs. Each specific comparison (e.g., same neuron recorded at intervals of 1 run) could usually be made on several pairs of neurons. The individual comparisons were made as described above, and the estimation of the overall value of R is discussed below.

5. Estimation of Combined R. The combined estimate of R was simply the average of the individual R_{raw} values. Care was taken to keep unlike distributions separate as mentioned in step 3. Therefore, R_M, R_O and R_R were separately averaged at this stage. The estimate of the standard error of the mean of R, sem, was also made at this stage, according to the formula:

$$sem = sqrt(\Sigma(sdev_{raw})^2)/(npairs * 10))$$

where npairs refers to all the histogram comparisons. For R_M, npairs would simply be the number of pairs of neurons being compared. However, for R_O and R_R there are histograms for each odorant, so npairs is thrice as large. The factor of 10 is an estimate of the number of cycles within each run, since the individual $sdev_{raw}$ values were obtained from the variance within a run.

6. Normalization of R. Control samples of unrelated neurons were obtained by randomly selecting pairs (several hundred) of recordings from different rats. The entire process 1 through 5 was followed to obtain control values of R_M, R_O and R_R, and also the corresponding error estimates. R_{final} is then simply the average of the normalized values:

$$R_{final} = (R_M/R_{Mc} + R_O/R_{Oc} + R_R/R_{Rc})/3$$

Sem_{final} is combined as described above, with each term being normalized before the summation:

$$Sem_{final} = \text{sqrt}(\Sigma(sdev_{raw}/R_c)^2)/(\text{npairs} * 10))$$

where R_c is R_{Mc}, R_{Oc} or R_{Rc} as appropriate.

SECTION 3. INTEGRATION OF MODELING AND EXPERIMENTS.

This section draws heavily on both the simulation and experimental aspects of the thesis work. The basic project undertaken here was to develop a model of the olfactory bulb which incorporated sufficient modeling detail and experimental information to be able to reproduce the observed behavior of the system. The construction of an explicit model of the bulb enabled us to explore the conditions under which the experimentally observed behavior could be replicated. Furthermore, we were able to suggest which of the organizational features of the bulb were essential to the functioning of the model, and to find respects in which our model description of the bulb needed further development.

Detailed biologically based simulations of the mammalian olfactory bulb.

INTRODUCTION.

This section draws heavily on both the simulation and experimental aspects of the thesis work. The basic project undertaken here was to develop a model of the olfactory bulb which incorporated sufficient modeling detail and experimental information to be able to reproduce the observed behavior of the system. The construction of an explicit model of the bulb enabled us to explore the conditions under which the experimentally observed behavior could be replicated. We were particularly interested in examining the two primary results of the experiments: first, the variability observed in individual neuron responses, and second, the spatial organization of response properties. The model was based directly on the single-cell models described in chapter 3, and utilized the same parameter search methods. The behavior of the model was analyzed using the same tools as had been developed for the experimental work, and the results were compared with the experiments.

Our general approach to modeling is to integrate as much of the relevant experimental information from the literature as possible, into the structure of the model. Having constructed a structurally accurate model, we then proceed to examine the electrical behavior of the model and to relate this to the corresponding experimental recordings. This approach closely follows the pioneering studies of Rall and co-workers (Rall et al. 1966; Rall and Shepherd 1968). In these previous modeling efforts, the mitral and granule cells were modeled to the level of detail possible at the time, and their responses in the context of the network were compared to experiments. The primary sources of electrophysiological data used in these earlier studies were current source density studies. These models successfully predicted the presence of reciprocal dendro-dendritic synapses between mitral and granule cells, for which considerable experimental evidence has since accumulated (reviewed in Mori 1987).

Numerous other models of the olfactory bulb have also been developed, representing a wide spectrum of detail from highly mathematical to detailed and realistic. White et al. (1992) have constructed one of the largest (> 7000 cells) and most detailed models, and have related this to their experimental

observations on the salamander olfactory bulb. The cells in their model were modeled with one to three compartments and used an integrate-and-fire scheme rather than active channels. They followed a similar sequence for parameterization of the model, first matching shock stimuli and then applying odorant input. Their model demonstrated that lateral interactions embodied in their model were important in reproducing single mitral cell firing patterns. A similar model has also been constructed by Anton et al. (1991). The cells in this model were also of the integrate-and-fire variety, and utilized a lumped circuit representation. This simulation was somewhat smaller (750 cells) and only represented a single glomerulus. The model demonstrated the ability of the glomerular unit to transform frequency of receptor input to a spatial encoding over the mitral cells in the glomerulus. Schild and Reidel (1992) have developed a model of synaptic interactions and organization in the glomerular tuft. Their model includes multiple compartments and synapses modifiable according to Hebb's rule, but does not incorporate voltage dependent channels. They have demonstrated that it is possible to derive differential specificities for odors through self-organization of the patterns of connectivity, but that such a process only takes place in multicompartmental models. Meredith (1992) has abstracted the synaptic interactions and cellular physiology of the bulb to build a network which qualitatively embodies the interactions in the bulb at both the glomerular (mitral-pg-ON connections) and external plexiform level (mitral-granule connections). This study indicates a mechanism for obtaining several of the observed spatio-temporal patterns of mitral cell activity in response to shock and odorant stimuli.

Several abstract models of the olfactory bulb have modeled the system as an assembly of coupled oscillators (Freeman et al. 1988; Li and Hopfield 1989). The emphasis in these studies has been on the emergent properties of networks of such oscillators. Such systems demonstrate a very robust classification of input signals and typically converge to a solution rapidly. Other studies (Hopfield 1991) have utilized even more abstract neuron-like elements to model the process of localization of odor sources. The exact mapping of such systems onto the detailed physiology and anatomy of the olfactory bulb is at present unclear.

The current modeling effort is distinguished by the much higher level of biological detail it incorporates, and by its size. Each of the neurons in our model is based on a detailed, multicompartment

single cell model whose electrical properties have been closely related to experiment. Each cell model incorporates a complement of voltage dependent channels modeled according to the Hodgkin-Huxley formalism. The geometry of each cell is carefully preserved, as are the geometrical relationships between them in the network. Our model is substantially larger than all but the model by White et al, including 12 glomeruli and over 600 neurons (Figure 1). With this level of detail, it has been possible to incorporate much of the available information from the literature into the model, as discussed above. In this manner the model is intended to represent a good approximation to the current understanding of the olfactory bulb.

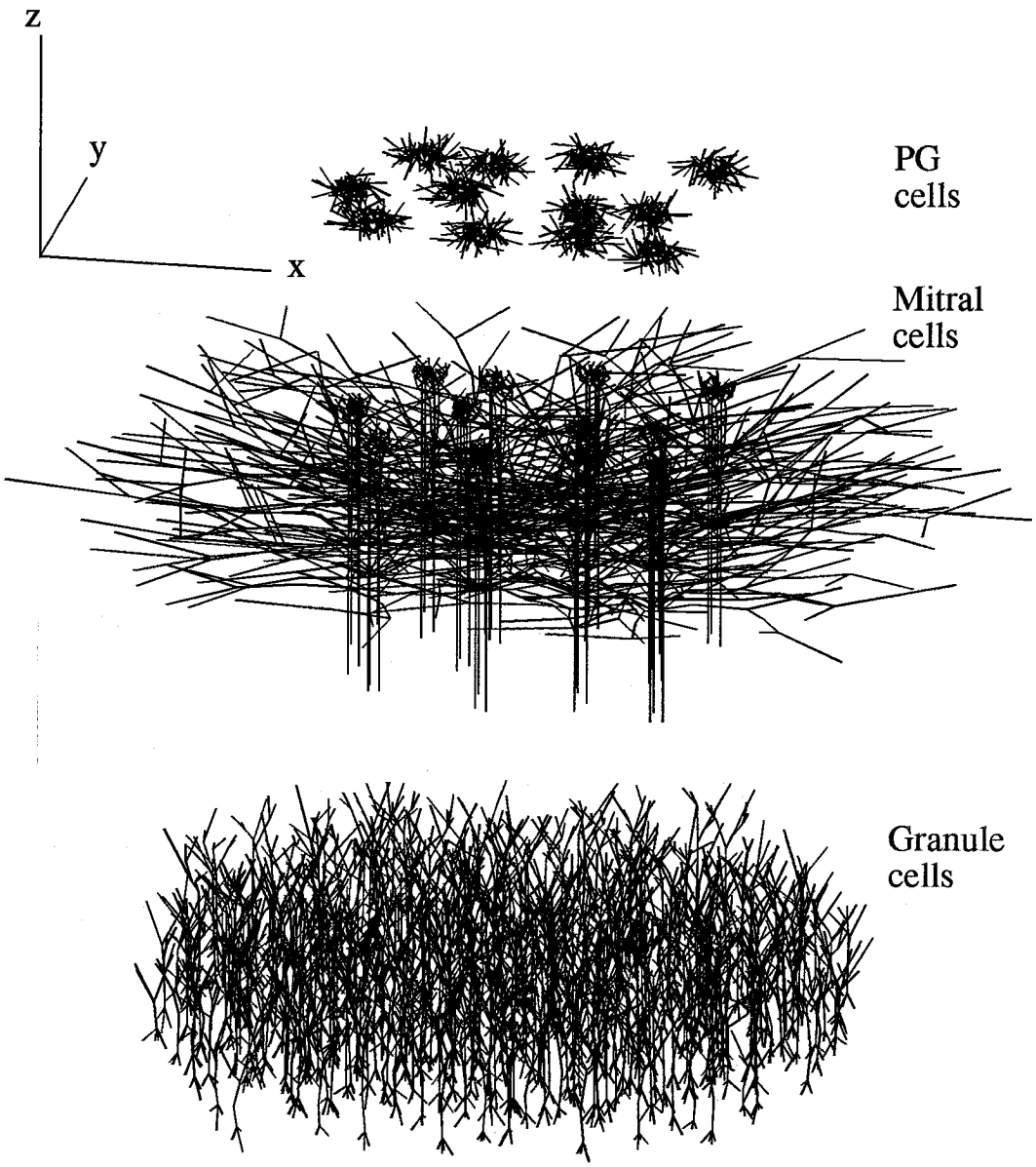

Figure 1. Exploded view of the bulb model. The periglomerular cells have been moved upwards and the granule type cells moved downwards, for clarity. In the actual network the periglomerular cells cluster around the glomerular tufts of the mitral cells visible in the figure. The large horizontal extent of the mitral cell secondary dendrites is immediately apparent. The granule cells occupy a larger radius that the cell bodies of the other cell types, in order to reduce boundary effects in the simulation. The cell density is much smaller than in the biological network. Scale bars: 1 mm on each axis.

METHODS.

Sources of data.

This study directly draws upon many previous experimental and simulation studies. First, the individual cell models are based on our previous models of the two major cell types in the olfactory bulb, mitral and granule cells, and their subclasses (Mori et al. 1983; Chapter 3). These in turn were based on experimentally obtained structural and electrophysiological data. The parameter search techniques developed for our previous study (Chapter 3) have also been utilized here.

The general organization and connectivity of the bulb have been well characterized by the combined efforts of many investigators (reviewed in Mori 1987). These formed the basis for our single cell models (Chapter 3).

An important source of information for establishing the parameters of the models were studies of intracellular responses of bulbar cells to shock and odorant stimuli. Olfactory nerve (ON) and lateral olfactory tract (LOT) stimulation studies have been carried out in several preparations (rabbit: Mori et al. 1978a; rat: Wellis et al. 1990; isolated turtle olfactory bulb: Mori et al. 1981b). In general, the responses of the three main cell types are consistent between these preparations. Anterior comissure stimulation studies (Mori and Takagi 1978b) have been performed in the turtle olfactory bulb. The advantage of using shock stimuli as the basis for determining model parameters is that the responses are extremely stereotyped and the bulk of the cell population is responding in the same way. This provides one with a good idea of the input driving each cell type in the network. Furthermore, events following shock stimuli typically last only a few tens of milliseconds, so the computational expense of comparing simulated responses is relatively small.

We have previously quantified several aspects of the spatial organization of the response properties of individual mitral cells in the olfactory bulb of awake behaving rats (Chapter 4) over a period of days. Other studies have also indicated that there is a pronounced degree of spatial organization in anesthetized (Buonviso et al. 1990) and awake (Freeman and Grajski 1987) animals. Our data is especially suited to direct comparison with modeling studies, since it involves a simple and consistent stimulus paradigm, a

quantitative measure of response similarity between neurons, and a sufficiently large sample size for estimation of the variability of responses.

The details of the projection from the olfactory epithelium to the olfactory bulb are a topic of active research (Reviewed in Shepherd 1993). It seems likely that the projection from the epithelium to the bulb is neither strictly topographical, nor completely scattered. Our study does not address this issue. Instead, we attempt to relate the observed spatial properties of bulbar response to the network properties of the bulb, without invoking additional spatial patterning at the input level.

Individual cell models.

Each cell model consists of multiple compartments in order to accurately incorporate known geometrical and electrical properties of the cell. The active electrical properties are modeled using voltage-gated ion currents based on the Hodgkin-Huxley formalism. These ion currents are distributed in the cells as predicted from our previous single-cell modeling efforts (Chapter 3). Synaptic channels are modeled using the alpha-function formalism, and distributed within the cell models according to previously published information about synaptic sites (Mori et al. 1983).

Due to constraints on computer resources, the individual cell models had to be simplified from the highly detailed models developed earlier (Chapter 3). This was done by using a coarser spatial subdivision of the cells. In the case of the mitral cells, this simplification could not be carried very far, because of the geometry and electrical properties of these cells. The simplified mitral cell model consisted of approx. 50 compartments, reduced from nearly 300.

The granule cells were considerably simplified, from 944 compartments to 12. This was possible because the cells are electrotonically compact, and because most of the compartments in the original models were dendritic spines, which we collapsed into the dendrites (Segev et al. 1990) in the simplified model.

Each of these simplified models was run through the same parameter search routines as the original models, in order to obtain the closest match to the original data.

Periglomerular cells have not been studied as closely as the other cell types, particularly with respect to the distribution of active channels. We therefore implemented a simple 5-compartment model for

these cells, with a soma and four dendrites. Voltage-dependent channels were placed in the soma of these cells. This simple model provided a good approximation to the experimentally observed spike waveforms of periglomerular cells (Figure 5).

Receptor models.

Our receptor models were intended to represent the consensus in the field that individual receptors respond to multiple odorants with varying degrees of affinity (Lancet 1986). We therefore allowed each receptor to respond to each of the presented odors, with randomly selected weights. Recent results (Boekhoff et al. 1990) regarding multiple pathways for transduction which can either depress or raise firing rates, were incorporated by assuming that a given odorant could result in either elevation or suppression of firing. Respiratory and background influences on the firing rates were also taken into account.

Receptor neurons were modeled as sources of random spikes with a mean rate determined by several parameters (Figure 2). These included the background rate, the product of the strength of each odor with a weight, and a sinusoidally varying respiratory modulation. Each receptor could potentially respond to each of the three odors depending on the combination of weights.

$$\text{rate} = B + WR * R(\text{phi} + t) + W1*O1(t) + W2 * O2(t) + W3 * O3(t)$$

where phi represents the randomly selected phase for each receptor, B, WR, W1,W2,W3 are the weights assigned to different components of the response, and O1, O2, and O3 are the time-dependent concentrations of the three odorants used in the experiment.

100 receptors were set up in this manner, each receiving the same odorant input but possessing different weights. These were connected randomly to the mitral cell dendritic tuft and the periglomerular cell dendrites. Care was taken to ensure that there was no spatial bias in the receptor input.

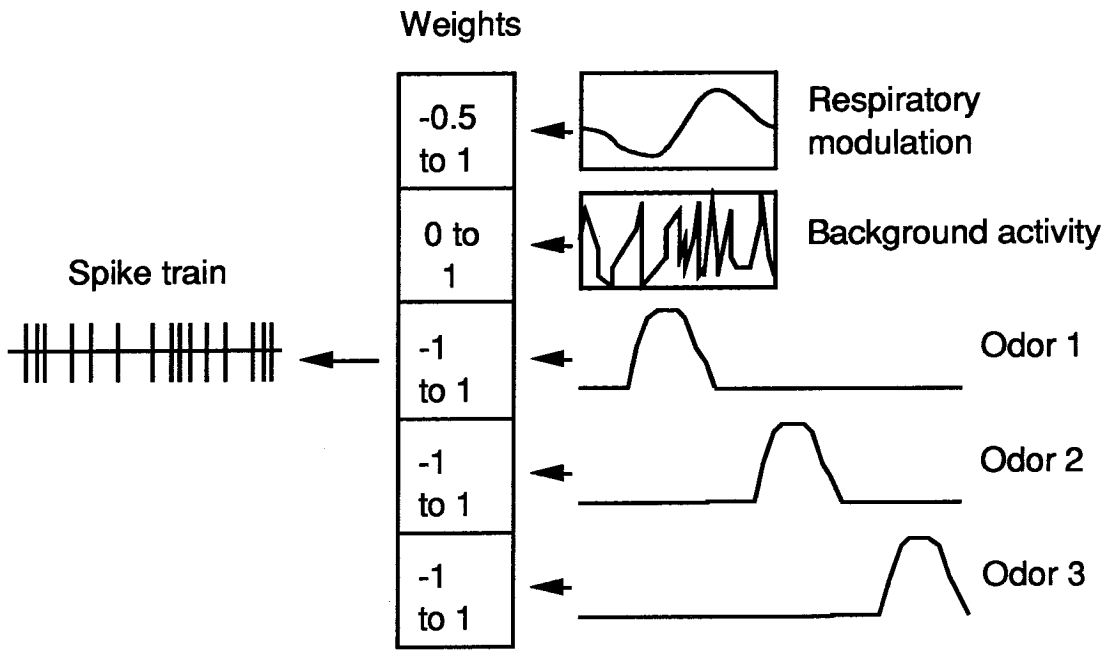

Figure 2. Model of the receptors. Each of the components driving the receptor firing is shown, along with the distribution of the weights. The respiratory modulation has a randomly selected phase for each receptor. The background activity was usually uniform, but in two models a variable background activity was applied. The three odors were delivered in a cyclical sequence. The shape of the odor waveforms in the figure represents the build-up and decay time courses for each odor stimulus.

Implementation of synapses.

The basic implementation of the synapses in the network was as a conductance changing as a two-time-course alpha function (Wilson and Bower 1991):

$$G(t) = \frac{\tau_1 \tau_2}{\tau_1 - \tau_2}(e^{-t/\tau_1} - e^{-t/\tau_2})$$

In the case of axo-dendritic synapses, the propagation of the action potential was implemented as a time delay related to the distance of propagation. The arrival of the action potential at the synapse initiated the alpha-function conductance change. In the case of dendro-dendritic synapses, the presynaptic voltage was first transformed using an approximately sigmoidal transfer function. This transformed value initiated the alpha-function based conductance change. Each reciprocal dendro-dendritic synapse was modeled as two independent dendro-dendritic synapses, with synaptic effects occurring in either direction.

Interconnections in the network.

The network included the known major synaptic interconnections in the bulb. In general, all interconnections were made on the basis of geometrical criteria which are most likely to correspond to the natural situation. Specifically, all dendrodendritic synapses were made simply on the basis of proximity of the pre- and post-synaptic compartments. Whenever the compartments were within a certain range, a reciprocal dendro-dendritic connection was established. Axo-dendritic synapses were made on the basis of experimentally determined projection patterns. As previously mentioned, the olfactory nerve projection was set up in a purely random manner.

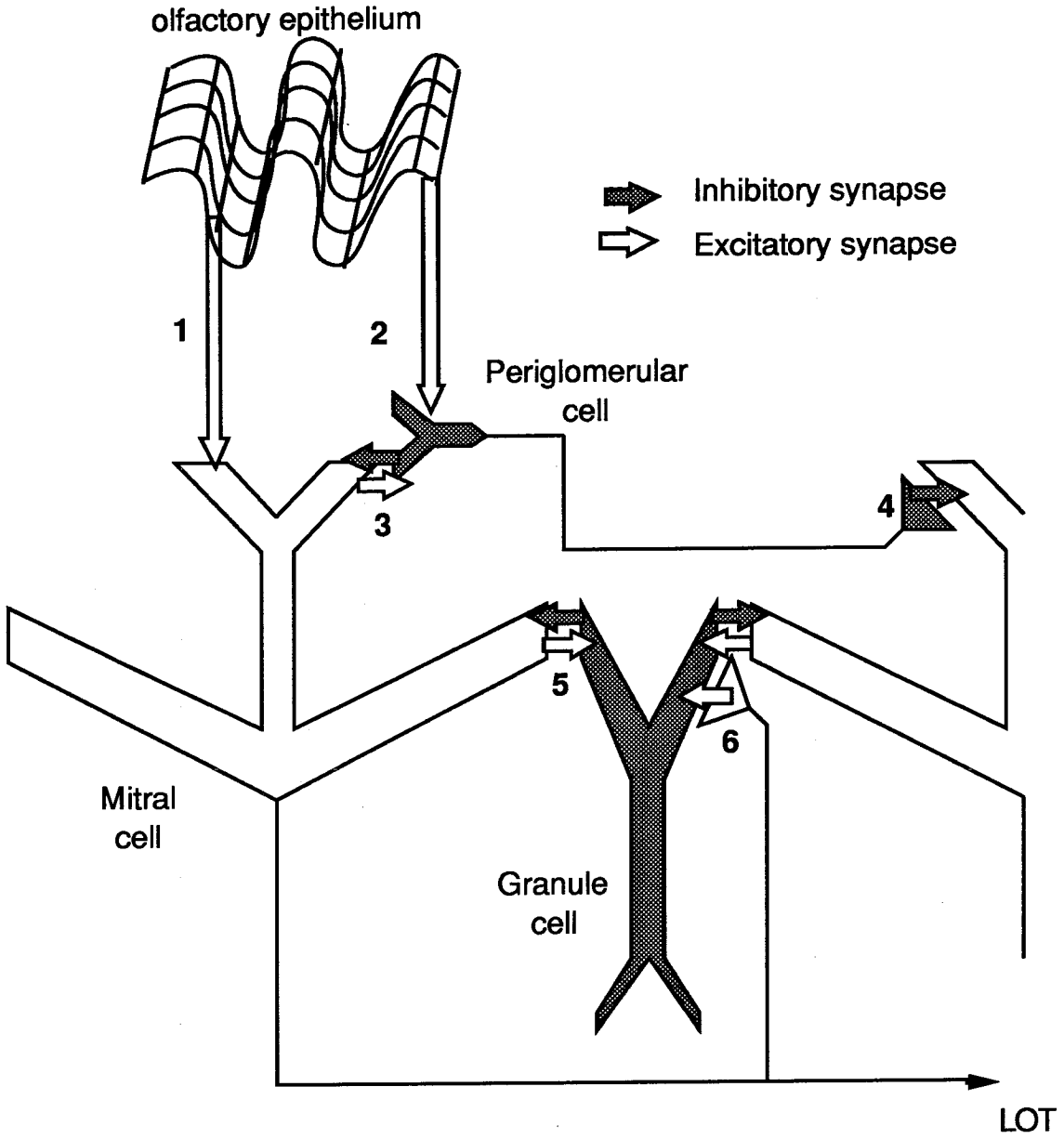

Figure 3. Interconnections modeled in the network. (Adapted from Shepherd, 1972). The synaptic pathways are numberd as follows. 1. Olfactory nerve to mitral cell glomerular tuft. 2. Olfactory nerve to periglomerular cell. 3. Reciprocal dendro-dendritic synapse between mitral and periglomerular cell. 4. Inhibitory axodendritic synapse from periglomerular cell onto mitral cell in nearby glomerulus. 5. Reciprocal dendro-dendritic synapse between mitral and granule cell. 6. Excitatory axo-dendritic synapse from mitral cell axon collaterals to granule cell.

The following synaptic interconnections were implemented in the model:

1. Olfactory nerve to mitral cell (axodendritic).

2. Olfactory nerve to periglomerular cell (axodendritic). These two projections were made in a non-topographic, random manner from a sheet of receptors.

3. Mitral-periglomerular reciprocal dendrodendritic synapses. These intra-glomerular connections were made in a purely geometrical manner. Whenever peri-glomerular cell dendritic compartments were within a specified distance (50 microns in this model) of a mitral cell apical tuft dendrite, a reciprocal dendro-dendritic connection was established.

4. Periglomerular to mitral cell axodendritic dendritic pathway. In accordance with anatomical observations (Pinching et al. 1971), these projections were made only to apical tuft dendrites of mitral cells in glomeruli between 100 and 300 microns distant.

5. Mitral-granule reciprocal dendro-dendritic synapses. Again, these connections were made on the basis of geometry and the proximity of dendritic compartments in the external plexiform layer. The same distance criterion of 50 microns was used.

6. Mitral-granule axodendritic synapses. Based on anatomical studies (Mori et al. 1983), these projections were made to the distal dendritic segments of the granule cells.

These interconnections are summarized in Figure 3.

Parameter search techniques.

We have previously presented a detailed description of our parameter search methods as applied to neuronal simulations (Chapter 3). Briefly, two basic approaches were used in our previous study: brute force methods, where parameter space was systematically sampled; and conjugate gradient methods, which use sophisticated algorithms to rapidly locate optimal sets of parameters. The former was conceptually simpler and preferable for performing a coarse search in an unknown region of parameter space. However, it was computationally very expensive. The conjugate gradient method is much more efficient, but prone to being trapped in local minima. Both these parameter search methods rely on an 'energy function,' which is a

measure of how close the simulated output is to the desired output. The desirable features of the energy function include smoothness, monotonicity, and a single-valued minimum. For this set of simulations, we devised an energy function which was closely related to the one used for the single cell simulations. This function compared spike properties such as amplitude, width and timing. In addition, the energy function also compared the voltage waveform following the initial spike, so as to include information on the subsequent network interactions into the calculations. Each of the cells in the model were compared with the 'correct' waveform using this energy function, and the sum of these comparisons was used for evaluating the network as a whole.

As a final, fine-tuning process, we visually inspected waveforms for each of the cell types under the various stimulus conditions, to select for features too subtle to be resolved using the existing energy functions (Figure 4). As in the previous study, preference was given to parameter sets which were insensitive to relatively small changes in parameter values.

In each parameter search run, the model ran for 150 msec of simulated time. This included a prestimulus duration of 50 msec to allow the network to equilibrate. The parameters varied were various aspects of each synaptic conductance: synaptic weights; slope, threshold, and offset of the synaptic transfer function for dendro-dendritic synapses; time constants of the synapses, and strength of stimuli. Up to 30 parameters were varied at a time. This number of parameters begins to pose problems of non-uniqueness. The issue of non-uniqueness is dealt with in the results section.

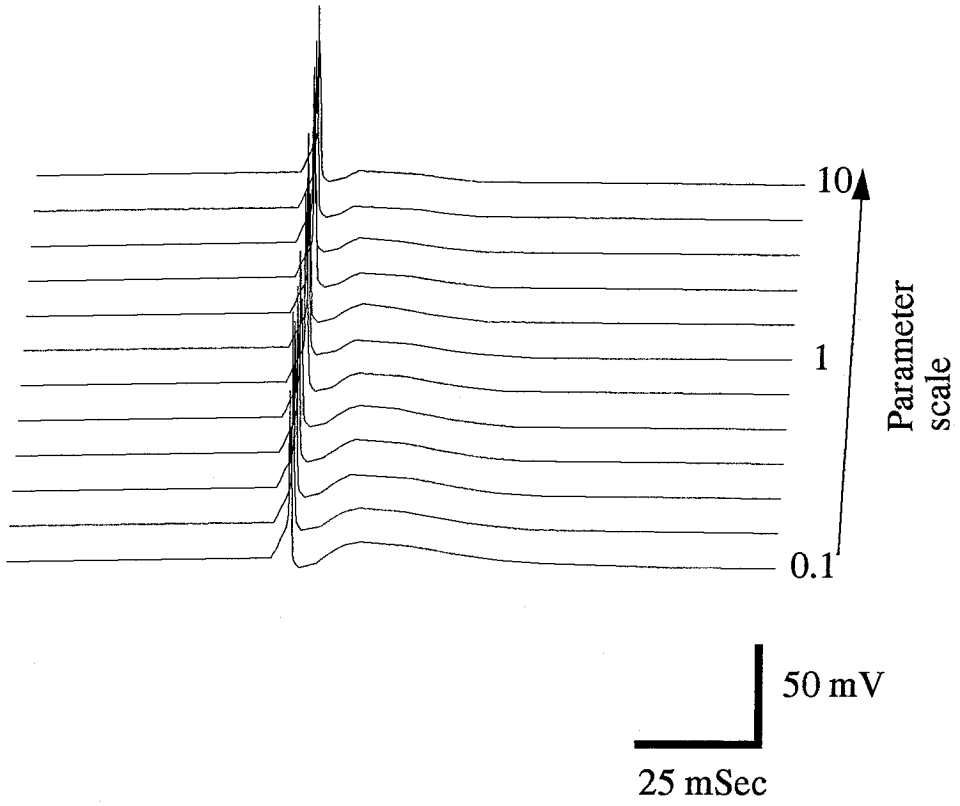

Figure 4. Example of one dimension of a parameter search. 11 mitral cell spike responses to an olfactory nerve stimulus are displayed, each offset slightly from the previous one for clarity. The parameter being varied is the granule to mitral cell synaptic weight. The value of the parameter is scaled from 0.1 to 10, where 1 is the reference value (in this case, the weight used in the final model). As the synaptic weight is increased, the size of the second depolarization decreases and the time course gets slightly shorter. By this measure, the effect of this parameter on network behavior is small, even over 2 orders of magnitude.

Computational issues.

All simulations were carried out using Genesis (Wilson et al. 1989, Chapter 1). Each cell model was solved using the Crank-Nicolson method for integration, based on the decomposition scheme proposed by Hines (1984). An integration time step of 100 msec was used for all simulations. At this timestep the error for single neuron models is under 5%, based on the Rallpacks in Chapter 2. The size of the network (over 600 neurons, 10,000 compartments, 20,000 active conductances, 100,000 interconnections) made it necessary to implement the bulb model in parallel. The model was implemented on three nodes of the Touchstone Delta parallel supercomputer, based on a geometrical decomposition. Each node was responsible for simulating about a third of the whole model. The neurons simulated on a given node were all spatially contiguous. In this configuration the communications to computation ratio was approx. 1:5, i.e., passing information between nodes accounted for 20% of the run time. Extended parameter searches were carried out using multiple copies of this three-node network. The ratio of simulated to real time was approx. 1:3800, so it took approx. one hour to simulate one second's worth of activity in the network. The total duration of each experimental run was around 390 sec, which was clearly not practical to run in serial. In order to perform simulation runs of the same duration as the experimental runs, multiple copies of the same model were run simultaneously. Each model received stimulus input corresponding to the section of time which it was simulating, including an equilibration time of 200 msec of simulated time before commencing data generation. This period is well over the longest time constants of the individual cells of the network (tau = 60 msec for the mitral cell) and of any synaptic interactions (the GABA channel had 20 msec kinetics). Longer term interactions (e.g., LTP) have not been sufficiently characterized in the olfactory bulb to justify their inclusion. We carried out 11 complete simulation runs of the entire odor delivery sequence, totaling approximately 15,000 hours of computer time.

RESULTS

Responses to shock stimuli.

The responses of bulb neurons to a variety of shock stimuli were computed for the final bulb model. The olfactory nerve shock stimulus was simulated as a 2.5 msec stimulation of the glutamate synaptic channels in the glomerular dendrites of the mitral and periglomerular cells. Following this simulation, the glomerular tuft region of the mitral cell underwent a calcium spike which propagated to the soma in a similar fashion to previous descriptions (Chapter 3). The periglomerular cells also spiked directly following the stimulus. After a short delay during which the mitral cell soma and secondary dendrites charged up and underwent action potential firing, the granule cells were also depolarized, which crossed spike threshold in a large fraction of the granule cells (Figure 5).

Particular attention was paid to the voltage waveform for the mitral cell (Figure 5). Following olfactory nerve stimulation, mitral cells display a characteristic multi-phasic voltage waveform (Mori et al. 1981a). Following the action potential (E_1) there is an initial inhibition (I_1), followed by a second depolarization (E_2) and finally a long lasting inhibition (I_2).

It was found that a large part of the I_1 - E_2 transition in the model was due to the intrinsic properties of the mitral cell. In particular, the long lasting calcium depolarization in the apical dendrite (Chapter 3) caused the elevation of somatic potential (E_2) following the initial after-hyperpolarization.

The shock stimulus in the model assumed that all the cells started out at resting potential. This may have failed to take into account the ongoing activity of the network in the experiments. Furthermore, the electrode penetration used in the experimental recordings would be a source of depolarization. The model therefore underwent a smaller voltage change during the inhibitory phases, since the reversal potential of the GABA A channel is only slightly below the resting potential of the mitral cells.

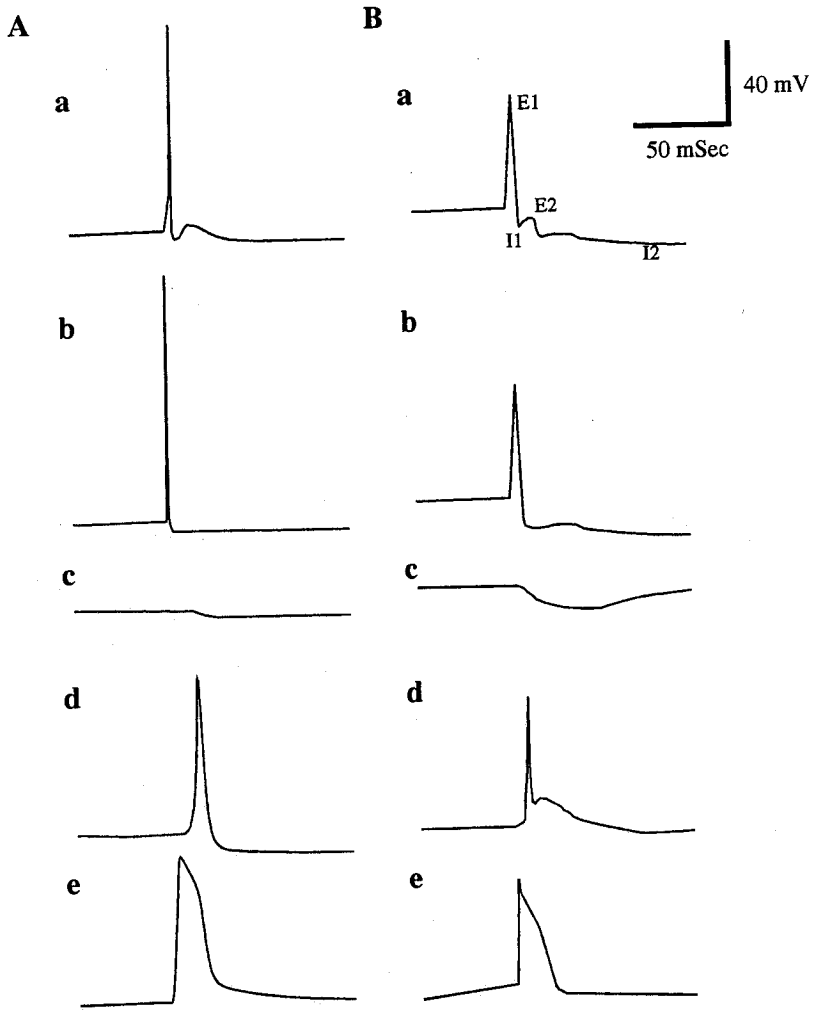

Figure 5. Shock stimulus responses in the olfactory bulb. A. simulated responses. B. experimental responses. A (a), B(a). Response of mitral cell to olfactory nerve stimulation. The multiphasic output waveform is evident. The phases of the waveform are labeled E1, I1, E2, I2 according to Mori et al (1981b). (b). Response of mitral cell to lateral olfactory tract stimulation. The E2 phase is distinctly absent in this case. (c). Response of mitral cell to AC stimulation. A hyperpolarizing effect is seen in both cases. (d). Response of granule cell to ON or LOT stimulation. In the experimental situation multiple spikes are frequently observed. There is a long lasting depression following the spikes. (e). Response of periglomerular cell to olfactory nerve stimulation.

It was possible to generate the second phase of hyperpolarization of the mitral cell (I_2) from several mechanisms in the simulations. First, the periglomerular-mitral interactions were capable of resulting in a hyperpolarization on this time scale. However, the effect was much stronger when granule-mitral interactions were considered. A close examination of the activation of these two interneurons was therefore carried out.

As mentioned earlier, periglomerular cells receive excitatory synaptic input through two pathways: directly through olfactory nerve synapses, and indirectly via dendrodendritic synapses from mitral cell apical tufts, which are in turn excited by the olfactory nerve (Figure 3). Other excitatory synaptic influences on periglomerular cells have been proposed, such as lateral excitation from other periglomerular/tufted cells (Martinez and Freeman 1984). However, the first two pathways are more generally accepted and were included in the model. A comparison was made of the efficacies of the two modes of excitation. It was found that almost identical voltage waveforms to Figure 5 B (e) could be elicited in periglomerular cell somas, through either pathway. We therefore set up the weights so that each pathway contributed roughly equal amounts to the periglomerular cell activation.

Granule cells also have at least two local pathways in the bulb for synaptic excitation. The first of these is the reciprocal dendro-dendritic synapse with the mitral cell. In addition, mitral cells also send axon collaterals to the granule cells. Previous interpretations of bulbar activity have focused on the former (Mori et al. 1981b). We compared the voltage waveforms that could be elicited in granule cells by specifically excluding one or the other connection. As with the periglomerular cells, it was found that almost identical waveforms could be elicited from either pathway (Figure 5 (d)). Furthermore, experimental protocols that depend on either orthodromic (Olfactory nerve) stimulation, or antidromic (LOT) stimulation would be expected to activate both pathways as well. In the absence of a clear method for determining relative importance of either pathway, we adopted the same compromise as with the periglomerular cells, and weighted the pathways so that they produced similar effects.

Mitral cells display a somewhat different response to LOT stimulation. Under these conditions, the glomerular tuft is not directly excited. Our previous single cell studies (Chapter 3) show that the

antidromically elicited spike does not easily propagate into the glomerular tuft to cause a calcium spike. Consequently, the brief depolarizing phase E_2 following the spike is not seen in the model. In this respect it closely matches experiment (Figure 5 A(b), B(b)). Granule cells respond with very similar spike waveforms to either LOT or ON stimulation. The experimental response tends to be somewhat broader, and sometimes additional spikes are seen (Wellis and Scott 1990). Other than confirmation of the parameters derived from the ON stimulation models, the granule cell spike waveforms did not provide much additional information at this level of detail in the models. It is likely that a finer model might reveal subtle differences based on the spike propagation and initiation, which differ in the two cases. Periglomerular cells usually do not show any response to LOT stimulation (Wellis and Scott 1990; Freeman 1974).

Experiments involving AC stimulation provided information about two parameters: the weights of the AC- to granule cell connections, and supplementary information on the granule-to-mitral cell dendro-dendritic synapse. However, the resolution of the latter was not as high, since the inhibitory action of GABA does not produce a large enough voltage change to reveal details of the interaction.

Responses to odorants.

As described in the methods section, we simulated the same sequence of odor delivery as had been used in our previous experiments. The spike times for mitral/displaced mitral/tufted cells in the model were recorded while this odor input sequence was delivered to the model. These spike times were subjected to the same analysis as had been applied to the experimental recordings. Briefly, we measured the response of a cell in terms of three measures: the mean firing rate, the phasic response to odor onset, and odor-dependent changes in respiration tuning. We found that one parameter regime, with a receptor-to-mitral dendrite connection probability of 0.03, led to responses similar to the experiments (Figure 6). At this level of convergence, approx. 35 distinct receptor types were converging onto the mitral cell, but only 3 were likely to contact any given compartment in the glomerular tuft.

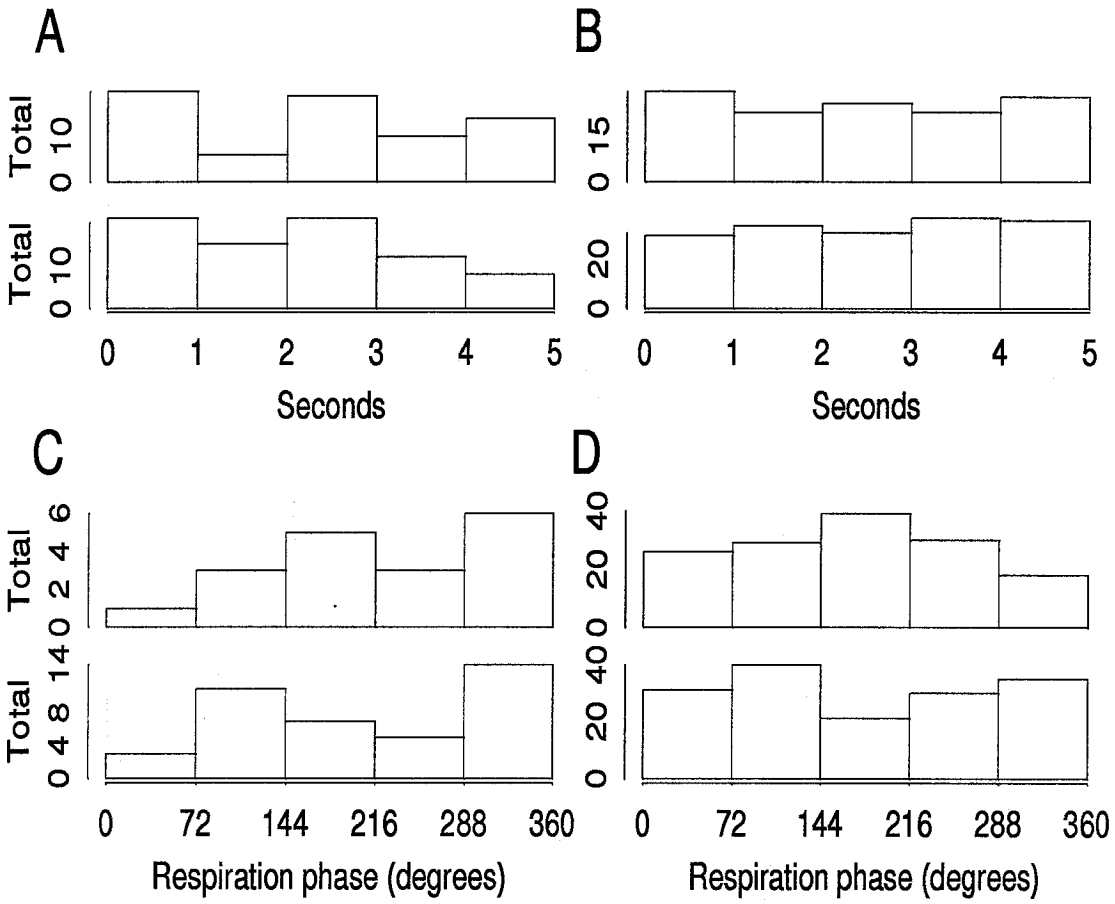

Figure 6. Examples of response histograms from the simulation. A, B. Histograms for odor onset responses. The upper histogram represents the response during odor presentation; the lower histogram is the immediately preceeding air delivery period. C,D. Examples of respiration related responses. The upper histogram is the odor period; the lower is the pure air period.

Mean firing rate response.

The percent of neurons responding by changes in mean firing rates was higher in the model than experimentally observed. The number of neurons having this type of response appeared to decrease slightly with increasing receptor convergence (Table 1).

Odor onset response.

The proportion of simulated mitral cells displaying odor-onset responses fell in the same range as for the experiment. This proportion tended to vary inversely with the number of receptor axons converging on the mitral cells (Table 1). When the convergence probability was 0.03, we observed odor-onset responses to each odor in approx. 10% of neurons. This is close to the proportion of cells responding in the experiments.

Respiration related responses.

Again, the proportion of cells responding in this manner was similar to that seen in the experiment, with the best match at a convergence ratio of 0.03. The dependence of this measure on convergence probability was less clear. In some cases a larger convergence ratio led to fewer cells with significant responses (Table 1(1,2)), as in the odor-onset case. However, there were examples where there was no response (Table 1(4,5)) and even a counter example (Table 1(6,7))

Table 1. Simulation parameters and responses.

	Receptor projections				Responses			R Values.	
Sim	RMP	RMW	RPW	Rate	M	POH	PRH	RNear	RFar
1	.04	2500	2500	20	69	12	3.4	1±.02	1.02±.01
2	.03	4500	4500	20	77	17	11	.99 ±.02	1.05±.01
3	.03	8000	4500	20	78	10	3.6	.83±.02	.87±.01
4	.02	500	50	200	80	18	6	.91±.02	.92±.01
5	.01	1000	50	200	85	23	6	.97±.02	.92±.01
6	.02	500	300	200	84	40	2		
7	.05	200	300	200	76	26	7.8		
8*	.03	1000	300	100	75	11	3		
9*	.03	4500	4500	20	63	277	25		
Experiment					5.7	11.6	9	.84±.01	1.06±.01

Meaning of abbreviations: Sim: simulation number. RMP: Receptor to Mitral cell projection Probability. RMW: Receptor to Mitral Weight. RPW: Receptor to Periglomerular cell projection Probability. Rate: Maximum firing rate of receptor 'neurons.' M: Mean firing rate responses (%). POH: Odor onset responses (%). PRH: Phasic responses to respiration (%). RNear: R for all adjacent neurons in the simulation. RFar: R for all distant neurons in the simulation.

*In these two simulations a randomly changing baseline input to the receptors was present.

Variability in responses

An aspect of the single neuron response that was noticeable in the experiments was the strong variability in firing rate between different cycles within the same run (nearly 50% of neurons showed a significant variability by the ANOVA test). In these simulations very low variability was seen. This clearly follows from the fact that there were no influences on the network other than the receptor input, which in turn was simplified and deterministic within known ranges. We investigated the variability in firing rate caused by applying a randomly varying baseline signal at the receptor level. This variability was 10% as large as the odorant signal. The mitral cell firing rate, however, remained almost constant between trials (2% of the neurons showed a significant variability). When a random modulation 50% as large as the range for odorant input was applied to the input, the number of neurons with significant inter-trial variability was still only 17% which is about a third of the variability seen in the experiments (Table 2). At this level of variability, the other responses of the system were significantly distorted as well (Table 1 (9)), making it unlikely that so much variability is present at the input.

Table 2. Variability between cycles

Simulation	Background variability (%)	Cycle variability (%)
3	0	0.76
8	20	2.03
9	50	16.8
Experiment		45.08

Spatial distribution of responses.

We further utilized the analysis tools developed for the experimental study to compare the responses of adjacent and separated neurons in the model. Briefly, the shapes of the histograms describing the responses of the two neurons are compared. The histogram bin values are used to construct vectors for each response, and the geometrical distance between these vectors is used for the measure of difference, R. The difference measure R is normalized against a control group of comparisons between unrelated neurons. On this measure, a value of 0 indicates that the responses are identical, values between 0 and 1 represent decreasing levels of similarity, a value of 1 indicates that they are unrelated, and values greater than 1 show that the responses are more dissimilar than chance.

Adjacent neurons.

These were defined as all mitral/displaced mitral/tufted cells projecting to a single glomerulus. Depending on the input parameters, R took on values greater as well as less than 1.

Distant neurons.

These were defined as all mitral class cells in different glomeruli. The geometry of the model was such that the closest glomeruli were 400 microns apart, which corresponds well to the experimental situation. Again a range of values was obtained for R, but it was usually 1 or greater (Table 1). It should be noted that in several cases (Table 1(5)), the distant neurons were unrelated to each other, while adjacent neurons were dissimilar. These examples are a reversal of the arrangement seen in the experiments.

DISCUSSION.

Parameters of the model.

The complexity of this model is reflected in the large number of parameters that had to be specified in it. A sequential process of parameter estimation somewhat reduces the magnitude of this problem. In particular, the individual cell models were held fixed during the parameter searches for the synaptic properties of the bulb model, and then the synaptic properties were held fixed while determining the input parameters. However, there were two outstanding cases where the available experimental data was not sufficient to resolve certain parameters. First, the input to the periglomerular cells could either be directly

from the receptors, or indirectly via the mitral cells and the reciprocal dendro-dendritic synapse. Second, the granule cells could be excited either through the dendro-dendritic synapses, or the axo-dendritic synapses from mitral cell collaterals. In principle both these cases should be resolvable with fine enough resolution in the recordings, but such data were not available. Our solution was to weight each of the two possible synaptic pathways so that they produced approximately the same effect on the postsynaptic cells. The justification is twofold. First, both pathways exist in the real system, and therefore presumably do play a role. Second, at least under the conditions of the parameter searches, there is no significant difference in the cell behavior and therefore the effects of incorrectly weighting the two pathways should also be small.

Our model suggests experimental manipulations which should be able to resolve some of these questions. First, our single cell models show that repeated antidromic stimulation may cause the glomerular tuft to charge up sufficiently to fire a calcium spike (Chapter 3). Since intracellular recordings from periglomerular cells under these conditions are feasible (Wellis and Scott 1990), it should be possible to characterize the PG cell response to activation through the dendro-dendritic contacts through mitral cells. This would allow us, by subtraction, to estimate the effect due to the olfactory nerve alone.

For the two mitral to granule synaptic pathways, it may be possible to separate the effects based on the relative timings involved in ON and LOT stimulation. In the first, the depolarization of the secondary dendrites is likely to begin slightly (a few msec) before the action potentials are initiated and arrive at the axodendritic synapses. For LOT stimulation, the reverse is true. Although the differences are subtle, they may be possible to resolve especially with close reference to detailed simulations.

With regards to the other parameters, the selected solution was quite robust to change. This was one of the criteria for selecting the parameters. It suggests that many of the approximations made in the construction of the model may not greatly affect the detailed model properties. The further implication is that the biological network is also a robust system, which has indeed been found following various manipulations (Slotnick et al. 1987).

Basic responses.

Our simulations, despite being based on a simplistic receptor model and random ON projections, reproduced several features of the experimentally observed responses. Purely on the basis of averaging of the

converging inputs, one would expect that a fortuitous combination of receptor specificities capable of producing a response would be a rare event. Assuming a linear summation of the inputs, one would expect the mean of the 35 inputs to vary by less than 10% between odorants, given the random distributions used in the receptor models. The two response properties that best agreed with experimental proportions were both phasic in nature. Again, given the complete lack of a phasic component in the input, other than the background respiration tuning, it is remarkable that such responses were observed. It is apparent that the network is deriving these phasic responses from the only aspect of the input signal that was non-uniform, i.e., the transitions between odor off and on. A likely mechanism for this process may relate to the stabilizing effects of feedback inhibition onto the mitral cells from the granule and periglomerular cells. In the event of an increase in firing rate of the mitral cell (e.g., by increased stimulation due to odor onset) the interneurons would receive an increase in excitation. The inhibitory feedback from the interneurons would then damp the mitral cell firing rate back towards its original value. Overall, the mitral cell firing would have experienced an initial increase, followed by a damping towards the equilibrium level. This would constitute the phasic response. In terms of electrical circuits, this response would be similar to that of a differentiator. An analysis of the response histograms (Figure 6 A) shows that in some cases this indeed appears to be the observed sequence of events. The previous study by Meredith (1986), as referred to in the introduction, also suggests an effect of this sort.

An important respect in which the simulations contrasted with experiment relates to the variability between cycles within a run. In the experiments this was one of the strongest statistical effects observed. However, under the basic simulation parameters, variability was essentially nonexistent. This was the case even when a very large random component (as large as the range for olfactory signals) was applied to the baseline. This makes it unlikely that a peripheral mechanism underlies the observed experimental firing rate variability. We suggest instead that the variability has a central origin. On the basis of the experiments, we had already hypothesized that the responses of individual neurons may undergo central modulation depending on the state of the network. The experimentally observed inter-trial variability may therefore be a manifestation of this central modulation.

Spatial aspects of responses.

In the experiments, we had observed that adjacent neurons responded more similarly than distant ones. This was also the case for the model with the parameters which gave the best match to experiment for single neuron responses (Table 1 (2)). In this simulation the distant neurons were significantly dissimilar, while the adjacent neurons actually did not show any relationship (R = 1). This sort of long-range interaction is likely to be mediated by spike propagation into the secondary dendrites of the mitral cells, which our single cell modeling had predicted (Chapter 3).

The lack of similarity in adjacent neuron responses in the model may indicate that its assumption of random projections is faulty, and in the biological network there may actually be similarity in the input from the olfactory nerve. An alternative possibility is that an as yet uncharacterized interaction is occurring in the glomeruli, which is increasing the response similarity of the mitral cells. The accumulation of K^+ ions in the glomerulus has been reported to occur under conditions of high activity (Khayari et al. 1988). This may provide a means for making mitral cell responses more similar. Another candidate glomerular-level interaction is NO, which has been shown to occur in high levels in the glomerular region and has been suggested as a possible mediator of information processing (Breer and Shepherd 1993).

Projection specificity.

This study demonstrates that it is possible to obtain many of the experimentally observed responses in bulbar neurons without invoking a precise mapping from highly tuned receptors to individual neurons in the bulb. In this model, a convergence of as many as 35 randomly selected receptors to each mitral cell still led to levels of response tuning that were as high or greater than seen in experiment. As described in the methods section, each of those receptors had randomly selected tuning properties. It is interesting to compare this with current estimates of the number of distinct receptor molecules in the family of putative olfactory receptors. It appears that this number is probably in the 500 to 1000 range (Buck and Axel 1991). The problem of individually specifying projections for each of these is reduced many fold if the intrinsic bulbar circuitry can resolve individual responses from mixtures of 35 at a time. In other words,

rather than chemically or otherwise specifying 1000 projection patterns, one could attain specificity of response by specifying perhaps 50 broad and overlapping response groups. Investigations of molecular markers for olfactory projections have already revealed a number of broad, overlapping groups of projections from the olfactory nerve to the bulb (Mori 1993). It is easy to expect that this number may rise to the region of 50 or so.

Further work.

A simulation such as this is capable of addressing a very wide range of questions. At this stage we have chosen only to investigate the variability and the spatial aspects of the model response, as being particularly relevant to the theme of the thesis. There are an enormous number of other potential questions. In general, the realism of the model makes it relevant for comparison with most physiological experiments. At the structural level of the model, one can ask questions about the role of particular network components, as illustrated by our treatment of the two pathways that might excite periglomerular cells. We have already suggested that central influences may play a major role in determining bulbar responses. This is an area that could be usefully studied with the model. A more detailed analysis of the responses and their dependence on the receptor and projection properties is likely to be relevant to outstanding questions discussed in the introduction.

A detailed simulation such as the bulb model is in some senses a functioning encapsulation of much of the available knowledge in the field. Beyond merely describing the bulb, it also predicts responses, and by its success or failure on certain predictions indicates where the available data may be inaccurate or insufficient. There are clearly many experimental details which could further improve the accuracy of the model, and several ways in which it should be extended. A number of models of different components of the olfactory system have previously been studied. These include olfactory receptor neurons (Firestein 1991) and the projections from the receptors to the bulb (Berkowicz, personal communication). These are clearly important for the development of a fuller model of the olfactory system. Several models at different levels of detail have also been proposed for the piriform cortex (Wilson and Bower 1992; Hasselmo et al. 1992). A long term goal in studying the olfactory system is to integrate all these subsystems into a coherent model

of the modality as a whole. The development of this model, and the initial manipulations described here, are only a first step towards fully utilizing it in the role of the theoretical counterpart of the experimental system.

REFERENCES

ANTON, P.S., LYNCH, G., AND GRANGER, R. Computation of frequency-to-spatial transform by olfactory bulb glomeruli. *Biol. Cybern.* 65: 407-414, 1991.

BREER, H., AND SHEPHERD, G.M. Implications of the NO/cGMP system for olfaction. *TINS* 16:5-9, 1993.

BUCK, L., AND AXEL, R. A novel multigene family may encode odorant receptors: a molecular basis for odor recognition. *Cell* 65: 175-187, 1991.

BUONVISO, N., AND CHAPUT, M. A. Response similarity to odors in olfactory bulb output cells presumed to be connected to the same glomerulus: Electrophysiological study using simultaneous single-unit recordings. *J. Neurophysiol.* 63: 447-454, 1990.

FIRESTEIN, S., AND SHEPHERD, G.M. A kinetic model of the odor response in single olfactory receptor neurons *J. Steroid Biochem. Molec. Biol.* 39: 615-620, 1991.

FREEMAN, W.J., AND GRAJSKI, K.A. Relation of olfactory EEG to behaviour: Factor Analysis *Behav. Neurosci.* 101: 766-777, 1987.

FREEMAN, W.J., YAO, Y., AND BURKE, B. Central pattern generating and recognizing in olfactory bulb: a correlation learning rule. *Neural Networks* 1:277-288, 1988.

HASSELMO, M.E., ANDERSON, B.P., AND BOWER, J.M. Cholinergic modulation of associative memory function. *J. Neurophysiol.* 67:1230-1246, 1992.

HINES, M. Efficient computation of branched nerve equations. *Int. J. Bio-Medical Computing.* 15: 69-76, 1984.

HOPFIELD, J.J. Olfactory computation and object perception. *Proc. Natl. Acad. Sci. USA* 88:6462-6466, 1991.

KHAYARI, A., MATH, F. AND DAVRAINVILLE J.L. Electrical stimulation of primary olfactory nerve induces two types of variation in the extracellular potassium activity within the glomerulus of the rat olfactory bulb. *Brain Res.* 457: 188-191, 1988.

LANCET, D. Vertebrate olfactory reception *Ann. Rev. Neurosci.* 9: 329-55, 1986.

LI, Z., AND HOPFIELD, J.J. Modeling the olfactory-bulb and its neural oscillatory processings. *Biol. Cybern.* 61: 379-392, 1989.

MARTINEZ, D.P., AND FREEMAN, W.J. Periglomerular cell action on mitral cells in olfactory bulb shown by current source density analysis. *Brain Res.* 308:223-233, 1984.

MEREDITH, M. Patterned response to odor in mammalian olfactory bulb: the influence of intensity. *J. Neurophysiol.* 56: 572-597, 1986.

MEREDITH, M. Neural circuit computation: Complex patterns in the olfactory bulb. *Brain Res. Bull.* 29: 111-117, 1992.

MORI, K., NOWYCKY, M. C., AND SHEPHERD, G. M. Electrophysiological analysis of mitral cells in the isolated turtle olfactory bulb. *J. Physiol. Lond.* 314: 281-294, 1981a.

MORI, K., NOWYCKY, M. C., AND SHEPHERD, G. M. Analysis of synaptic potentials in mitral cells in the isolated turtle olfactory bulb. *J. Physiol. Lond.* 314: 295-309, 1981b.

MORI, K., KISHI, K., AND OJIMA, H. Distribution of dendrites of mitral, displaced mitral, tufted, and granule cells in the rabbit olfactory bulb. *J. Comp. Neurol.* 219: 339-355, 1983.

MORI, K., AND TAKAGI, S. F. An intracellular study of dendrodendritic inhibitory synapses on mitral cells in the rabbit olfactory bulb. *J. Physiol. Lond.* 279: 569-588, 1978a.

MORI K., AND TAKAGI, S.F. Activation and inactivation of olfactory bulb neurones by anterior commisure volleys in the rabbit. *J. Physiol* 279:589-604, 1978b.

MORI, K. Membrane and synaptic properties of identified neurons in the olfactory bulb. *Progress in Neurobiology.* 29: 275-320, 1987.

MORI, K. Molecular and cellular properties of mammalian primary olfactory axons. *Micr. Res. and Tech.* 24: 131-141, 1993.

PINCHING, A.J., AND POWELL, T.P.S. The neuropil of the periglomerular region of the olfactory bulb. *J. Cell Sci.* 9: 379-409, 1971.

RALL, W., SHEPHERD, G.M., REESE, T.S., AND BRIGHTMAN, M.W. Dendrodendritic synaptic pathway for inhibition in the olfactory bulb. *Exp. Neurol.* 14:44-56, 1966.

RALL, W., AND SHEPHERD, G. M. Theoretical reconstruction of field potentials and dendrodendritic synaptic interactions in olfactory bulb. *J. Neurophysiol.* 31: 884-915, 1968.

SCHILD, D., AND RIEDEL, H. Significance of glomerular compartmentalization for olfactory coding. *Biophys J.* 61: 704-715, 1992.

SEGEV, I., FLESHMAN, J. W., AND BURKE, R. E. Computer simulation of group 1a EPSPs using morphologically realistic models of cat a-motoneurons. *J. Neurophysiol.* 64(2): 648-660, 1990.

SHEPHERD, G. M. Principles of specificity and redundancy underlying the organization of the olfactory system. *Micr. Res. and Tech.* 24:106-112, 1993.

SLOTNICK, B.M., GRAHAM, S., LAING, D.G., AND BELL, G.A. Detection of propionic acid vapor by rats with lesions of olfactory bulb areas associated with high 2-DG uptake. *Brain Res.* 417: 343-346, 1987.

WELLIS, D. P., AND SCOTT, J. W. Intracellular responses of identified rat olfactory bulb interneurons to electrical and odor stimulation. *J. Neurophysiol.* 64(3): 932-947, 1990.

WHITE, J., HAMILTON, K.A., NEFF, S.R., AND KAUER, J.S. Emergent properties of odor information coding in a representational model of the salamander olfactory bulb. *J. Neurosci.* 12: 1772-1780, 1992.

WILSON, M. A., BHALLA, U. S., UHLEY, J. D., AND BOWER, J. M. Genesis: A system for simulating neural networks. In: *Advances in Neural Information Processing Systems, Vol 1.* Edited by D. Touretzky. San Mateo, Morgan Kaufman Publishers, 1989, p. 485-492.

WILSON, M., AND BOWER, J.M. Cortical oscillations and temporal interactions in a computer simulation of piriform cortex. *J. Neurophysiol.* 67:981-995, 1992.

CONCLUSION.

"... such substances as agreeably titillate the senses are composed of smooth round atoms. Those that seem bitter and harsh are more tightly compacted of hooked particles and accordingly tear their way into our senses... "

(Lucretius, 47 BC).

Theories of information processing in the bulb.

The objective of these projects was to study information processing in the olfactory bulb. Despite it being the object of considerable attention since the beginning of the century, it has been difficult to determine the nature of this processing. Given that the input has been ill-defined, and the output barely touched upon, it is not surprising that our picture of the intervening processing has remained somewhat nebulous.

In this study we have found two distinct spatial organizations of olfactory bulb responses, which are related to different behavioral states. We suggest that these represent distinct modes of processing in the bulb, and that there may be multiple such modes controlled by centrifugal inputs in a manner that optimizes the operation of the bulb for specific tasks. The observed variable component in single-neuron responses may be related to changes between such processing modes. Our proposals about olfactory bulb processing draw together many of the ideas that have been previously put forth, as described below.

The first modern framework for thinking about olfaction was proposed by Adrian (Adrian 1950). It is remarkable how many of his suggestions remain relevant to current research. On the basis of multiunit recordings and histology, he formulated a picture of diffuse but broadly topographic projections from the receptors to the bulb, and suggested that the representation of odorants in the bulb was encoded in the spatial pattern of activity they elicited. This spatial representation of odorants in the bulb has been

a topic of investigation for many years, with techniques of increasing resolution. A number of different ideas about how the spatial representation relates to information processing have emerged. As discussed in the introduction, these ideas generally fall under the headings of 'specific' and 'distributed' representation. The spatial processing proposed by Adrian is evident in the organization of bulbar responses seen in our experiments.

Another perspective on spatial encoding of olfactory information has been the analogy, particularly due to Shepherd, between the retina and the olfactory bulb (Shepherd 1979). The basic resemblance between the two circuits is in the lateral interactions at two levels of the circuit. In the retina the levels are the horizontal cells, which mediate interactions immediately following the photoreceptors, and the amacrine cells contributing another level of lateral interactions prior to the ganglion cells. The analogous components in the bulb, according to this viewpoint, are periglomerular cell interactions at the glomerular layer and the mitral-granule cell dendro-dendritic connections in the external plexiform layer.

Other aspects of encoding have also been established. The early work of Kauer and Shepherd (Kauer and Shepherd 1977) began to highlight the importance of temporal encoding of olfactory information in the spike trains of neurons. This theme has been developed to include the complex issue of respiration-related tuning, where the reference respiratory signal itself is subject to odor and behavior dependent changes.

One of the early methods for studying spatial aspects of bulbar responses was EEG recordings. These methods have been developed and refined by Freeman and co-workers for many years. On the basis of these they have propounded a somewhat isolated viewpoint in the olfactory literature. Their proposition is that the basis of olfactory processing is not single unit activity, but group action. Accordingly, they have utilized EEG recordings as a means of measuring the activity of ensembles of neurons. Due to the cell geometry and populations in the bulb, most of the EEG signal arises from granule cells. A theory of odorant recognition based on chaotic dynamics controlled by feedback from central olfactory structures has been developed on the basis of this data (Freeman, 1975). Despite the differences in the details of these

ideas, however, the underlying concept of multiple state-dependent representations of odorants is similar to other hypotheses, including ours.

The development of 2-DG techniques established the pivotal role of glomeruli in olfactory processing and strongly reinforced the idea of specific representations of odorants on the bulb (Lancet et al. 1982). Extreme versions of this theory relate each odorant to a small number of glomeruli - nicknamed the 'grandmother glomerulus' theory. With the gradual formulation of a clearer picture of spatial aspects of bulbar organization, however, the differences between the distributed and specific views of olfactory processing have also come into sharper focus. The identification of specific sets of glomeruli as related to the processing of odorants led to the logical next step of ablating them (Slotnick et al. 1987), and this uncovered a serious gap in the emerging framework of understanding olfactory processing. The 'grandmother glomerulus' idea had already been challenged on the entirely different grounds of anatomical projections to the cortex (Haberly and Price 1977). Our study suggests a way of reconciling these two views. We find that response consistency lies on a continuum. At one extreme responses are stable, and would fit with ideas on highly specific projections and tuning. On the other extreme we also observe highly variable responses, which would be expected for a distributed representation. Since these extremes lie on a continuum, it is easy to see how examples of each kind of response can be found.

In recent years single unit studies have begun to characterize the more dynamic aspects of spatial organization of bulbar responses predicted by Adrian. These were initially described as center-surround, by analogy with corresponding properties in the visual system. Since then it has been appreciated that there is a more subtle aspect of complementary responses (Scott et al. 1993; Chapter 4), which a simple sign flip does not fully describe. Techniques for optical recording from the olfactory bulb (Kauer 1988; Cinelli and Salzberg 1992) have vastly broadened the spatial extent that can be monitored, and improved the time and spatial resolution.

Another ongoing development is the infusion of results and concepts from molecular biology, starting with the identification of a putative family of odorant receptors (Buck and Axel 1991). There is a

strong tendency to favor familiar molecular concepts of specificity and clonal exclusion, and these ideas have brought many of the comfortable compromises of diffuse projections under closer scrutiny.

Results and hypothesis from these studies.

Our basic experimental results have two facets. First, we have found that the responses of an individual neuron can be represented as a combination of a consistent response, and a variable component. Second, and more fundamentally, we have found two distinct cases of spatial organization in bulbar responses, related to normal respiration and sniffing respectively. Our simulations complement these observations. They demonstrate a mechanism for the interactions that may underlie the spatial organization in the form of active spike propagation in the secondary dendrites of mitral cells. Furthermore, they suggest that the degree of variability seen in individual neuron responses is unlikely to be due to variability at the receptor input level, and thereby indicate a central mechanism for this effect.

Based on these observations, we propose that the olfactory bulb has multiple modes of operation. The variable component of single neuron responses is not random, but due to these different processing modes. Under central control, and according to behavioral state, the system switches between these modes in order to obtain the best possible information about the olfactory signal.

Implications for further studies.

Our study suggests several directions for additional research. It would be enlightening to obtain corresponding results for spatial patterns in animals performing specific behavioral tasks. A number of studies (Freeman and Grajski 1987 ; Gray and Skinner 1988a) indicate that such tasks might also involve state-dependent response patterns in the bulb. A broadening of the domain addressed by our experiments would help to place the results in better perspective. In particular, the range of odor concentrations, the duration and number of recordings, and the arrangements of recording sites in the bulb could all be usefully extended. Reversible blockage of centrifugal input to the bulb (Gray and Skinner 1988b) would be an excellent test of these ideas relating to central modulation of bulbar activity.

We have only begun to address a range of issues that the model of the bulb is relevant to. More careful analysis of the bulbar responses and parameters will undoubtedly highlight the interactions in the model that are most important for its correct behavior. The bulb model itself represents only a small part of the olfactory system, other components of which are already being studied using simulations (receptor neurons: Firestein and Shepherd 1991; projections from epithelium to bulb: Berkowicz (personal communication); Piriform cortex: Wilson and Bower 1992; Hasselmo et al. 1992). With additional experimental and modeling work, it should be feasible to aim for a combined model of the olfactory system as a whole which can more closely address some of the theories of olfactory processing and its relation to central control and behavior.

The field of olfaction is experiencing a renaissance as new methods: physiological, anatomical, molecular, and simulation based, are developed and begin to relate to each other. This project has been very much in keeping with this theme. We have begun to see how behavioral state may direct information processing in the bulb. As our understanding deepens, we may begin to see how information processing in sensory systems directs behavior.

REFERENCES

ADRIAN, E.D. Sensory discrimination with some recent evidence from the olfactory organ. *Br. Med. Bull.* 6:330-331, 1950.

BUCK, L., AND AXEL, R. A novel multigene family may encode odorant receptors: a molecular basis for odor recognition. *Cell* 65: 175-187, 1991.

CINELLI, A. R., AND SALZBERG, B. M. Dendritic origin of late events in optical recordings from salamander olfactory bulb evoked field potentials from salamander olfactory bulb. *J. Neurophysiol.* 68: 786-806, 1992.

FIRESTEIN, S., AND SHEPHERD, G.M. A kinetic model of the odor response in single olfactory receptor neurons. *J. Steroid Biochem. Molec. Biol.* 39: 615-620, 1991.

FREEMAN, W.J., AND GRAJSKI, K.A. Relation of olfactory EEG to behavior: Factor Analysis *Behav. Neurosci.* 101: 766-777, 1987.

FREEMAN, W.J. *Mass Action in the Nervous System.* 1975. Academic Press.

GRAY, C.M., AND SKINNER, J.E. Field potential response changes in the rabbit olfactory bulb accompany behavioral habituation during the repeated presentation of unreinforced odors. *Exp. Brain Res.* 73: 189-197, 1988a.

GRAY, C.M., AND SKINNER, J.E. Centrifugal regulation of neuronal activity in the olfactory bulb of the waking rabbit as revealed by cryogenic blockade. *Exp. Brain Res.* 69: 378-386, 1988b.

HABERLY, L. B., AND PRICE, J. L. The axonal projection patterns of the mitral and tufted cells of the olfactory bulb in the rat. *Brain Res.* 129: 152-157, 1977.

HASSELMO, M.E., ANDERSON, B.P., AND BOWER, J.M. Cholinergic modulation of associative memory function. *J. Neurophysiol.* 67:1230-1246, 1992.

KAUER, J. S., AND SHEPHERD, G.M. Analysis of the onset phase of olfactory bulb unit responses to odour pulses in the salmander. *J. Physiol. Lond.* 272:495-516, 1977.

KAUER, J. S. Real-time imaging of evoked activity in local circuits of salamander olfactory bulb. *Nature* 331: 166, 1988.

LANCET, D., GREER, C.A., KAUER, J. S., AND SHEPHERD, G. M. Mapping of odor-related neuronal activity in the olfactory bulb by high-resolution 2-deoxyglucose autoradiography. *Proc. Natl. Acad. Sci.* 79: 670-674, 1982.

SCOTT, J.W., WELLIS, D.P., RIGGOTT, M.J., AND BUONVISO, N. Functional organization of the main olfactory bulb. *Micr. Res. and Tech.* 24:142-156, 1993.

SHEPHERD, G.M. *The synaptic organization of the brain. 2nd edn.* OUP, Oxford. 1979.

SLOTNICK, B.M., GRAHAM, S., LAING, D.G. AND BELL, G.A. Detection of propionic acid vapor by rats with lesions of olfactory bulb areas associated with high 2-DG uptake. *Brain Res.* 417: 343-346, 1987.

WILSON, M., AND BOWER, J. M. Cortical oscillations and temporal interactions in a computer simulation of piriform cortex. *J. Neurophysiol.* 67(4): 981-995, 1992.